Anti-Prion Effect of Polythiophenes

DISSERTATION

zur

Erlangung der naturwissenschaftlichen Doktorwürde

(Dr. sc. nat.)

vorgelegt der

Mathematisch-naturwissenschaftlichen Fakultät

der

Universität Zürich

von

Ilan Margalith

von

Lausanne, VD

Promotionskomitee

Prof. Dr. Adriano Aguzzi (Vorsitz und Leitung der Dissertation)

Prof. Dr. Ueli Suter

Prof. Dr. Fritjof Helmchen

Zürich, 2013

TABLE OF CONTENT

SUMMARY

Prion diseases are invariably lethal transmissible diseases for which no efficient treatment currently is available. These include in humans the sporadic form called sporadic Creutzfeld-Jakob Disease (sCJD), the iatrogenic form acquired upon transmission of prion infectious particles (iCJD), several heritable forms including Gerstmann-Sträussler-Scheinker syndrome (GSS) and Fatal Familial Insomnia (FFI), the Papua New Guinea-endemic Kuru and the BSE-derived form new variant CJD (nvCJD). The normal prion protein, termed PrP^{C}, for which no physiological function has been yet convincingly demonstrated is coded by the gene *Prnp* and happens to be converted into a misfolded form, termed PrP^{Sc}, which can be transmitted, for example through blood donation. In addition, several conformational isoforms of PrP^{Sc} are possible, yielding the puzzling phenomenon called “prion strains”. In addition, several cell and tissue culture assays enable the determination of infectivity titer of tissue samples. Finally, naturally- or experimentally-occurring prion deposits characterizing different prion strains can be discriminated in tissue sections by using novel molecules called luminescent conjugated polymers (LCPs). In particular, polythiophene acetic acid (PTAA) has been used to unravel conformational variants of the mouse prion protein in animals infected with several mouse-adapted prion strains.

The strong interaction of LCPs with prion aggregates and amyloid structures related to various amyloid-involving diseases provides the rationale for testing their potential antiprion effect. In the first part of my thesis I show that incubation with anionic, cationic or zwitterionic LCPs not only depleted the infectivity of a prion-containing brain homogenate but also limited prion accumulation in cerebellar organotypic cultured slices (COCS). In addition, by using several techniques for quantifying prion content, I link decreased infectivity with structural changes of prion aggregates. Surprisingly, I could show that PrP^{Sc} resistance to proteolysis was enhanced and LCP-treated recombinant $mPrP_{23\text{-}231}$ fibers were visualized as more compact aggregates that were also more stable to proteolysis. These results suggest that LCPs exert their antiprion effect by rendering PrP aggregates more compact, which may prevent release of infectious prion seeds. In addition, ELISA on COCS as well as a conversion

assay using recombinant $mPrP_{23-231}$ show that PTAA may also prevent the transition of PrP^{C} to PrP^{Sc} by interacting with PrP^{C} or an intermediate molecular variant.
I therefore propose LCPs as a new class of antiprion compounds that prevent propagation of prion infectious species by enhancing compactness of PrP^{Sc} deposits.

In the second part of my thesis I describe the development of a method for using LCPs as a tool to study phenomena related to prion strains in COCS, such as prion strain adaptation and prion strain competition. LCPs have previously been proven to be powerful tools to investigate the structure of PrP^{Sc} aggregates linked with different prion strains. Here I propose to combine the use of these molecules with the prion organotypic slice culture assay to study prion strains in a fast manner: Indeed, prion propagation in COCS enables analysis of amyloid aggregates that are readily stainable and observable in COCS after already five weeks, versus several months in mice. Notably, I could reproduce the results previously obtained by C. J. Sigurdson and K. P. R. Nilsson in mice in a very fast manner in COCS.

In the third part of my thesis I describe collaborative work that has led to the identification of human stem cell-reconstituted *Prnp* knockout mice as a bioreactor for human prions. In particular, I have shown that these mice had efficiently replicated CJD prions.

ZUSAMMENFASSUNG

Prionenerkrankungen sind ausnahmslos letale übertragbare Erkrankungen, für die keine effiziente Behandlung zur Verfügung steht. Zu diesen Erkrankungen gehören die sogenannte Creutzfeld-Jakob Erkrankung (sCJD), die iatronische Form (iCJD), die durch die Übertragung von infektiösen Prionenpartiklen erworben wird, sowie mehrere erbliche Formen, wie z.B. das Gerstmann-Sträussler-Scheinker-Syndrome (GSS) und die familiäre fatale Insomnie (FFI), die in Papua-Neuguinea auftretende endemische Erkrankung Kuru und die durch BSE-übertragene neue Variante der CJD (nvCJD). Die normale Form des Prionproteins, PrP^{C}, für das noch keine physiologische Funktion überzeugend beschrieben worden ist, wird von dem Gen *Prnp* kodiert und kann in eine falschgefaltete Form, PrP^{Sc}, umgewandelt werden, welche übertragbar ist, z.B. bei der Blutspende. Weiterhin kann PrP^{Sc} verschiedene konformationelle Isoformen annehmen, was zu dem Auftreten des verwirrenden Phänomens verschiedener Prionenstämme geführt hat. Die Infektiösität von Prionen-infizierten Gewebeproben kann mittels verschiedenen Zell- und Gewebekulturuntersuchungen bestimmt werden. Schlussendlich, natürliche und experimentell-auftretende Prionenablagerungen verschiedener Prionenstämme können in Gewebeschnitten mittels neuer Moleküle, welche als “luminescent conjugated polymers (LCPs)“ bezeichnet, unterschieden werden. Namentlich, “polythiophene” Essigsäure (PTAA) wurde zur Unterscheidung von verschiedenen konformationellen Varianten des Mausprionproteins von Tieren, welche mit verschieden Maus-adaptierten Prionenstämmen infiziert wurden, verwendet.

Die starke Wechselwirkung von LCPs mit Prionenaggregaten und Amyloidstrukturen, die mit verschiedenen Amyloid-Erkrankungen in Verbindung gebracht werden, hat die Untersuchung von LCPs auf deren Anti-Prionen-Effekt nahegelegt. Im ersten Teil meiner Arbeit zeige ich, dass die Inkubation mit verschiedenen LCPs, darunter anionische, kationische und zwitterionische, die Infektiosität von prioneninfiziertem Hirnhomogenat senkte und die Prionenaggregation in zerebellaren organotypischen kultivierten Hirnscheiben (COCS) hemmte. Unter Anwendung diverser Techniken zur Quantifizierung des Prionengehalts konnte ich einen Zusammenhang zwischen der verminderten Infektiosität und der strukturellen Veränderungen der Prionenaggregate

zeigen. Überraschenderweise zeigte sich, dass die Resistenz von PrP^{Sc} gegenüber Proteolyse wuchs und LCP-behandelte rekombinante $mPrP_{23-231}$ Fasern kompaktere Aggregate bildeten, die ebenfalls resistenter gegenüber Proteolyse waren. Diese Befunde legen nahe, dass die LCPs ihren Anti-Prionen-Effekt erzielen, indem sie PrP-Aggregate kompakter machen, und somit die Freisetzung von infektiösen Keimen verhindern. Darüber hinaus zeigen ELISA-Daten der COCS sowie Konvertierungsexperimente mit rekombinantem mPrP23-231, dass PTAA möglicherweise auch die Umwandlung von PrP^{C} in PrP^{Sc} durch Wechselwirkung mit PrP^{C} oder einem molekularen Zwischenprodukt verhindert. Ich schlage deshalb vor, dass LCPs eine neue Klasse von Anti-Prionen-Verbindungen darstellen, die die Ausbreitung von prioneninfiziertem Partikeln verhindert, in dem sie die Kompaktheit von PrP^{Sc}-Ablagerungen erhöhen.

Im zweiten Teil meiner Arbeit beschreibe ich die Entwicklung einer Methode, die es ermöglicht, LCPs einzusetzen, um Phänomene im Zusammenhang mit Prionenstämmen in COCS zu beobachten, wie z.B. Prionenstamm Kompetition und Prionenstamm Anpassung. Vor kurzem konnte gezeigt werden, dass LCPs gut geeignet sind, um die Struktur von PrP^{Sc}-Aggregaten in Verbindung mit verschiedenen Prionenstämmen zu untersuchen. Ich zeige auf, dass die Verwendung dieser Moleküle kombiniert mit einem Prion organotypischen Kokultur-Assay die Untersuchung von Prionenstämmen vereinfacht: Prionvermehrung in COCS erlaubt die Analyse von Amyloidaggregaten, die bereits gefärbt und beobachtet werden können, in COCS schon nach fünf Wochen versus mehrere Monate in Mäusen. Ich konnte vorgängige Resultate von C. J. Sigurdson and K. P. R. Nilsson in Mäusen auf diese Weise in sehr kurzer Zeit reproduzieren.

Der dritte Teil meiner Arbeit beschreibt eine Zusammenarbeit, die zur Identifikation von mit menschlichen Stammzellen rekonstituierten *Prnp* Knockout-Mäusen als Bioreaktor für menschliche Prionen geführt hat. Insbesondere konnte ich zeigen, dass diese Mäuse CJD Prionen sehr effizient replizierten.

DEFINITIONS

Prion: Agent of transmissible spongiform encephalopathy (Khoor et al.), with unconventional properties. The term does not have structural implications other than that a protein is an essential component.

'Protein-only' hypothesis: Maintains that the prion is devoid of informational nucleic acid, and that the essential pathogenic component is protein (or glycoprotein). Genetic evidence indicates that the protein is an abnormal form of PrP (perhaps identical with PrP^{Sc}). The association with other 'non-informational' molecules (such as glycosaminoglycans, or maybe even short nucleic acids) is not excluded.

PrP^{C}: The naturally occurring form of the mature *Prnp* gene product. Its presence in a given cell type is necessary, but not sufficient, for replication of the prion.

PrP^{Sc}: An 'abnormal' form of the mature *Prnp* gene product found in tissue of TSE sufferers, defined as being partly resistant to digestion by proteinase K (PK) under standardized conditions. It is believed to differ from PrP^{C} only (or mainly) conformationally, and is often considered to be the transmissible agent or prion.

Adapted from Aguzzi and Weissmann (Aguzzi and Weissmann, 1997)

ABBREVIATIONS

BBB	Blood-brain barrier
BH	Brain homogenate
BSE	Bovine spongiform encephalopathy
CGN	Cerebellar granule neuron
CJD	Creutzfeldt-Jakob disease
CNS	Central nervous system
COCS	Cultured organotypic cerebellar slices
COCSBH	Brain homogenate prepared from COCS
CR	Congo red
CWD	Chronic wasting disease
DPI	Days post-inoculation
DIV	Days *in vitro*
FFI	Fatal familial insomnia
GPI	glycosylphosphatidylinositol
GSS	Gerstmann-Sträussler-Scheinker disease
LCP	Luminescent conjugated polythiophene
MPA	Misfolded protein assay
PK	Proteinase K
POSCA	Prion organotypic slice culture assay
PPS	Pentosan polysulfate
PrP^{C}	Cellular prion protein
PrP^{Sc}	Scrapie-associated prion protein
recPrP	Recombinant PrP
RML	Rocky Mountain laboratory prion strain
SDS	Sodium dodecyl sulfate
SCA	Scrapie cell assay
SCEPA	Scrapie cell assay end point assay
LogID50	Prion infectivity units
TEM	Transmission electron micrscopy
TSE	Transmissible spongiform encephalopathy
vCJD	Variant Creutzfeldt-Jakob disease

INTRODUCTION

TRANSMISSIBLE SPONGIFORM ENCEPHALOPATHIES

Prion diseases, also called transmissible spongiform encephalopathies (TSEs), are a large group of lethal neurodegenerative disorders affecting both humans and animals (Aguzzi, 2006). These diseases share similarities on the epidemiologic, pathological and biochemical levels: TSE refers to the transmissibility of the disease and to the neuropathological feature of songiform vacuolation classically seen in the CNS of sick individuals. TSEs can be dominantly inherited (as a result of a mutation of the prion gene) or transmitted (by infection with prion infectious seeds). If a genetic or infectious transmission can be excluded, they are classified as sporadic. Independently of their origin, however, all TSE can be transmitted experimentally and are therefore regarded as infectious diseases. Although many similarities to other neurodegenerative protein misfolding diseases such as Alzheimer's, Huntington's and Parkinson's disease have been described (DeArmond, 1993; Aguzzi and Haass, 2003), prion diseases distinguish themselves by their transmissibility. The transmitting agent, called prion (from *pr*oteinaceous *i*nfectious *o*nly), distinguishes itself from conventional bacterial or viral infectious agents by its resistance to usual sterilization means (high temperature, treatment with formaldehyde or UV irradiation) and by the unusually long incubation time of the associated disease. The prion seems to be devoid of informational nucleic acids (Alper et al., 1966; Alper et al., 1967) and prion infectivity tends to associate with accumulation in the brain of PrP-scrapie (PrP^{Sc}), a proteinase-resistant isoform of the naturally occurring, physiological cellular protein termed PrP^{C} (Chesebro et al., 1985; Oesch et al., 1985b; Basler et al., 1986). The notion that a protein might be the infectious agent causing TSEs was first proposed by Griffith (Griffith, 1967). This idea was later on supported by Stanley Prusiner who named this protein the prion protein (Prusiner, 1982). Major neuropathological hallmarks of TSEs are extensive spongiosis, neuronal cell loss in the CNS, gliosis (DeArmond, 1993), and deposition of amorphous PrP aggregates (amyloid plaques) (Bendheim et al., 1984; DeArmond et al., 1985; Aguzzi, 1996; Manuelidis et al., 1997). The accumulation in the brain of PrP aggregates and the transmissibility of the disease are the defining traits of TSEs.

Animal prion diseases

The naturally occurring prion disease called Scrapie has been recognized in sheep and goats since the 18th century (Aguzzi, 2006) and was initially termed “tremblante” in French because of the quivering syndrome developed by sick animals. Several other widespread occurrences of TSEs have recently been observed in other wild or domesticated species of animals. Animal TSEs include sheep and goat Scrapie (Cuille and Chelle, 1939), the original animal TSE that has been recognized more than 200 years ago, but also transmissible mink encephalopathy (TME) (Marsh and Hadlow, 1992), chronic wasting disease (CWD) of mule deer and elk (Williams and Young, 1980), feline spongiform encephalopathy (FSE) (Pearson et al., 1991; Eiden et al., 2010) and bovine spongiform encephalopathy (BSE) (Wells et al., 1987). The first cases of CWD, a prion disease of captive and free-ranging mule deer and elk, were reported in the late 1960s in Colorado. This newly recognized TSE is currently spreading across the American continent (Sigurdson and Aguzzi, 2007). The unidentified path of horizontal transmission is still preventing means of controlling this epidemic. In the UK, a previously unobserved neurological disease in cattle associated with pathologic changes in the brain that were similar to those characteristic of TSEs was first recognized in 1986. This new form of TSE, called BSE or more commonly “mad-cow disease”, rapidly developed into a worrying epidemic in the UK and in other European countries. BSE was possibly caused by transmission of sheep Scrapie to cattle through infected fodder prepared from carcasses of sacrificed animals (Wilesmith, 1988; Aguzzi and Weissmann, 1996). Another hypothesis for the origin of BSE is the possible contamination of feed prepared from cattle with BASE, a possibly atypical sporadic form of BSE (Capobianco et al., 2007). The transmissibility of BSE to various animal species, including humans, unlike previously known prion diseases such as sheep scrapie, has raised enormous public health concerns. Even though the routes for transmission of prions in Scrapie and CWD remain elusive, several possible routes of horizontal transmission have been recently described, such as nephritis-associated transmission through urine (Seeger et al., 2005), mastitis-associated transmission through milk (Ligios et al., 2005), as well as transmission through saliva (Mathiason et al., 2006). Furthermore, transmission of prion infectivity through olfactory routes has been recently demonstrated (Haybaeck et al., 2011).

Human prion diseases

Human TSEs include familial, sporadic and variant Creutztfeldt-Jakob diseases (CJD) (Gibbs et al., 1968), Fatal Familial Insomnia (FFI) (Medori et al., 1992), Gerstmann-Sträussler-Scheinker syndrome (GSS) (Gajdusek, 1977) and Kuru (Gajdusek et al., 1966). These diseases can be either genetically inherited (Mastrianni, 2010), acquired by transmission of prion infectivity (Weissmann et al., 2002; Aguzzi and Polymenidou, 2004a; Haybaeck et al., 2011) or occur sporadically (Edgeworth et al., 2010) (Figure 1, adapted from: (Aguzzi and Calella, 2009)).

Disease	Etiology
Kuru	Infection
Creutzfeldt-Jakob disease	
Iatrogenic	Infection
Sporadic	Unknown
Familial	*PRNP* mutation
Variant	Presumed BSE infection
Gerstmann-Sträussler-Scheinker disease	*PRNP* mutation
Fatal familial insomnia	*PRNP* mutation

Figure 1: Human prion diseases

Adapted from: (Aguzzi and Calella, 2009).

Sporadic CJD occurs with an equal incidence in men and women and accounts for 85% of human prion diseases. Its rate of occurrence worldwide is 1 to 3 cases per million inhabitants per year. The origin of sporadic CJD is unknown. Different hypothesis propose that sporadic CJD could be triggered as a rare event by spontaneous conversion of PrP^{C} into disease-associated PrP^{Sc} or by somatic *Prnp* mutations. A predisposition to the development of sporadic and acquired CJD results from homozygosity for the M allele at a common coding polymorphism at codon 129 of *Prnp* gene encoding either methionine or valine (Collinge et al., 1991; Palmer et al., 1991; Windl et al., 1996). Individuals that are homozygous for the V allele are more resistant to infection than heterozygous ones (Baker et al., 1991). The observation of a very long incubation period (up to 50 years) between the time of infection and the clinical manifestation of Kuru has led to the concept that this disease was caused by “slow viruses” (Collinge et al., 2006). About 15 % of human prion diseases are associated with autosomal dominant mutations in the *Prnp* gene. Most pathogenic mutations in *Prnp* are

thought to trigger an increased tendency of PrP^{C} to convert into PrP^{Sc}, however not all disease-causing *Prnp* mutations are associated with PrP^{Sc} and infectivity. The discovery of a new form of CJD in the UK in 1996 was epidemiologically and experimentally linked to the widespread BSE epidemic in the early 1990s. Although it is not yet possible to estimate the extent of a potential vCJD epidemic, preliminary data indicate a significant dietary exposure to BSE-infected meat in the UK. Although it seems that the annual new cases of vCJD have peaked (Aguzzi et al., 2007), all patients suffering from vCJD so far were homozygous for methionine at codon 129 of *Prnp*. Experiments in mice expressing different isoforms of human PrP^{C} show that valine at codon 129 of *Prnp* inhibits transmission of BSE whereas mice homozygous for methionine develop BSE rapidly. The fact that heterozygous mice show a delayed onset of disease, but still develop clinical disease nonetheless (Wadsworth et al., 2004), raises the concern of a delayed vCJD outbreak in humans that are heterozygous at codon 129. In addition, transmission of vCJD through blood donation from a donor, who developed vCJD several years after donating blood, to multiple recipients was recently described (Llewelyn et al., 2004; Wroe et al., 2006). This represents the formal proof of efficient transmission of vCJD through blood. Although many different assays for sensitive detection of prions in blood are currently under development, the danger of propagation of vCJD through blood donation cannot, at the moment, be obviated (MacGregor and Prowse, 2004). Therefore, research efforts to understand the molecular basis of prion diseases, understand the mechanisms underlying species barrier and interspecies transmission, improve methods of diagnosis, and develop therapeutic strategies for treatment and prevention of the disease have been intensified.

PRION CONVERSION REACTION

As prion diseases are associated with brain accumulation of PrP^{Sc}, prion research has largely focused on the transition from PrP^{C} to PrP^{Sc}. These two molecules were found to share a similar amino acid structure and no known covalent modifications could differentiate them (Stahl et al., 1993). It is therefore generally accepted that PrP^{Sc} is a posttranslational derivative of PrP^{C} that has acquired an alternative structure. The protein-only hypothesis proposes that the nature of the infectious entity responsible for the triggering of any prion disease consists mainly of PrP^{Sc}, an abnormally-folded, protease-resistant, β-sheet-rich isoform of the normal cellular prion protein, termed PrP^{C} (Prusiner, 1991, 1998). This concept has been further precised by Charles Weissmann (Weissmann, 1991): the prion is an infectious protein that does not contain any informational nucleic acids, and that propagates

by recruitment and "autocatalytic" conformational conversion of the normal cellular prion protein PrP^{C} into disease-associated PrP^{Sc} (Aguzzi et al., 2007). The resolution of the 3D structure by NMR of mouse (Riek et al., 1996a) and human PrP (Hosszu et al., 1999) and the development of newer techniques to study amyloids such as hydrogen/deuterium exchange (Lu et al., 2007) have provided useful information about a possible conversion mechanism: since PrP^{Sc} appears to have more β-sheet content than PrP^{C}, it is proposed that non-covalent interactions between compatible nucleic acid strands in PrP^{C} make this molecule tend towards the structural state of PrP^{Sc}. Furthermore, it is proposed that pathologic PrP^{Sc} may operate the template-promoted further conversion of PrP^{C}. The structural transition is accompanied by profound changes in the physicochemical properties of the prion protein. While PrP^{C} is soluble in mild detergents and sensitive to proteinase K (PK) digestion, PrP^{Sc} forms insoluble aggregates and is partially resistant to PK (Bolton et al., 1982; Oesch et al., 1985a; Meyer et al., 1986). Attempts to purify PrP^{Sc} by fractionation and correlating the mass of the purified protein complexes to the infectivity of the samples, indicates that the most infectious prion particle has a mass corresponding to 14-28 PrP molecules (Silveira et al., 2005). However, the failure to establish a high resolution of the structure of PrP^{Sc} has precluded a full understanding of the conversion process. Nevertheless, two hypotheses have been developed to explain the pathological refolding of PrP^{C} into PrP^{Sc}. The "refolding model" postulates a template assisted mechanism where a strong kinetic energy barrier prevents PrP^{C} to misfold spontaneously into PrP^{Sc}. Overcoming of the high energy barrier is possible in the presence of a misfolded PrP^{Sc} template, possibly with the help of a chaperone (Telling et al., 1995) or another type of molecule (Priola et al., 2003) (Figure 2A, adapted from: (Aguzzi and Polymenidou, 2004b)) . The second hypothesis, "the seeding model" proposes that PrP^{C} and PrP^{Sc} are in a natural equilibrium privileging PrP^{C} although bi-directional conversion of PrP^{C} and PrP^{Sc} is possible spontaneously. Secondary exposure to exogenous PrP^{Sc} induces a nucleation-polymerisation process promoting stabilization of PrP^{Sc} and further recruitment of endogenous PrP^{C} into a PrP^{Sc} conformation (Jarrett and Lansbury, 1993) (Figure 2B). Mutations in PrP^{C} could predispose PrP^{C} to aggregate in PrP^{Sc} by destabilizing its conformation.

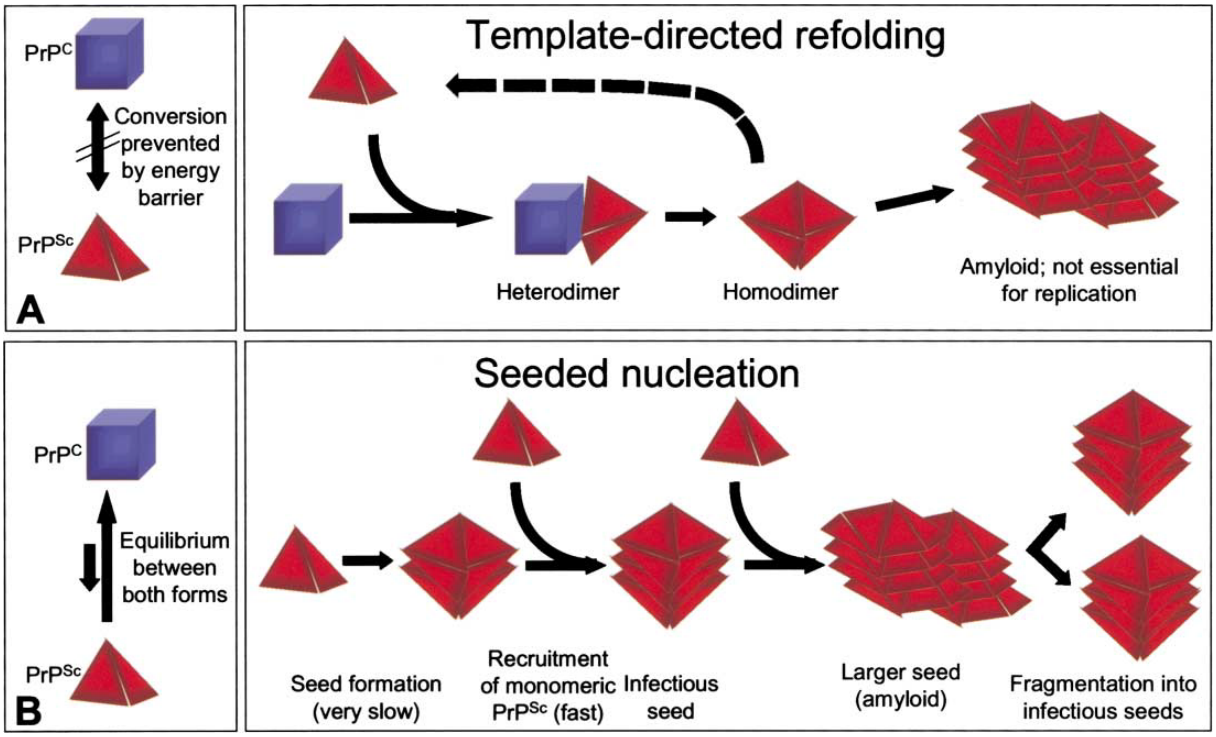

Figure 2: Models for the Conversion of PrP^C into PrP^{Sc}. Adapted from: (Aguzzi and Polymenidou, 2004b).

(**A**) The "refolding" or template assistance model postulates an interaction between exogenously introduced PrP^{Sc} and endogenous PrP^C, which is induced to transform itself into further PrP^{Sc}. A high energy barrier may prevent spontaneous conversion of PrP^C into PrP^{Sc}.

(**B**) The "seeding" or nucleation-polymerization model proposes that PrP^C and PrP^{Sc} are in a reversible thermodynamic equilibrium. Only if several monomeric PrP^{Sc} molecules are mounted into a highly ordered seed, further monomeric PrP^{Sc} can be recruited and eventually aggregates to amyloid. Within such a crystal-like seed, PrP^{Sc} becomes stabilized. Fragmentation of PrP^{Sc} aggregates increases the number of nuclei, which can recruit further PrP^{Sc} and thus results in apparent replication of the agent.

PRION PATHOGENESIS

The mechanisms of prion pathogenesis leading to glial activation, neuronal cell death and the associated spongiosis and clinical signs are not yet understood. Mice lacking PrP^C do not show significant behavioral phenotype or signs of neurodegeneration (Büeler et al., 1992), suggesting that prion diseases are not caused by a PrP^C-associated loss-of-function. In fact prion replication and clinical signs upon intracerebral inoculation with prions are not observed if no PrP^C is present (Büeler et al., 1993), which clearly shows that PrP^C expression is crucial for prion replication. However, the link between PrP^{Sc} accumulating outside the cells and the damage to surrounding tissue is missing. Brandner *et al*. investigated this question by transplanting wild-type and PrP overproducing neuroectodermal grafts into brains of PrP knockout mice (Brandner et al., 1996). After the mice were intracebrally inoculated with prions the grafts accumulated high levels of PrP^{Sc} and prion infectivity and the tissue

developed typical Scrapie pathogenesis-induced histopathological changes. The surrounding tissue, which was not expressing PrP, remained healthy despite substantial accumulation of PrP^{Sc} occurred, which shows that cytotoxicity of PrP^{Sc} needs target cells to express cellular PrP^{C} by. This was more recently confirmed in mice expressing a secreted form of PrP^{C} ('GPI-anchorless': a secreted PrP molecule lacking the glycosylphosphatidylinositol-anchor (GPI)) (Chesebro et al., 2005): Prion-inoculated mice replicated PrP^{Sc} without developing histopathological changes, illustrating that PrP must be membrane-bound to exert cellular toxicity. In addition, early signs of prion pathogenesis such as spongiosis and behavioral symptoms can be reversed by conditionally removing PrP^{C} selectively in neurons after disease onset (Mallucci et al., 2003; Mallucci GR, 2007). Altogether this suggests that prion replication at the cell level could be a target for anti-prion intervention strategies.

THE PRION STRAIN PHENOMENON

Prion strains are defined by different disease phenotypes in identical hosts, such as incubation times, histological lesion profiles, organ-tropism, biophysical and biochemical features and targeted cells (Aguzzi et al., 2007). Circumstantial evidence points toward strain-specific properties being defined by different conformations of PrP^{Sc} present in the inoculum. The different stability against chaotropic salts and heat (Safar et al., 1998) and susceptibility to digestion with proteinase K (PK) of PrP^{Sc} isolates derived from different prion strains support this view: PrP^{Sc} tertiary structure defines resistance to denaturation and site of protease digestion. As a result, naturally occurring TSEs present different running patterns on western blots after digestion with PK (Casalone et al., 2004; Zanusso et al., 2004). In addition, different prion strains can co-exist within one individual (Polymenidou et al., 2005; Yull et al., 2006), suggesting a possible competition between different PrP^{C}-recruiting PrP^{Sc} templates for prion conversion. Therefore, it is possible that a prion strain with a higher affinity for PrP^{C} but less profound pathological consequences would decrease the pathogenesis caused by a co-existing strain with more important physiological consequences. However, the formal demonstration that the biological basis of prion strains is encoded within structural differences of PrP^{Sc} has not been possible yet, in part because of the difficulty of performing structural studies on infectious isolates. It has been suggested that the ratio of distinct glycoforms of PrP (un-, mono- and diglycosylated) (Collinge et al., 1996) may influence the structure of infectious PrP species, determining strain properties (Collinge, 2005). However, more recent results deny this view (Piro et al., 2009). Finally, strain properties are also defined by host-encoded PrP^{C} (Nonno et al., 2006). As a result, cell-based

assays can only replicate prion strains to which the cell clones have been selected for (Klohn et al., 2003; Solassol et al., 2003). This limitation, though, provides an opportunity to investigate the so far unidentified factors governing cell tropism and the phenomena of prion mutation and selective amplification of prion strains (Li et al., 2010).

THE CELLULAR PRION PROTEIN

The expression pattern of PrP^C

Expression of the cellular prion protein is highly conserved in mammals and has been identified in birds (Harris et al., 1993), in amphibian (Strumbo et al., 2001), in turtles (Simonic et al., 2000) and more recently in fish (Rivera-Milla et al., 2003). Although PrP-deficient mice are generally believed to perform well despite the absence of PrP, an evolutionary pressure must exist to counterbalance the susceptibility of *Prnp*-expressing individuals to prion disease (Mead et al., 2003). It is therefore plausible that PrP^C must have an important function. PrP^C is highly expressed in the CNS and in several peripheral tissues including heart, skeletal muscle, kidney and lymphocytes (Dodelet and Cashman, 1998; Ford et al., 2002). However, ectopic PrP^C expression can be triggered by inflammatory conditions in organs that normally express very low amounts of PrP^C, thereby supporting prion replication competence (Heikenwalder et al., 2005). In the CNS PrP^C is mainly expressed on neurons, and to a lower extent on other neural cell types including astrocytes and oligodendrocytes (Moser et al., 1995).

The biosynthesis of PrP^C

Upon transcription, an unprocessed PrP polypeptide comprising 254 amino acids is directed towards the membrane of the endoplasmic reticulum (ER) by a 22 amino acids N-terminal hydrophobic signal sequence (in mice and hamsters) which is removed after ER translocation (Stahl et al., 1987). A GPI-anchor replaces 23 amino acids at the C-terminus (Stahl et al., 1987) and high mannose glycans are attached to the polypeptide at residues 180 and 196 and processed to complex glycans during transport through the Golgi apparatus (Bolton et al., 1985). Mature PrP^C molecules are then transported by secretory vesicles to the plasma membrane and anchored by the GPI-moiety at the outer cell surface. The deletion of both glycosylations causes intra-cellular accumulation of PrP^{Sc} (Cancellotti et al., 2005), although the presence of 1 out of the 2 glycosylations is sufficient for appropriate cellular trafficking of PrP. In cell culture, most PrP^C undergoes endocytosis and degradation via the lysosome or

proteasome pathway (Caughey et al., 1989), however 10 to 30 % of PrP^C is shed into the medium (Borchelt et al., 1990).

The structure of PrP^C

Murine, bovine, canine, feline and human mature PrP^C, as well as a prion protein recently characterized in other mammals (e.g.: tammar wallaby (Christen et al., 2009)) have a similar three-dimensional structure comprising a globular domain (residues 125 to 228) and a flexible N-terminal part of about 100 residues (residues 23 to 124 (Donne et al., 1997; Riek et al., 1997; Viles et al., 2001)). The fold of the globular domain is defined by a two-stranded anti-parallel sheet, three □-helices, and a disulphide bond linking helices two and three (Riek et al., 1996b; Hornemann et al., 1997; Riek et al., 1997). The unstructured N-terminal part contains two defined and conserved regions: the first one is a segment of five repeats of an eight amino acids sequence and is called the octarepeat region. This region was suggested to be involved in copper binding and may be involved in prion pathogenesis since its expansion by insertional mutations provokes inherited prion disease (Brockes, 1999). The octarepeat region is flanked by two positively charged sequences named “charge clusters”, CC1 (residues 23–27) and CC2 (residues 95–110). These domains are linked by a hydrophobic stretch of amino acids (residues 111–134), also termed hydrophobic core. This region is evolutionarily extremely well conserved although its potential function is so far unknown (Figure 3, adapted from: (Aguzzi et al., 2008)).

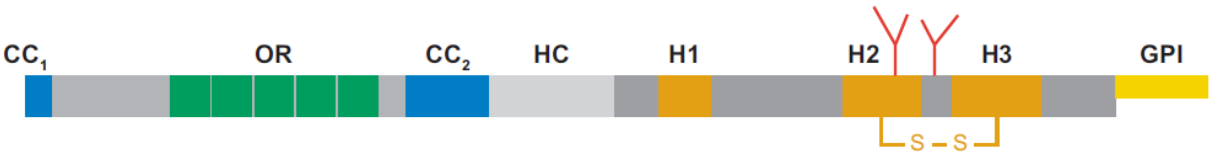

Figure 3: The structure of the human PrP^C. Adapted from: (Aguzzi et al., 2008).
The mature human PrP^C protein contains 208 amino acid residues. It features two positively charged amino acid clusters denoted CC1 and CC2 (*blue boxes*), an octapeptide repeat region (OR) (*green boxes*), a hydrophobic core (HC) (*gray box*), three α-helixes (H1-H3) (*red boxes*), one disulphide bond (S–S) between cysteine residues 179 and 214, and two potential sites for N-linked glycosylation (*red forks*) at residues 181 and 197. A glycosylphosphatidylinositol anchor (GPI) (*yellow box*) is attached to the C-terminus of PrP.

The physiological function of PrP^C

The presence of PrP on the cell surface as a GPI-anchored extracellular molecule suggests a role in cell adhesion, intercellular interaction or as a signaling molecule. Mice devoid of PrP^C were initially reported to have no phenotype (Büeler et al., 1992). Later reports, however, suggested mild alterations in hippocampal synaptic function (Collinge et al., 1994) as well as in circadian rhythm and sleep-pattern of PrP-deficient mice (Tobler et al., 1996). Furthermore, post-developmental ablation of PrP^C was reported to lead to subtle alterations in hippocampal synaptic function, identical to what was seen in PrP-null mice, excluding that compensatory developmental effects are masking a stronger PrP-related phenotype (Mallucci et al., 2002). Unfortunately, most of these results could not be reproduced by other groups (Herms et al., 1995; Lledo et al., 1996). PrP^C was recently proposed to be important for the self-renewal of long-term repopulating haematopoietic stem cells (Zhang et al., 2006) and a positive regulator of neural precursor proliferation during developmental and adult neurogenesis (Steele et al., 2006). More recently, chronic demyelinating polyneuropathy has been evidenced in PrP^C-deficient mice (Bremer et al., 2010), which suggests a role of PrP in myelin maintenance. The relatively low impact of the absence of PrP^C on animal's life and physiology blur the view of a direct function of PrP in any of the above-mentioned roles and confronts with the fact that PrP^C is nevertheless evolutionarily conserved.

ANTIPRION THERAPY

Known antiprion compounds

To date, no efficient treatments against protein aggregation diseases are available (Appleby and Lyketsos, 2011). The assumption that PrP^{Sc} plays a central role in prion disease has motivated approaches based on the identification of compounds that influence amyloid formation or clearance of PrP^{Sc} and PrP^{Sc} stability. Another important aspect of potential antiprion compounds is their bioavailability, as medicaments targeting the brain would need to be able to cross the blood-brain barrier (BBB). Inhibition of PrP^{Sc} conversion in cultured cells chronically infected with prions (Korth et al., 2001) or in animal models (Pocchiari et al., 1987) have been reported for molecules that are known to cross the BBB such as amphotericin B (Pocchiari et al., 1987), quinacrine and chloropromazine (Korth et al., 2001). However, clinical trials in humans revealed no significant improvements of the course of chronic disease (Benito-Leon, 2004; Martinez-Lage et al., 2005; Collinge et al., 2009). Amyloid deposition is thought to progress within one organism by the propagation of

infectious seeds (Aguzzi and Calella, 2009) and prion fibrils may propagate through breaking and elongation of infectious seeds into new fibrils (Wang et al., 2011). Thus, fibril frangibility may be a critical parameter of their infectivity (Caughey and Lansbury, 2003; Knowles et al., 2009). Compounds that stabilize aggregated prion particles may decrease prion infectivity and therefore could be valuable tools for the treatment of prion diseases or prophylactic measures. Congo red (CR) (Ingrosso et al., 1995) and the fluorescent antracycline iododoxorubicin (Tagliavini et al., 1997) were reported to prolong incubation time in rodents upon co-inoculation with prions. Although many prion disinfectants degrade or disaggregate PrP^{Sc}, CR was found to interfere with one or more steps in the conversion of PrP by stabilizing PrP aggregates (Caspi et al., 1998). In addition, several polyanions can interfere with prion replication. The structural requirements for anti-scrapie activity of sulphated polyanions in chronically infected cells were investigated in detail (Ouidja et al., 2007). The most promising compound, pentosan polysulfate (PPS) (Tsuboi et al., 2009; Terada et al., 2010) is currently undergoing clinical trials, although its hydrophobic nature hinders CNS penetration (MacGregor et al., 1985). However, these compounds are believed to interfere with the interaction of endogenous glycosaminoglycans with PrP^{C} and/or PrP^{Sc} rather than acting directly at the level of PrP^{Sc} aggregates. Finally, complex polyamines have been shown to disaggregate PrP but also suffer poor bioavailability (Supattapone et al., 2009). The discovery of new classes of compounds with better bioavailability that directly influence amyloid formation is therefore of high interest.

Conjugated polythiophenes

Conducting polymers (CPs) are a particular group of chemically engineered polymers with electronic and ionic conductivity. CPs were initially developed for broad applications in the field of electronics, however the chemical synthesis of numerous derivatives has extended their potential use in various fields such as the food industry but also the development of biomedical devices, neural prosthetics, antioxidants and biosensors (Ravichandran et al., 2010). Luminescent conjugated polythiophenes (LCPs) (Figure 4) are a subgroup of CPs that have good electrical conductivity and optical properties and have recently been proven as novel tools to investigate amyloids (Herland et al., 2005; Nilsson et al., 2005; Nilsson et al., 2006; Nilsson et al., 2010). Upon binding to the amyloid scaffold the LCPs are able to adopt distinct conformations with characteristic spectral properties that have recently been used for prion strain discrimination (Sigurdson et al., 2007) (Figure 5, adapted from (Sigurdson et al.,

2007)) and the characterization of amlyoid aggregates associated with other protein aggregation diseases (Nilsson et al., 2010).

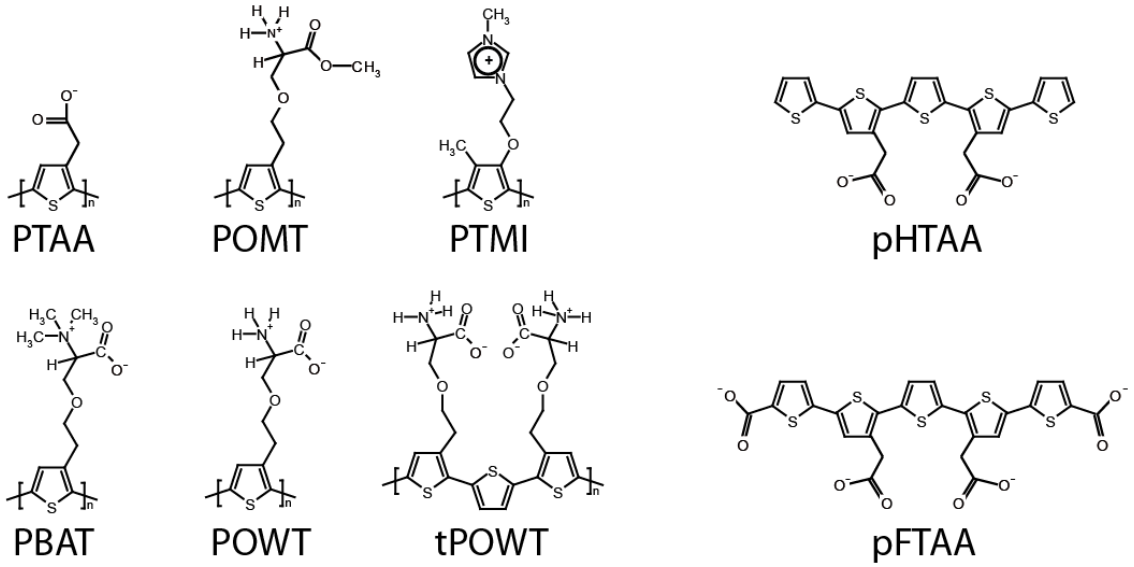

Figure 4: Molecular structures of LCPs.

Luminescent conjugated polythiophenes (LCPs). pHTAA and pFTAA are homodispersed preparations of chemically defined molecules with molecular weights of 897 and 704.7 Da, respectively. All other compounds are polydisperse preparations with average molecular weights ranging from 3000 to 11000 Da and number of monomers of n=11-20 or 1500 Da with n=3 for tPOWT. PTAA and its derivatives pHTAA and pFTAA are anionic compounds. POMT, PTMI and PBAT are cationic and POMT and tPOMT are zwitterionic.

The use of LCPs as novel dyes for aggregated proteins associated with several neurodegenerative disorders illustrate their very strong affinity and specificity for amyloid aggregates. This suggests a potential as anti-prion compounds, because molecules that are able to bind PrP aggregates may stabilize them, thereby preventing the release of prion infectious seeds. In fact, this would not be the first time that a molecule initially used as a dye for amyloid structures would present antiprion activity, and indeed CR has been shown to bind to and stabilize PrP^{Sc} (Caspi et al., 1998). Recently, a new generation of these molecular probes called luminescent conjugated oligomers (Aslund et al., 2007; Aslund et al., 2009) (Figure 4, pHTAA and pFTAA) has been developed for broadening their use in protein aggregation research. As these molecules cross the BBB they enable further development of visualization of protein aggregates *in vivo* as well as prophylactic and therapeutic trials in laboratory animals. In this thesis I refer to all luminescent polythiophenes that I used as LCPs.

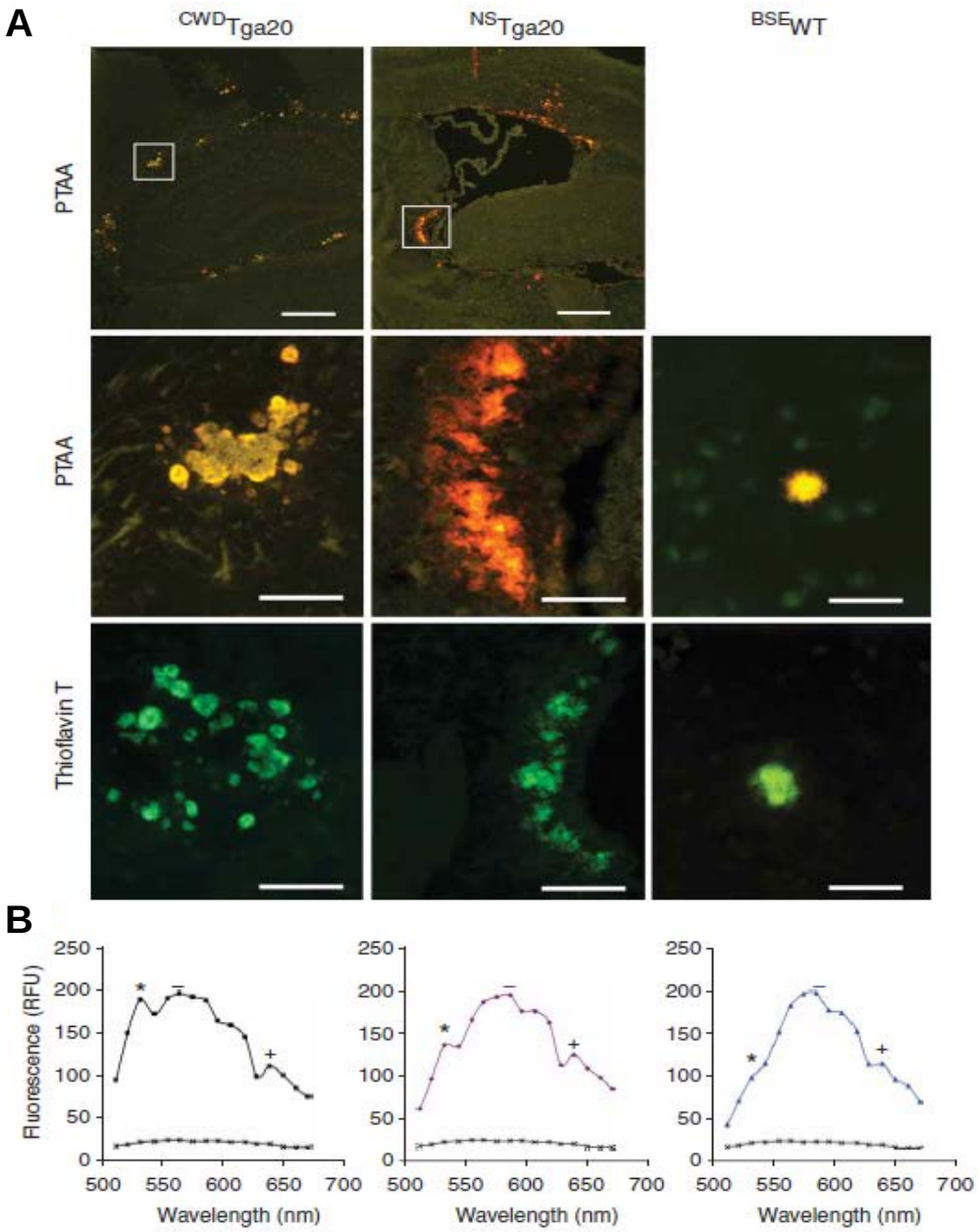

Figure 5: PTAA and thioflavin T staining of PrP deposits in prion-infected brain cryosections. Adapted from (Sigurdson et al., 2007)

(**A**) Images showing PTAA and thioflavin T bound to PrP aggregates from ^{CWD}tga20, ^{NS}tga20 and some ^{BSE}WT. To show the localization and the selective staining of the PrP aggregates, low and high magnifications of the boxed regions are shown for ^{CWD}tga20 and ^{NS}tga20.

(**B**) Spectra of PTAA bound to ^{CWD}tga20 (black), ^{NS}tga20 (purple) and ^{BSE}WT (blue) deposits. –, Emax; *, E532 nm; +, E639 nm. Background signal, black line. Scale bars, 500 μm (A; PTAA, top), 50 μm (A; PTAA, middle, and thioflavin T).

The prion organotypic slice culture assay

The prion organotypic slice culture assay (POSCA) (Falsig and Aguzzi, 2008; Falsig et al., 2008) is a novel, flexible and robust experimental system to study prion infection in cultured organotypic cerebellar slices (COCS), which allows for determination of prion infectivity and for studying prion replication *ex vivo* in a complex cellular environment. The POSCA is a versatile research platform that enables various manipulations of the tissue such as depletion or addition of specific cell types or treatment with various compounds. COCS are morphologically relevant as they retain the architecture of the originating brain tissue (e.g.: intercellular connections) while harboring disease-induced changes such as accumulation of aggregated PrP and prion-induced neuronal loss, allowing for the study of the role of different cell types in prion replication and pathogenesis. The operating characteristics of the POSCA are close to the most commonly used prion titration assays: the Scrapie cell end point assay (SCEPA) (Klohn et al., 2003; Falsig and Aguzzi, 2008; Falsig et al., 2008) and the mouse endpoint bioassay (Fischer et al., 1996). Furthermore, *ex vivo* organotypic brain slice cultures can be prepared from mice of any genotype and allow for depletion of specific cell types. This makes it a versatile tool to study the phenomena of strain adaptation and strain propagation (Weissmann, 2004). Multiple passages of a prion strain can be generated in a well-controlled manner in a relative short period of time. In addition the tissue can easily be manipulated and drugs and other compounds can be administrated via the culture medium.

PRION STRAIN TYPING USING LCPs

Prion strain adaptation

Prion strain adaptation is usually observed when an infectious prion isolate is transmitted across different species (Beringue et al., 2008). As an example, when prions obtained from a Scrapie-sick sheep are inoculated (in the form of a brain homogenate) to a cohort of mice, the incubation period is typically long. Successive passages in mice can be performed by transmitting brain homogenates into further generations of mice. As a result, the incubation time shortens and the attack rate and severity of the disease stabilizes, yielding what is referred as a “mouse-adapted prion strain”. Recently, LCPs have been used to reveal discrete structural changes of PrP aggregates upon strain adaptation of cervid prions into mice (Sigurdson et al., 2007) (Figure 6, adapted from (Sigurdson et al., 2007)).

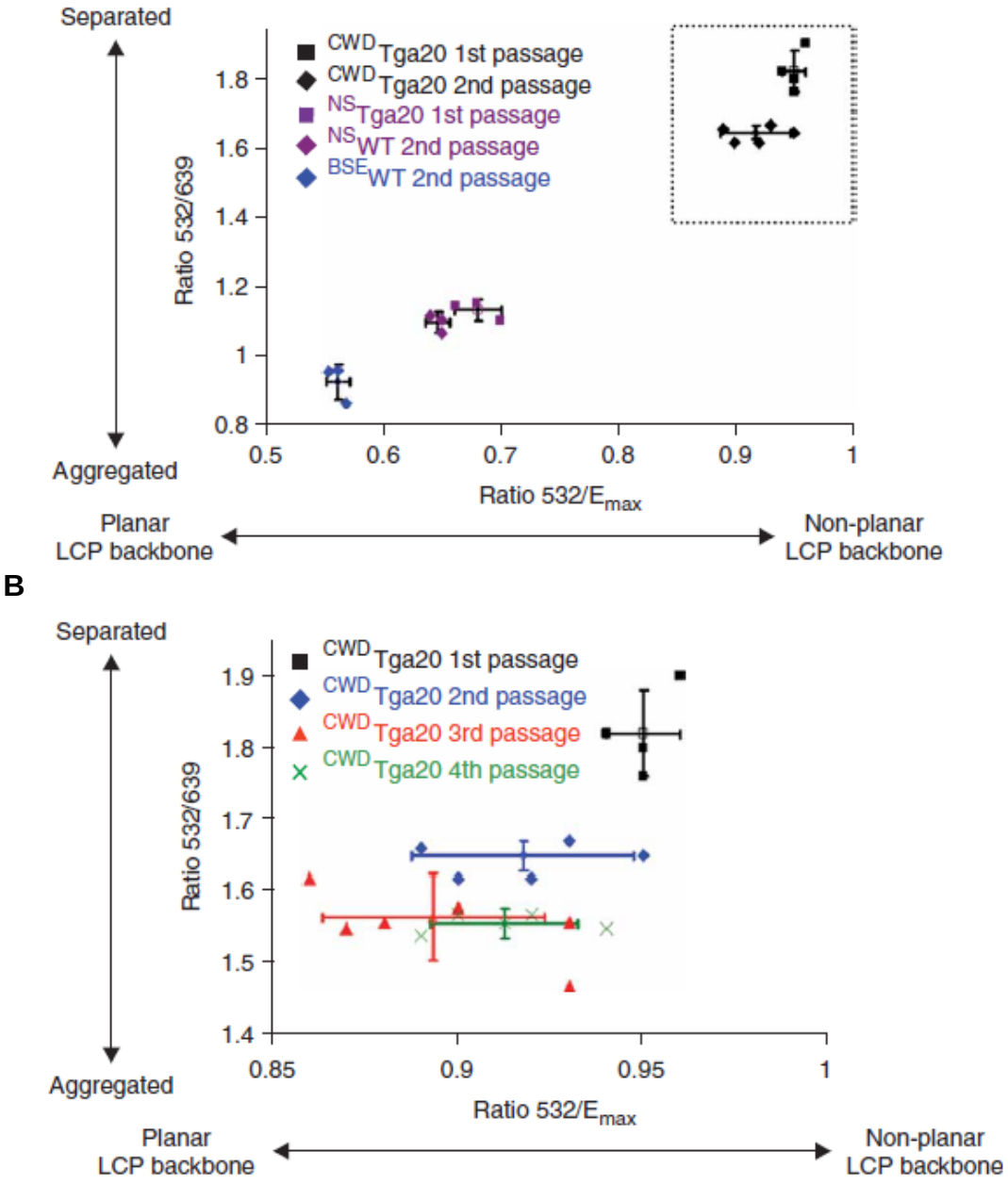

Figure 6: Spectral data of mouse PrP deposits stained with PTAA. Adapted from: (Sigurdson et al., 2007)

(**A**,**B**) Correlation diagram of the ratios of emitted intensities, R532/639 and R532/*E*max, of the intensity of the emitted light from PTAA bound to PrP plaques in individual ^{NS}tga20, ^{CWD}tga20, ^{NS}WT and ^{BSE}WT. The image in (B) is an expansion of the marked region in (A), and depicts four passages of CWD in tga20 mice.

AIM OF THE THESIS

To date no treatment is available for TSEs, which remain invariably lethal diseases. The strong interaction of LCPs with the amyloid scaffold was the rationale for the main focus of my thesis: investigate and characterize the antiprion effects of LCP treatment on COCS and unravel the underlying mechanisms. The first milestone was to establish that LCPs do have an effect on prion accumulation in prion-replicating COCS by using different methods as a read-out. I used quantitative methods such as SCEPA, MPA and ELISA. I also wanted to directly visualize prion aggregates and/or PK-resistant prions by using non- or semi-quantitative methods such as histoblot and Western blot. Finally, another important aspect was to appreciate if the effects of LCPs on prion replication would reduce prion-induced neurotoxicity by using a semi-quantitative method recently developed by my colleague Dr. Jeppe Falsig (neuronal cell death measurement in COCS by quantification of $NeuN^+$ area in a fluorescent microscope). This technique also enabled investigation of the potential toxicity of LCPs to brain cells. The second milestone was to unravel the mechanisms underlying the anti-prion effect of the selected LCP candidate PTAA. I used semi-quantitative methods such as Western blot and conformation-stability assay to investigate proteolysis of PrP in the presence of LCPs. I used quantitative methods such as bioassays in mouse or in cells. Finally I also investigated fibrilization of recombinant PrP (recPrP) in the presence of LCPs in a quantitative manner to elucidate the potential of an LCP to block PrP conversion.

The second part of my thesis focuses on prion strain discrimination in COCS. The goal was to partly reproduce the work of Sigurdson et al. in COCS in order to develop a straightforward method to study phenomena such as prion strain adaptation and prion strain competition in a fast manner.

In the third part of my thesis I describe collaborative work that I performed during my first year of PhD under the supervision of PD Dr. Mathias Heikenwälder. The goal of this work is to investigate peripheral prion pathogenesis of human prions by using a model of transgenic mice lacking B and T cells ($C\gamma^{-/-}RAG2^{-/-}$) which immune system was reconstituted with human embryonic stem cells.

RESULTS

PART I: LCPs INHIBIT PRION PROPAGATION BY STABILIZING PRION AGGREGATES

In the first part of my thesis I describe the antiprion potential of LCPs in prion-infected brain slices and the putative mechanism by which LCPs interfere with prion replication upon reacting with aggregated PrP.

Chronically prion-infected, LCP-treated COCS have variable signal for PK-resistant material on Western blot

I used the cationic and anionic LCPs PBAT and PTAA respectively for preliminary experiments to determine whether LCPs inhibit prion replication in COCS. However, for the further characterization of LCP treatment of COCS I focused on PTAA as this molecule was available in suitable amounts. COCS were prepared from 11 days-old PrP^{C}-overexpressing *tg*a20 pups, infected with RML6 and harvested after 35 or 42 days according to Falsig et al. (Falsig and Aguzzi, 2008; Falsig et al., 2008) with treatment started at 21 DIV (LCPs were added to the culture medium three times per week) (Figure 7).

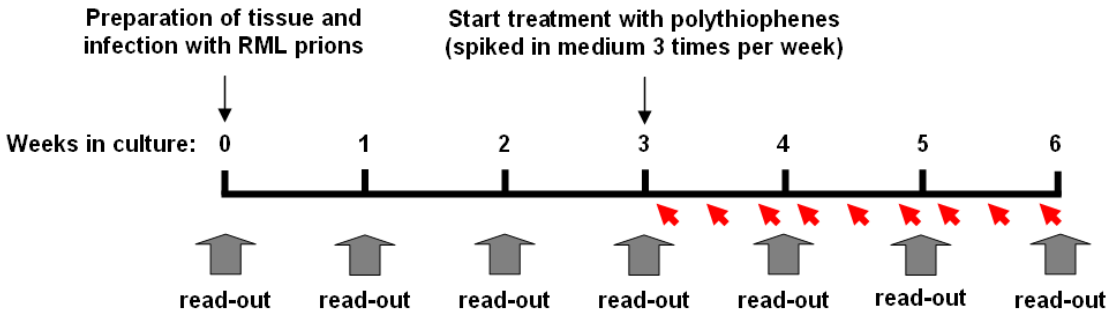

Figure 7: Experimental setup for treatment of prion-infected slice cultures with polythiophenes.

Red arrows: addition of LCPs to the culture medium. Grey arrows: tissue can be analyzed at various time points.

For clarity I refer to brain homogenate obtained from COCS as COCSBH. The presence of PrP^{Sc} in COCSBH was analysed by controlling for PK-resistant material on a Western blot (WB) (Figures 8A, lane 4). After PK digestion, prion-infected COCSBH yielded PK-resistant material migrating as three bands with molecular sizes between 18-27 kDa. In some cases, as in normal BH, additional bands can be observed between 37 and 75 kDa and are referred as "higher order aggregates", although their appearance on the nitrocellulose membrane is

generally of a weaker intensity. My first attempt to treat chronically-infected slices with PBAT and PTAA yielded a surprising result: treated cultures had increased PK-resistant material on WB (Figure 8A, lane 6 and Figure 9A, lanes 6-9). In addition, I observed an increased amount of higher-order aggregates. Immunoblots of non-digested COCSBH show that treatment with PBAT does not affect PrP^C levels (Figure 8B, lane 8) in accordance with the experiment conducted in N2a-PK1 cells by C. Julius and K.P.R. Nilsson (see discussion).

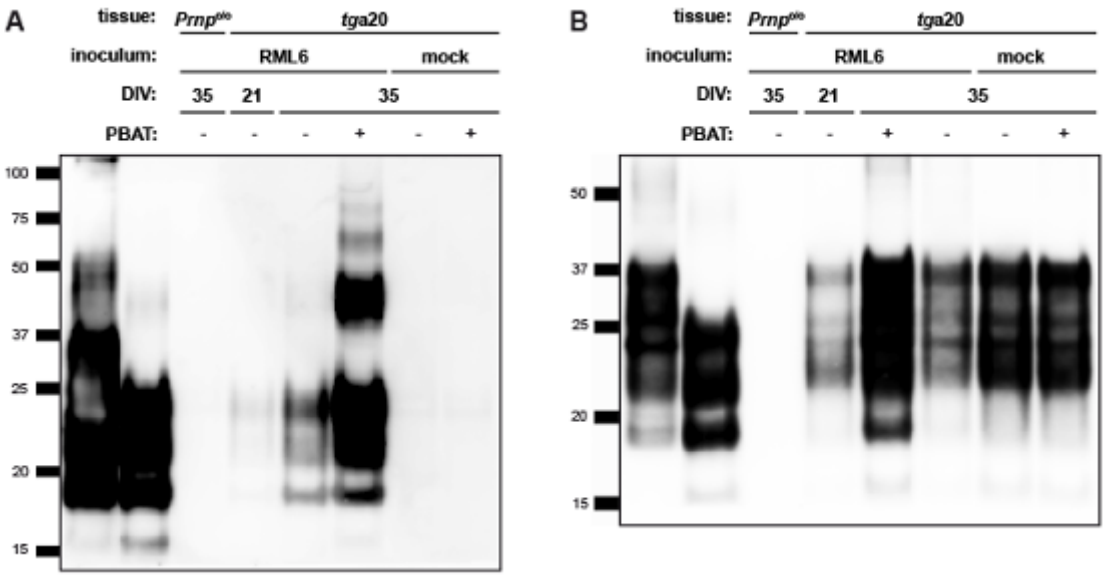

Figure 8: PBAT-treated slice culture homogenates have increased signal for PK-resistant material on Western blot.

(**A**) Immunoblot of PK-digested slice culture homogenates harvested after 21 or 35 DIV, untreated (PBAT -) or treated with 10 μg/ml PBAT (PBAT +).

(**B**) Immunoblot of samples shown in (A), undigested. On lane 1 in (A) and (B) 2 μg undigested RML6 BH was loaded. On lane 2 in (A) and (B) 20 μg PK-digested RML6 BH was loaded. In all other lanes 20 μg total protein from slice culture homogenates was loaded. Mock: slice culture homogenates from *tg*a20 slices exposed to non-infectious BH from a CD1 mouse. This experiment was repeated twice. The anti-PrP antibody POM1 was used for the detection. Molecular sizes are indicated in kDa.

Figure 9, in which all cultures were harvested at 35 DPI, shows the dose-dependent effect of PTAA. Surprisingly, high-dose PTAA treatment (60 μg/ml) (Figure 9, lane 5) lowered the signal for PK-resistant material.

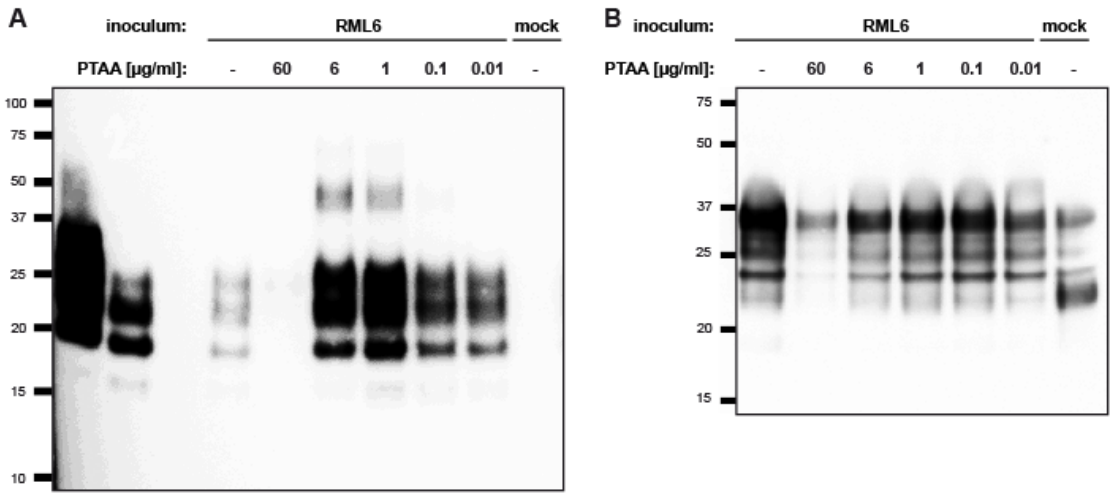

Figure 9: PTAA-treated COCSBH have modified signal for PK-resistant material on immunoblot.

(**A**) Immunoblot of a titration of PTAA for treatment of prion-replicating slice cultures. COCSBH harvested after 35 DIV, untreated (PTAA -) or treated with various dilutions of PTAA were digested with PK. 2 µg undigested RML6 BH was loaded in lane 1 and 20 µg PK-digested RML6 BH was loaded in lane 2. In all other lanes 20 µg total protein from COCSBH was loaded.

(**B**) Immunoblot of samples shown in (A), undigested. The anti-PrP antibody POM1 was used for the detection. Molecular sizes are indicated in kDa.

As the correlation of PK-resistant material with other markers for prion load (e.g. prion infectivity, presence of PK-sensitive prion aggregates) is not clear, I sought to determine the prion content of PTAA-treated slices with other methods. For this purpose, I repeated the titration experiment shown in Figure 9 in biological triplicates, including prion-infected cultures treated with pentosan polysulfate (PPS) as a control for reduction of prion accumulation. I chose to use PPS because its anti-prion effect is widely recognized and because my colleague Dr Falsig used it to develop the POSCA. I extended the culturing period to a total of six weeks and included prion-infected cultures that were harvested at 21 DPI. Immunoblots from one series of these replicas is shown in Figure 10. This experiment reproduces well the results shown in Figure 9. Treatment with PPS resulted in a signal for PK-resistant material that lies between that of untreated slices harvested at 21 or 42 DPI. Immunoblots from the other two series of biological replicas revealed identical patterns of PK-resistant material (not shown).

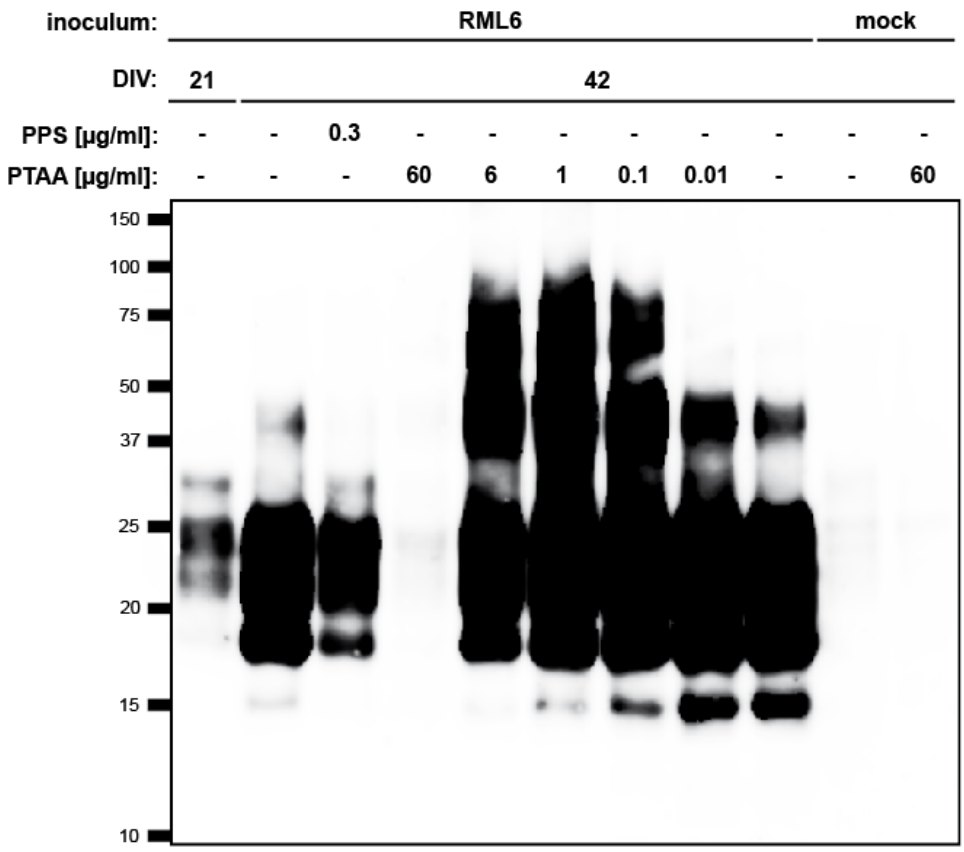

Figure 10: Immunoblot of a series of biological triplicates of prion-replicating COCS treated with a titration of PTAA.

20 µg total protein from COCSBH harvested after 21 or 42 DIV, untreated (PTAA -) or treated with PPS (PPS: 0.3 µg/ml) or with various dilutions of PTAA were digested with PK. The anti-PrP antibody POM1 was used for the detection. Molecular sizes are indicated in kDa.

Chronically prion-infected, PTAA-treated COCS have lower prion infectivity titre

In collaboration with Carlo Suter, I used the SCEPA to measure prion infectivity titres of biological triplicates (Figure 11). The average infectious titre of prion-infected, untreated COCSBH ranges from 5.66 for tissue harvested at 21 DIV to 7.38 $\log ID_{50}$ for tissue harvested at 42 DIV. Treatment with PPS or with 6 to 60 µg/ml PTAA significantly decreased prion infectivity (respectively $p = 0.012$, $p = 0.001$ and $p < 0.001$, Table 1). Notably, treatment with 60 µg/ml PTAA brought infectivity titres of COCSBH below those of samples harvested at 21 DIV. COCSBH from cultures treated with 0.01 µg/ml PTAA were excluded from the statistical analysis for mathematical reasons.

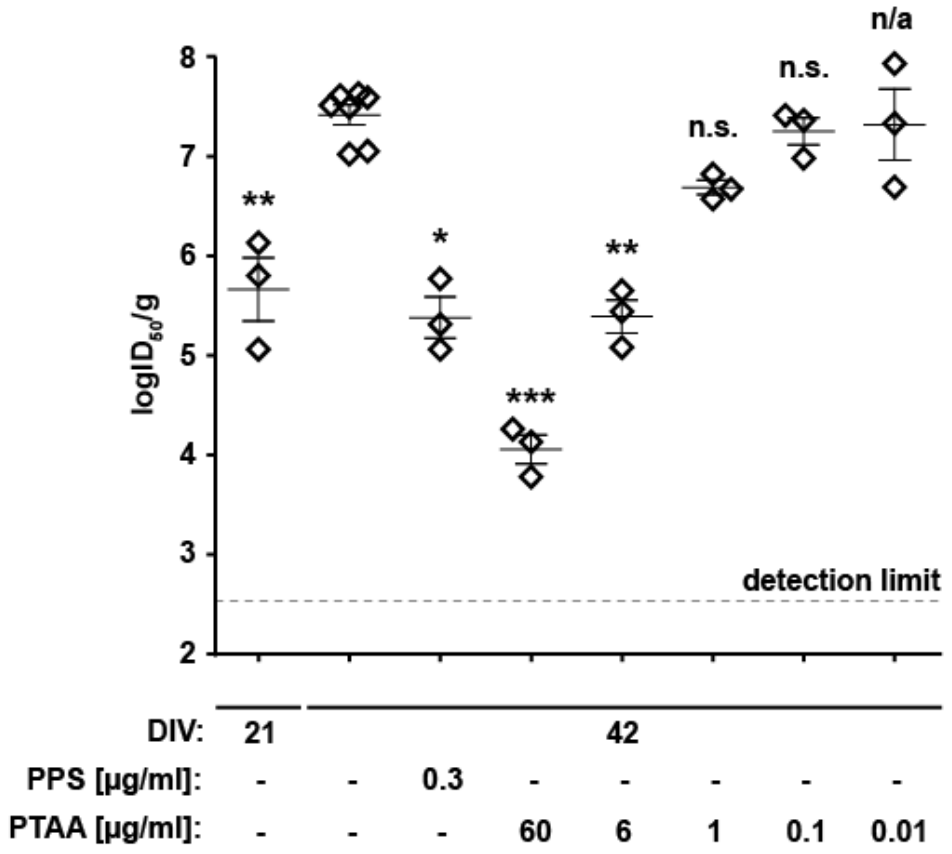

Figure 11: PTAA treatment decreases prion infectivity of COCS in a dose-dependent manner.

Prion infectivity titres of biological triplicates of COCSBH from COCS untreated or treated with PPS or PTAA were determined in the SCEPA. Infectivity titres of uninfected cultures harvested after 21 or 42 DIV are shown for comparison. Each diamond represents the infectivity titre of a COCSBH determined by serial tenfold dilution from 10^{-4} to 10^{-8} on a 96-well plate. Error bars represent the mean ± SEM of biological triplicates. P-values represent ID_{50} difference to control and are shown in Table 1. ***: $p < 0.001$. **: $p < 0.01$. *: $p < 0.05$. Detection limit: Theoretical titer based on the observation of false positives at concentrations between 10^{-2} and 10^{-3} of non-infectious inoculum (CD1). n.s.: non significant. n/a: these results were not included into the statistical analysis. Part of the SCEPA analysis was performed by Carlo Suter.

Chronically prion-infected, PTAA-treated COCS have lower reactivity with prion-specific binding peptoids

To further investigate prion accumulation in our cultures, I quantitatively determined prion load in COCSBH by using the misfolded protein assay (MPA) (Lau et al., 2007; Kranich et al., 2010; Polymenidou et al., 2011) (Figure 12). The MPA is a novel assay that enables sensitive and quantitative detection of prion aggregates without the use of PK. Paramagnetic beads coated with prion-specific binding peptoids are used to specifically capture prion aggregates, whereas monomeric PrP is not captured. After elution of PrP from the beads it is detected by a standard ELISA using the PrP-specific antibody POM19. Treatment of cultures

with PPS as well as with PTAA concentrations ranging from 0.1 to 60 µg/ml significantly decreased the signal in the MPA. Thus, this analysis further indicates that treatment with PTAA brings prion content of COCS below that of untreated tissue.

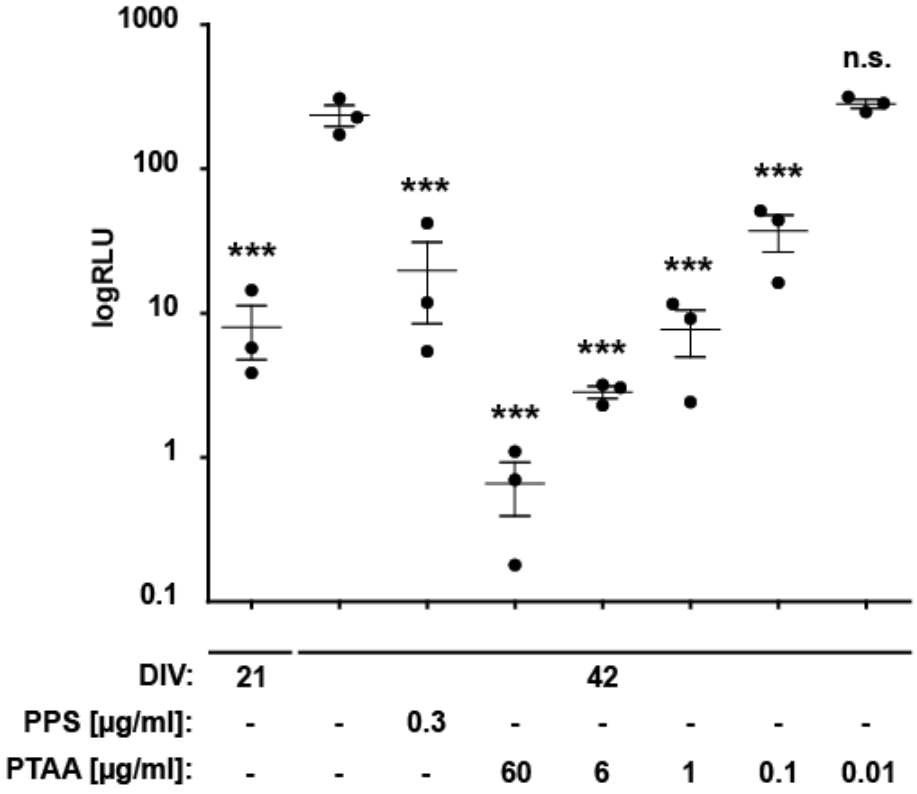

Figure 12: PTAA treatment decreases reactivity with prion-specific binding peptoids of COCSBH in a dose-dependent manner.

MPA of COCSBH shown in Figure 10. Each dot represents the average value of technical triplicates for one COCSBH. Error bars represent the mean ± SEM of biological triplicates. All data were corrected for the negative control (CD1 BH) and represented as relative light units (RLU). P-values represent difference to control and are shown in Table 2. ***: $p < 0.001$. n.s.: not significant.

To exclude the possibility that accumulation of PTAA in COCS could interfere with my methods I quantified fluorescence from COCSBH. I generated a standard curve by spiking PTAA into CD1 or RML6 BH or water and compared fluorescence from PTAA in COCS BH. I found that treatment of cultures with 60 µg/ml PTAA for three weeks resulted in a fluorescent signal in COCSBH that corresponds to less than 15 ng/ml PTAA spiked in brain homogenate (Figure 13). As the treatment of a brain homogenate with 1 µg/ml PTAA had no effect on the signal for RML6 prions in the MPA (see Figure 30), nor on the release of prion infectivity measured in the SCEPA (see Figure 26A) (Margalith et al., 2012), I conclude that PTAA treatment of COCS results in a concentration of PTAA within COCSBH that does not affect my methods.

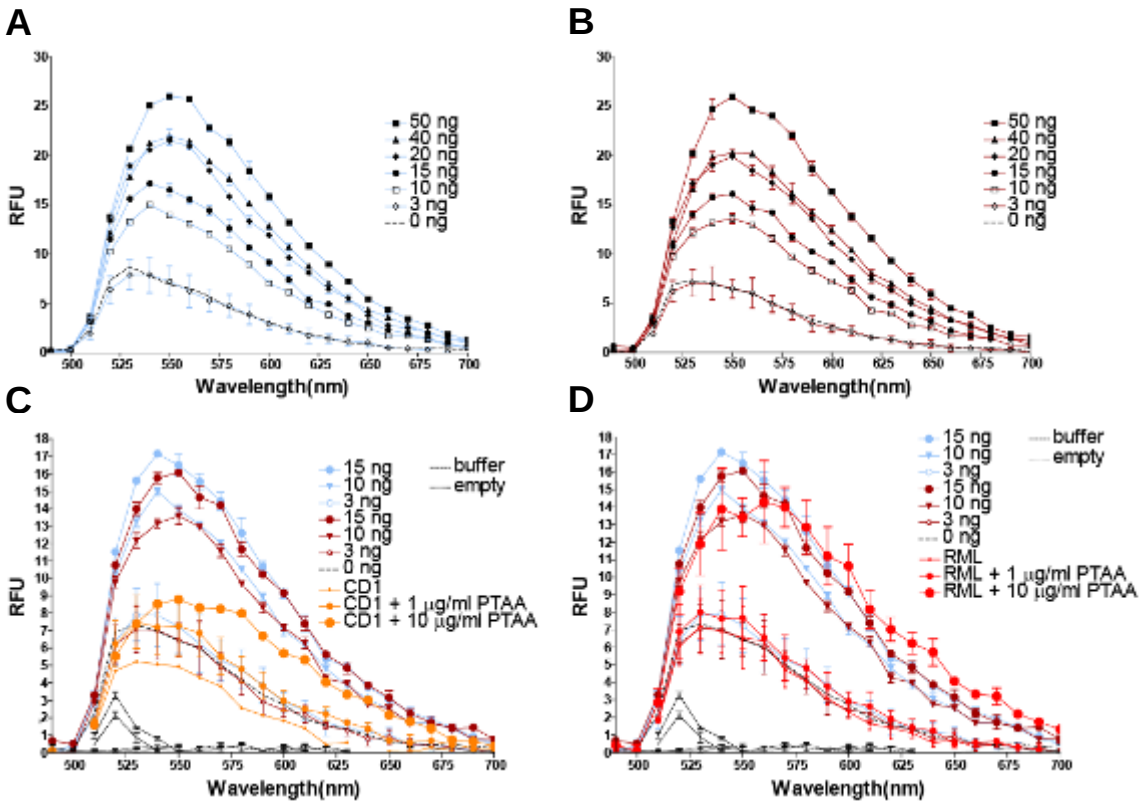

Figure 13: PTAA is present in negligible amounts in COCSBH from PTAA-treated cultures.

Fluorescence of PTAA or vehicle only (water, grey dotted line) spiked in (**A**) CD1 BH, (**B**) RML6 BH, or present in (**C**) COCSBH from PTAA-treated, non-infected cultures (CD1) and (**D**) COCSBH from PTAA-treated, RML6-infected cultures (RML). (C, D) Buffer: PBS. Empty: empty well of a 96-well plate.

Chronically prion-infected, PTAA-treated COCS have less PK-resistant material by ELISA

In order to investigate the discrepancy between the results of immunoblots and SCEPA/MPA, I sought to measure PK-resistant material of COCSBH using an ELISA for PrP. In collaboration with Boris Ballmer I measured PrP epitopes to POM1 in undigested as well as PK-digested COCSBH from the biological triplicates shown in Figures 11 to 12. COCSBH from PTAA-treated cultures had less PK-resistant material than COCSBH from untreated cultures (Figure 14A). No signal for PK-resistant PrP could be detected in COCSBH from cultures treated with 60 µg/ml PTAA. PrP^C levels remained relatively constant (no statistically significant difference) apart in COCSBH from infected tissue treated with 60 µg/ml PTAA where a significant decrease could be observed (Figure 14B) (Table 4).

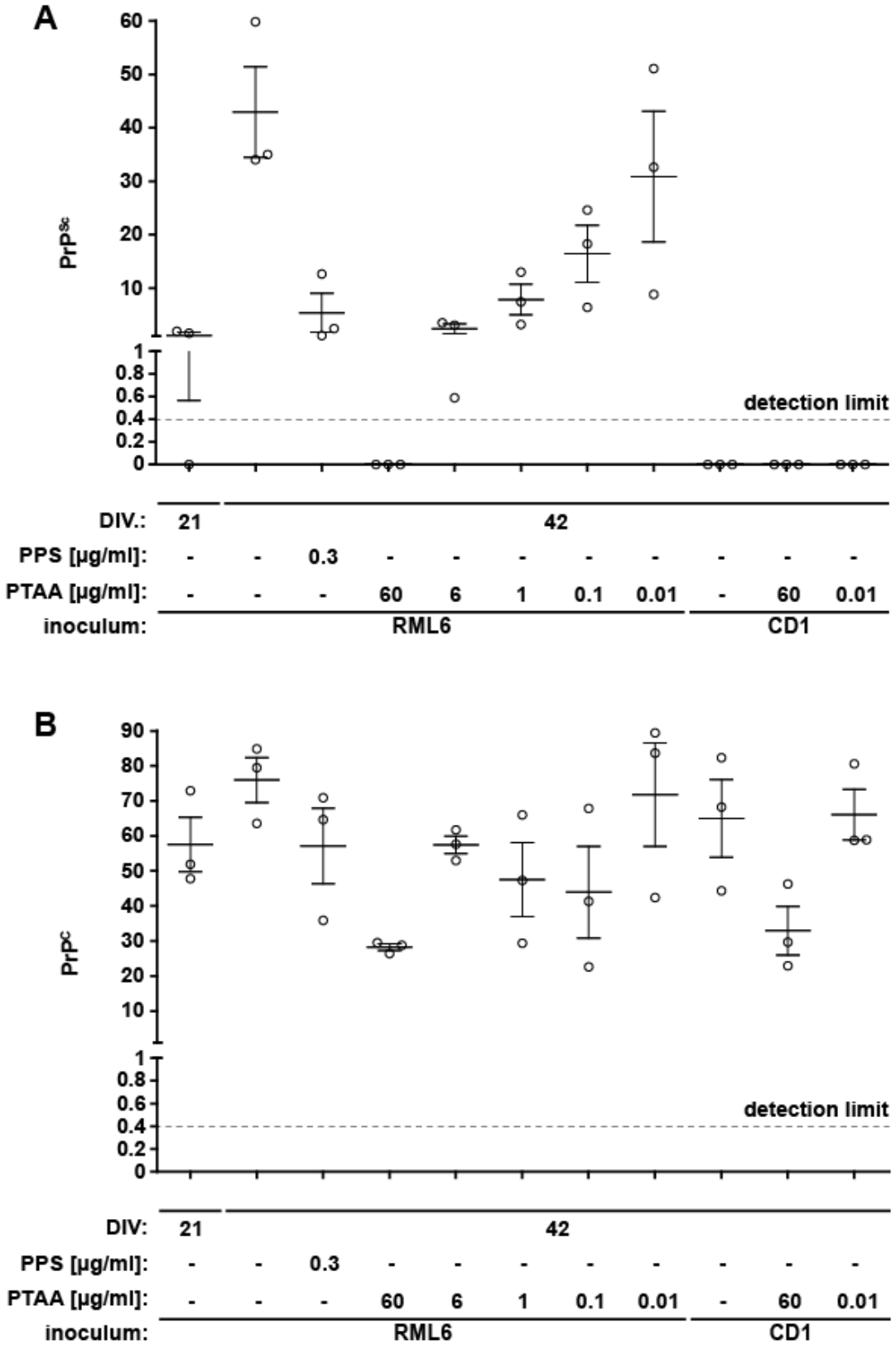

Figure 14: PTAA treatment of COCS decrease PK-resistant material measured by ELISA.

(**A**) PrP^{Sc} levels of COCSBH shown in Figures 9-11, PK-digested. Each dot represents the average value of technical duplicates for one COCSBH. Error bars represent the mean ± SEM of biological triplicates. All data were normalized to protein concentration of the corresponding sample. P-values represent difference to control and are shown in Table 3.

(**B**) PrP^{C} levels of COCSBH shown in (A). P-values represent difference to control and are shown in Table 4. The technical part of the ELISA analysis was performed by Boris Ballmer.

Correlation between MPA, SCEPA and ELISA

In order to validate my methods in the frame of the use of PTAA as an anti-prion compound as well as to convince myself of the anti-prion effect of PTAA I sought to better picture the correlation between data harvested by SCEPA, MPA and ELISA. Figure 15 displays correlation diagrams between for data shown in figures 11 (SCEPA), 12 (MPA) and 14 (ELISA).

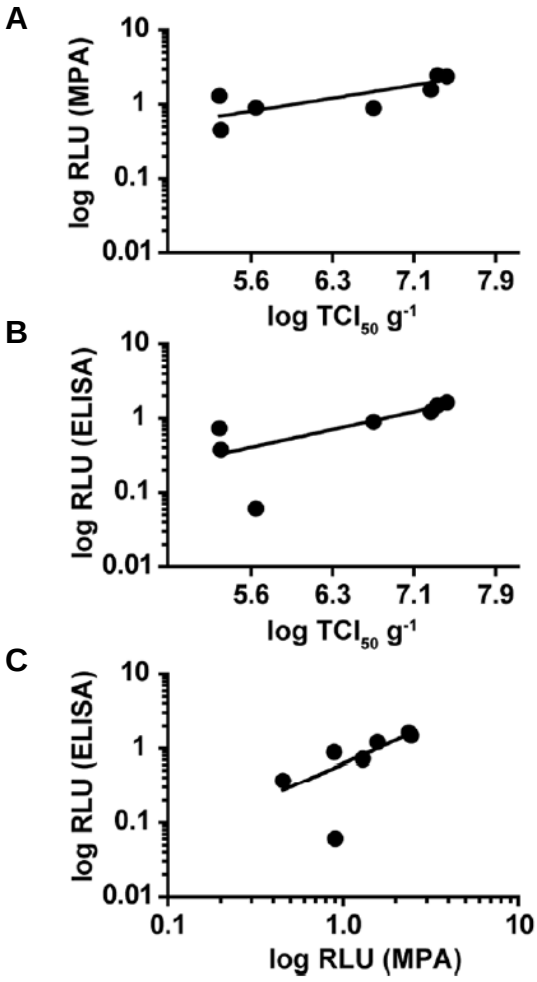

Figure 15: Correlation diagrams for data measured by SCEPA, MPA and ELISA.

(**A**) Correlation diagram to show the relationship between SCEPA and MPA data presented in Figures 11 and 12. (**B**) Correlation diagram to show the relationship between SCEPA and ELISA data presented in Figures 11 and 14. (**C**) Correlation diagram to show the relationship between MPA and ELISA data presented in Figures 12 and 14.

Chronically prion-infected, PTAA-treated COCS have fewer foci of deposition of PK-resistant PrP on histoblots

In order to visualize the areas of deposition of PK-resistant material in COCS I prepared tissue for histoblots. Briefly, tissue was applied onto nitrocellulose membrane which allows for transfer of proteins to the membrane. PK-digestion was performed and PrP epitopes were revealed using an HRP-conjugated anti-PrP antibody (POM1-HRP). Non-infected COCS digested with PK were devoid of PrP epitopes, whereas PrP^{C} was present in non-infected, undigested COCS (Figure 16A). Discrete foci of deposition of PK-resistant material could be seen in RML-infected, PK-digested COCS at 21 DPI and were more abundant at 42 DPI (Figure 16B). Treatment with PPS (300 ng/ml) or with PTAA (0.1 to 100 μg/ml) decreased foci of deposition of PK-resistant material to a level that was comparable to the situation at 21 DPI. Petra Schwartz performed the histoblot analysis.

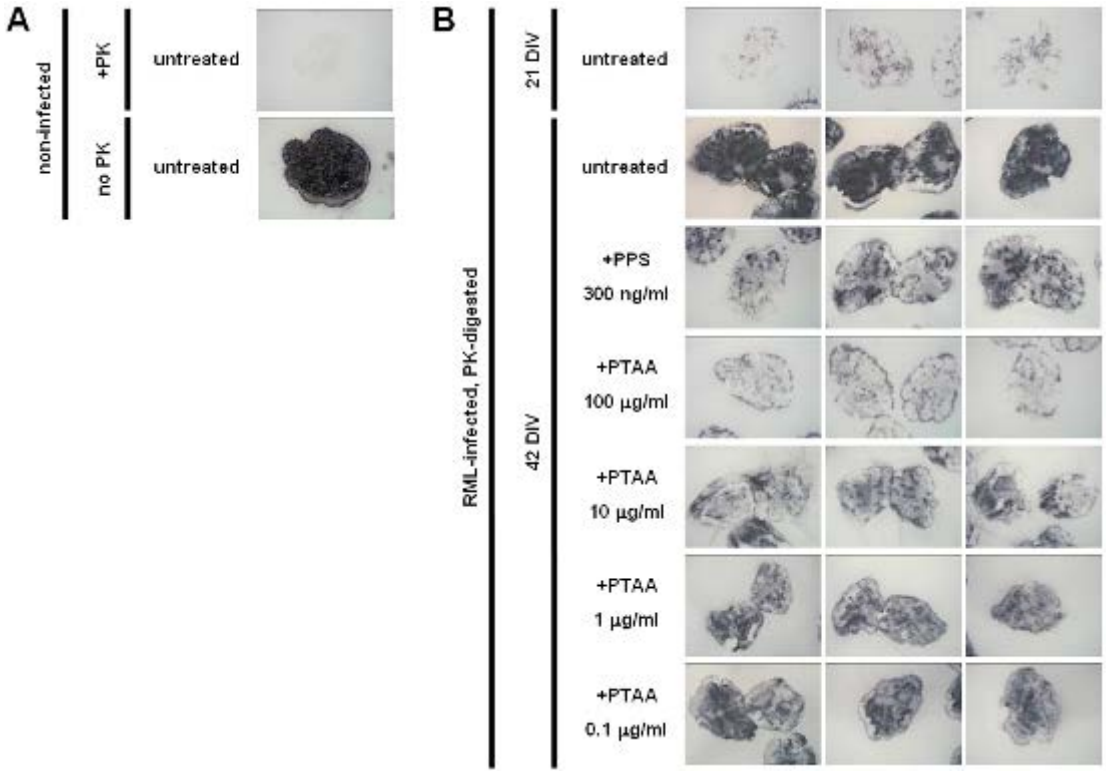

Figure 16: PTAA-treated COCS have fewer foci of deposition of PK-resistant material.

(**A**) Histoblots of non-infected COCS (negative controls).

(**B**) Histoblots of RML-infected COCS treated with PPS or PTAA. Histoblots were performed by Petra Schwartz.

PTAA treatment of chronically prion-infected COCS in a time-course manner

Next I wanted to investigate the effect of PTAA treatment in a time-course manner. I prepared and prion-infected slice cultures in biological duplicates and harvested the tissue at 7, 19, 21, 28, 35 and 42 DIV. In parallel, I performed PTAA treatment (fixed concentration: 10 μg/ml) of cultures by starting the administration of PTAA from day 7, 19, 21, 28 or 35. All cultures were harvested at 42 DPI. Treatment with PTAA started from either time-point resulted in an absence of signal in the MPA (Figure 17A). As PrP aggregates can be detected by the MPA at 7 DPI already in prion-infected COCS, the impossibility to detect them in prion-infected, PTAA-treated COCS may be due to a modification of PrP aggregates by the presence of PTAA.

I then measured PrP epitopes of the samples shown in Figure 17A by ELISA (Figure 17B and C). For this part (Figure 17B and C), additional cultures were prepared later on to obtain a third replica for each time point as well as additional time points (45, 49 and 56 DIV). PK-resistant PrP in untreated COCS could be detected at 21 DIV and increased during the course of the experiment (Figure 17B). Treatment with 10 μg/ml PTAA from day 28 kept the level of PK-resistant PrP at the level of the corresponding time point in untreated tissue, whereas treatment started from day 35 resulted in a decrease of PK-resistant PrP. Thus, PTAA-treated cultures seem to contain equal or lower levels of PK-resistant material than untreated cultures. It cannot be excluded, however, that PTAA treatment induces a modification of PrP aggregates that interferes with my method. PrP^{C} levels of COCS are shown in Figure 17C. PTAA treatment started at either time-point decreased PrP^{C} levels about two fold.

Figure 17 (next page): PTAA inhibits prion accumulation in RML6-infected slice cultures from different time points

(**A**) MPA of homogenates from RML6 infected slices harvested at days 7, 19, 21, 28, 35 and 42 DIV. PTAA was administered at a concentration of 10 μg ml^{-1} at the time of medium change freshly into the medium from days 7, 19, 21, 28 or 35 DIV. Slice cultures were harvested at 42 DIV and analyzed for PrP aggregates. Each dot represents the average value of technical triplicates for one slice culture homogenate. Error bars represent the mean ± SEM of biological duplicates. All data were corrected for non-infectious brain homogenates obtained from CD1 mice as negative control (mock) and represented as the ratio between relative light units (RLU) and protein concentration for each sample. P-values are shown in Table 5. (**B**) Sandwich ELISA of the same homogenates as in (A) analysed for PrP^{Sc}. The data are represented as biological triplicates. The signal for the negative control (mock) is shown as single replica. (**C**) Sandwich ELISA of the same homogenates as in (A) analysed for PrP^{C}. The ELISA was developed by chemiluminescence. The detection limit of 600 pg ml^{-1} (dashed line) was determined as the mean background levels plus three times SD.

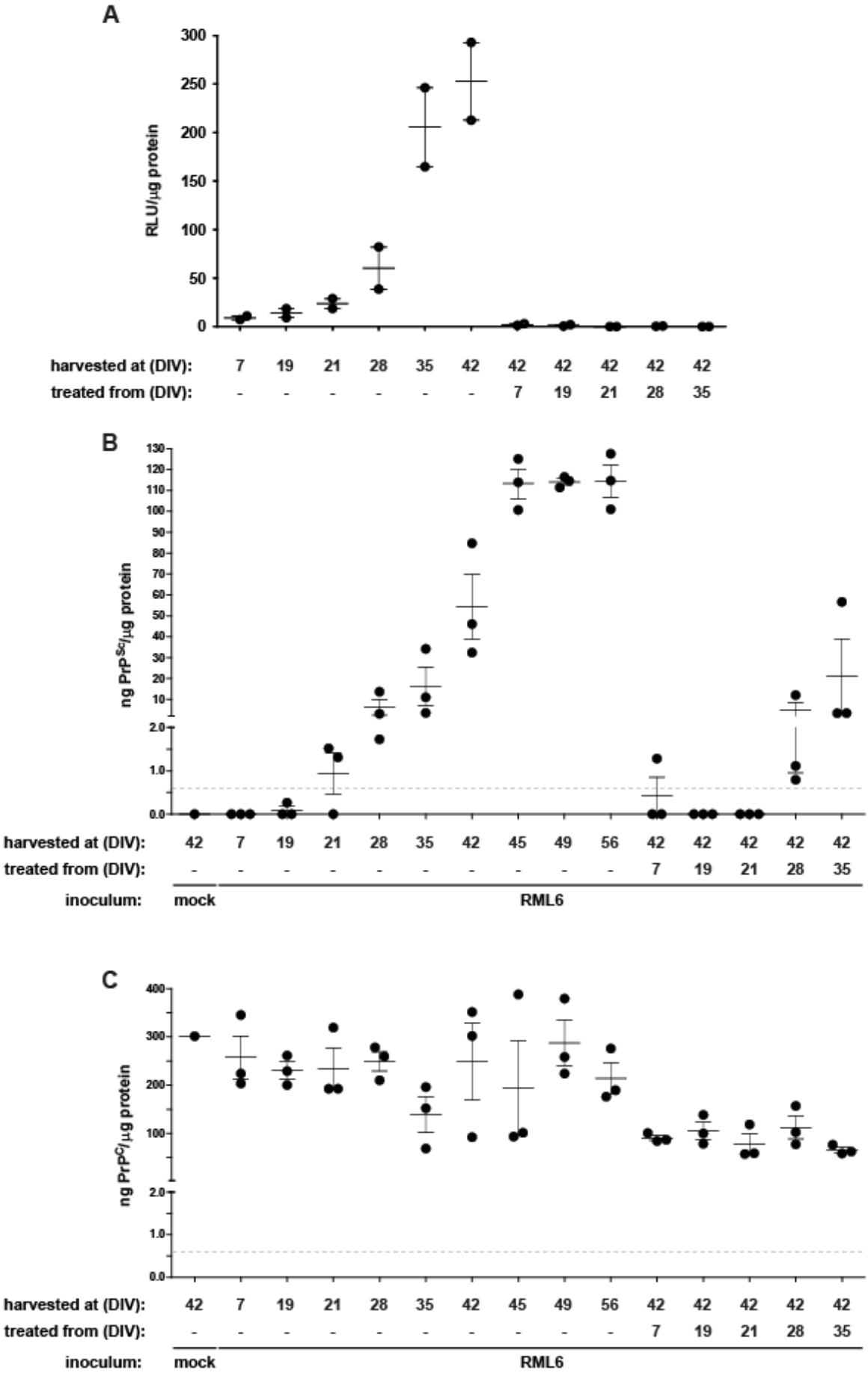
A
RLU/µg protein
300
250
200
150
100
50
0
harvested at (DIV): 7 19 21 28 35 42 42 42 42 42 42
treated from (DIV): - - - - - - 7 19 21 28 35
B
ng PrP^Sc/µg protein
harvested at (DIV): 42 7 19 21 28 35 42 45 49 56 42 42 42 42 42
treated from (DIV): - - - - - - - - - - 7 19 21 28 35
inoculum: mock RML6
C
ng PrP^C/µg protein
harvested at (DIV): 42 7 19 21 28 35 42 45 49 56 42 42 42 42 42
treated from (DIV): - - - - - - - - - - 7 19 21 28 35
inoculum: mock RML6

PTAA treatment rescues prion-induced neurodegeneration of chronically prion-infected COCS

Next, I asked if the inhibitory effect of PTAA on prion accumulation in chronically prion-infected COCS would prevent neurodegeneration. Prion-induced neurodegeneration in brain slices is generally appreciated as a 40-70% loss of cerebellar granule neurons (CGNs) at 42 DPI, which can be quantified upon staining with the antibody NeuN. I recorded the NeuN-positive area in 10 to 30 slices per condition (Figure 18) and observed a marked loss of CGNs in prion-infected COCS as compared to non-infected tissue ($p < 0.001$, $n = 30$). Treatment with PPS or PTAA led to a significant rescue of CGNs in prion-infected COCS ($p < 0.001$, $n = 10$), showing that inhibition of prion replications by PPS or PTAA blocks prion toxicity. In contrast, there was no statistically significant difference between uninfected cultures left untreated or treated with PPS or PTAA (6 and 60 μg/ml).

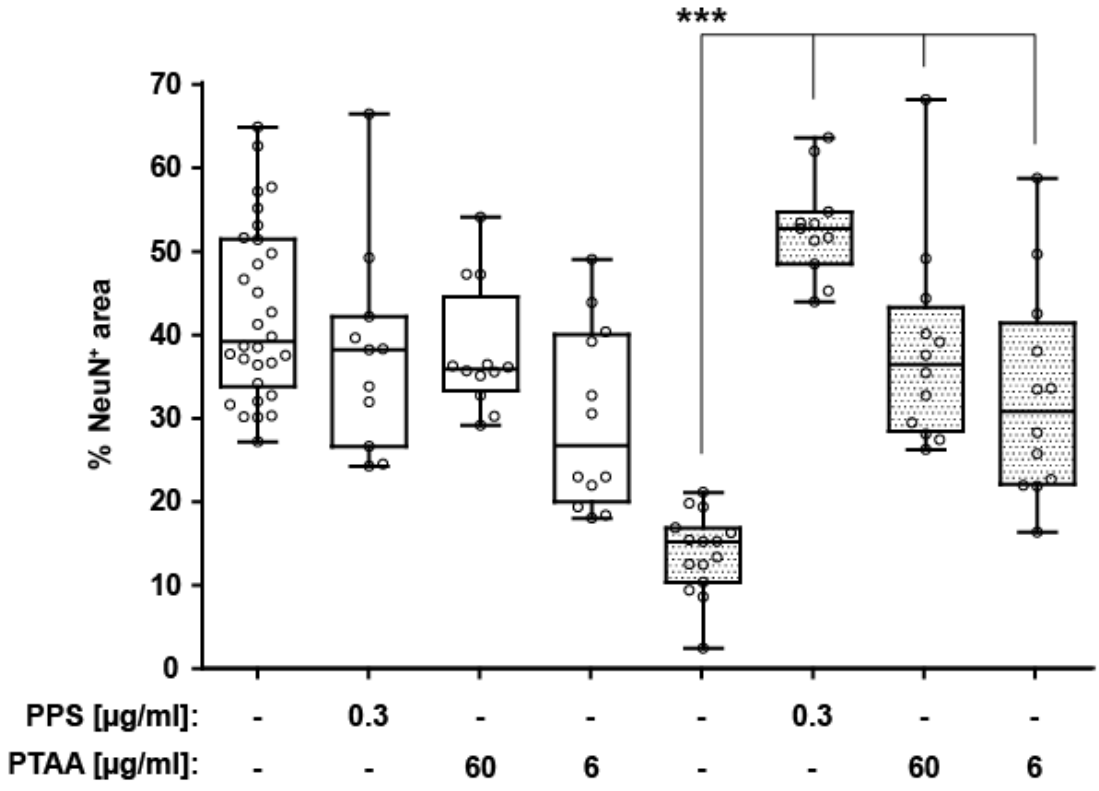

Figure 18: Neurodegeneration is prevented in PTAA-treated slice cultures.

Viability of slice cultures determined by quantification of NeuN+ area in 11 to 30 slices per condition. Empty boxes: COCS exposed to non-infectious BH (CD1). Boxes with pattern: prion-infected COCS. The boundaries of the boxes represent the 25th to 75th percentiles. Whiskers represent the minimal and maximal values. The line in the middle of the box represents the median. Each data point represents one measurement taken on an entire slice. Data was collected from 11 to 30 slices. ***: $p < 0.001$. Statistical analysis is provided in Table 6.

LCPs increase the resistance to proteolysis of RML6 prions

In this part of my work I sought to characterize the effects of LCPs on a prion-containing BH. A comprehensive library of different LCPs with different charged side-chains and/or different length of their thiophene backbone (Figure 4) was used in this study, including the anionic PTAA (Nilsson et al., 2005; Nilsson et al., 2006; Aslund et al., 2007; Nilsson et al., 2007) and its derivatives pHTAA and pFTAA (Aslund et al., 2009); the cationic POMT (Nilsson et al., 2006; Aslund et al., 2007; Nilsson et al., 2007), PTMI (Ho et al., 2002), and PBAT (unpublished); and the zwitterionic POWT (Nilsson and Inganas, 2003; Nilsson et al., 2003; Aslund et al., 2007), and tPOWT (Aslund et al., 2007). As PK-resistant PrP^{Sc} is a surrogate marker for prion diseases that can be observed upon proteolysis of a prion-containing BH, I first tested whether LCPs affect the proteolysis of RML6 prions. Figure 19 shows that incubation of 1% RML6 BH with increasing concentrations of the LCPs ranging from 1 to 900 μg/ml increased the level of PK-resistant PrP^{Sc} on a Western blot in a dose-dependent manner and caused the occurrence of higher-order aggregates.

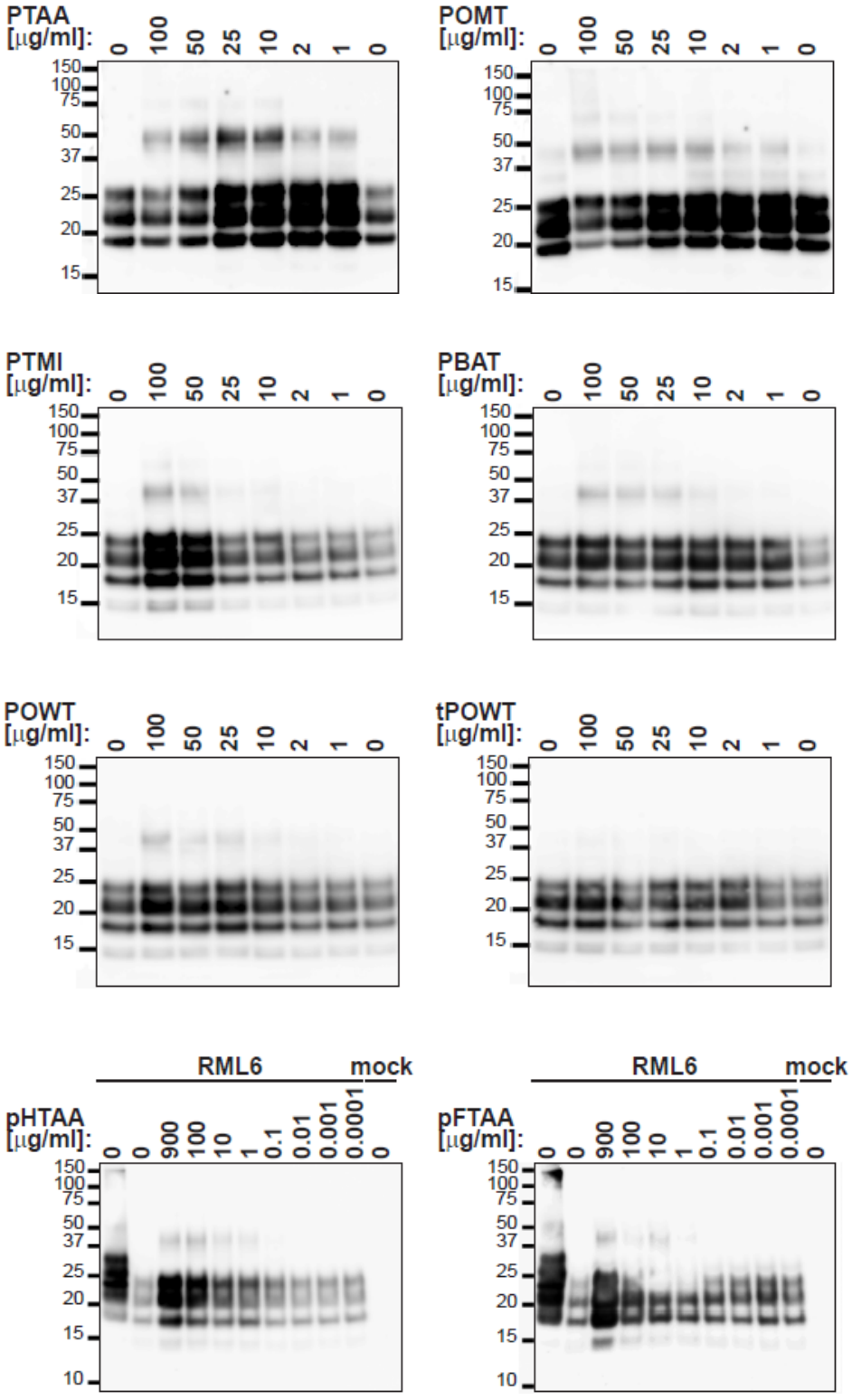

Figure 19: LCPs increase the resistance of PrP^{Sc} to PK digestion and induce the formation of higher order aggregates.

Immunoblots of PK-digested RML6 samples after treatment with increasing concentrations of the different LCPs. On lane 1 in the blots of the pHTAA and pFTAA titrations, 2 µg undigested RML6 BH was loaded. On all other lanes 20 µg PK-digested uninfected (mock) or RML6-infected BH was loaded. This experiment was repeated four times with PTAA, and twice with the other LCPs. The anti-PrP antibody POM1 was used for the detection. Molecular sizes are indicated in kDa.

Next, I wanted to exclude that the addition of PTAA to already PK-digested RML6 prions affects the level of PrP^{Sc}. Figure 20A shows that the addition of PTAA to readily PK-digested RML prions does not change the signal for PrP^{Sc}. Therefore, the increase of the signal for PrP^{Sc} is only obtained by proteolysis of RML prions after they had interacted with PTAA.

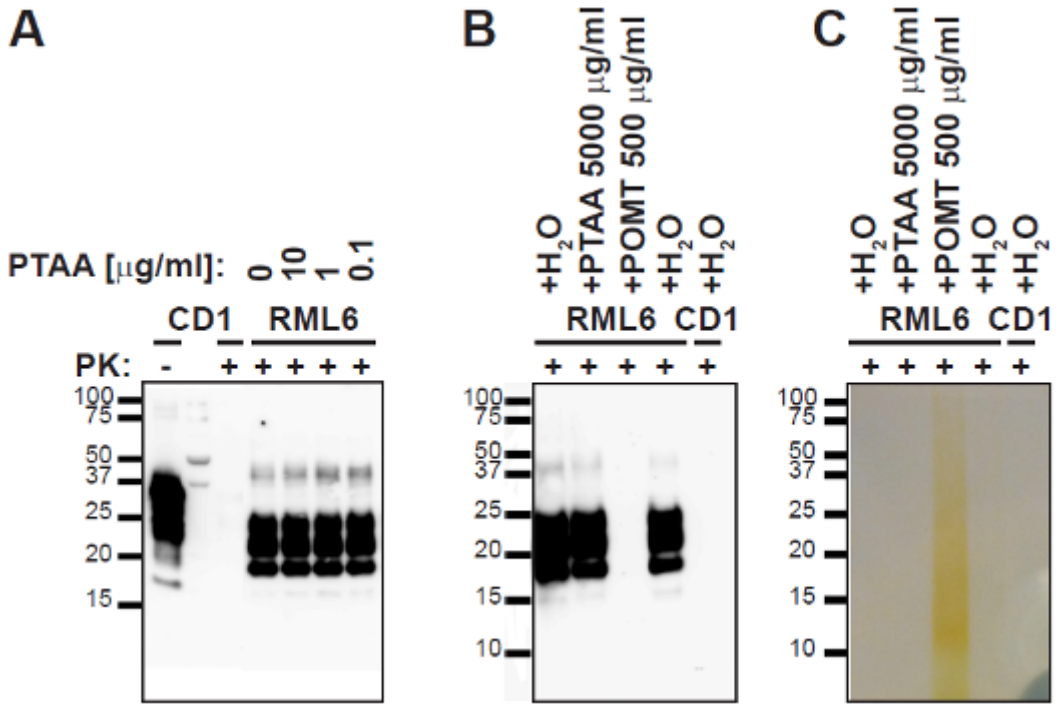

Figure 20: PTAA does not affect PK-digested prions.

Proteolysis of RML before the addition of LCPs. All samples were digested with PK before addition of water or LCP.

(**A**) Lane 1: 2 μg protein from CD1 BH, undigested. Lane 2: marker. Lane 3: 10 μg CD1 BH, digested. Lane 4: 10 μg RML6 BH digested before addition of water. Lanes 5-7: 10 μg RML6 BH digested before addition of PTAA, respectively: 10, 1 and 0.1 μg/ml.

(**B**) Lanes 1-4 contain 20 μg PK-digested protein from RML6 BH mixed either with water (lanes 1 and 4) or PTAA 5000 μg/ml (lane 2) or POMT 500 μg/ml (lane 3). Lane 5 contains 20 μg CD1 BH.

(**C**) Nitrocellulose membrane of blot shown in (B).

If PTAA or POMT were used at the highest concentrations of 50 and 100 μg/ml (Fig. 19, lanes 2 and 3 of upper blots), a decrease of signal was observed. In the case of POMT this was due to the presence of the LCPs on the nitrocellulose membrane which causes a reduction in the immunoreactivity of the anti-PrP antibody POM1. Indeed, 500 μg/ml POMT completely blocked immunoreactivity of POM1 (Figure 20B, lane 3). Protein transfer, however, occurred normally (Figure 21). The decrease of signal in PTAA-treated PrP^{Sc} with the highest doses of

50 and 100 μg/ml cannot be attributed to a similar artefact as with POMT because fewer or no PTAA binds to the membrane (Figure 20C, lane 2) (PTAA is anionic, POMT is cationic).

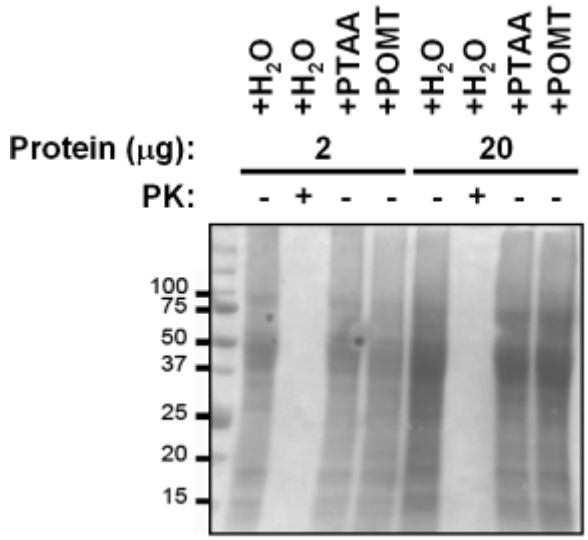

Figure 21: PTAA and POMT do not affect protein transfer.

Ponceau red staining of a nitrocellulose membrane with 2 or 20 μg total protein from CD1 BH, PK-digested (+) or undigested (-), in the absence (+H_2O) or presence of LCPs.

Incubation of RML6 with PBAT and POWT affected only weakly the relative signal for PrP^{Sc} but still caused the formation of higher order aggregates. Longer exposures of the blots revealed that the higher order aggregates are present for all LCPs, with the exception of tPOWT (Figure 22), which was also the only compound that did not affect the intensity of the signal for PrP^{Sc} (Figure 19).

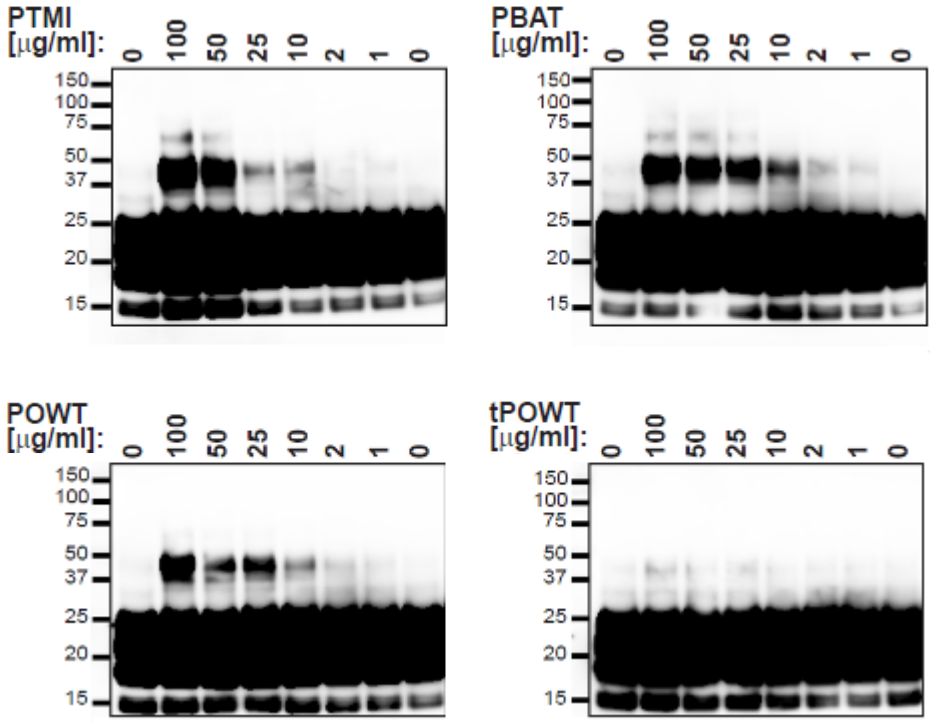

Figure 22: Longer exposures of selected immunoblots from Figure 19 to evidence the appearance of higher-order aggregates in the samples treated with PTMI, PBAT and POWT and their absence in the samples treated with tPOWT.

I also performed, in collaboration with Carlo Suter, a PK digestion with a 40-fold higher concentration of PK on PTAA-treated RML6 and doubled the incubation time for the proteolysis to investigate the efficiency of PTAA on the protection of PrP^{Sc} to protolysis. The signal for untreated PrP^{Sc} was completely abolished under these conditions, PrP^{Sc} in PTAA-treated samples remained detectable even under these harsh conditions (Figure 23), indicating that the LCPs strongly protect the PK-resistant core of PrP^{Sc} against proteolysis.

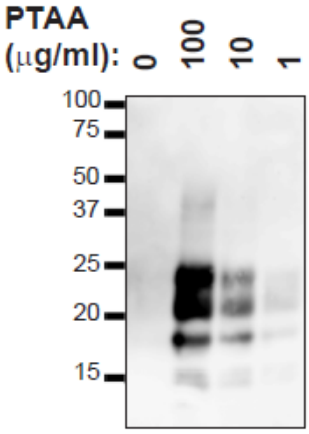

Figure 23: PTAA increases the resistance of PrP^{Sc} to PK digestion.

Immunoblot of PK-digested RML samples incubated with water (lane 1) or with PTAA (lanes 2-4). Each sample is a 45 μg protein aliquot. Proteolysis of all samples was performed with 2 mg/ml PK for 60 min. The anti-PrP antibody POM1 was used for the detection. Molecular sizes are indicated in kDa. This experiment was performed by Carlo Suter.

The finding that the LCPs render PrP^{Sc} more resistant against proteolysis was rather unexpected, because therapeutic compounds usually operate in the way that they increase the sensitivity of PrP^{Sc} to PK digestion. I performed therefore several control experiments with PTAA to exclude that the presence of the LCPs affected the assay. I digested CD1 BH in the absence and presence of PTAA with PK to eliminate that the LCPs interfere with the function of the PK enzyme (Figure 24) and observed no noticeable difference in the efficiency of proteolysis neither for the PTAA-treated nor untreated PrP^{C}.

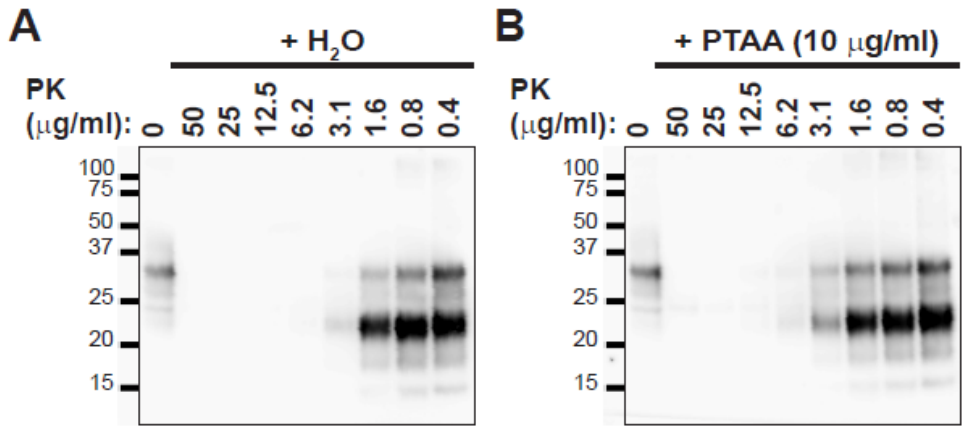

Figure 24: PTAA does not affect the digestion of PrP^{C} by PK.

Proteolysis of PrP^{C} (**A**) in the absence and (**B**) presence of PTAA. Lane 1 of each blot was loaded with 2 μg undigested protein (CD1 BH). Lanes 2-9 were loaded with 20 μg protein (CD1 BH) that was digested with limiting concentrations of PK.

Exposure of RML6 prions with LCPs reduces infectivity titre

In order to evaluate the anti-prion potential of the LCPs on RML6 prions I used the SCEPA to perform a screening of the different LCPs to identify those with the strongest effects on a reduction of the infectivity titer. Figure 25 shows that all LCPs apart from tPOWT (data not shown) significantly reduced the infectivity titre of RML6 prions when used at a concentration of 300 μg/ml. pFTAA was found to be the most efficient compound (Table 7).

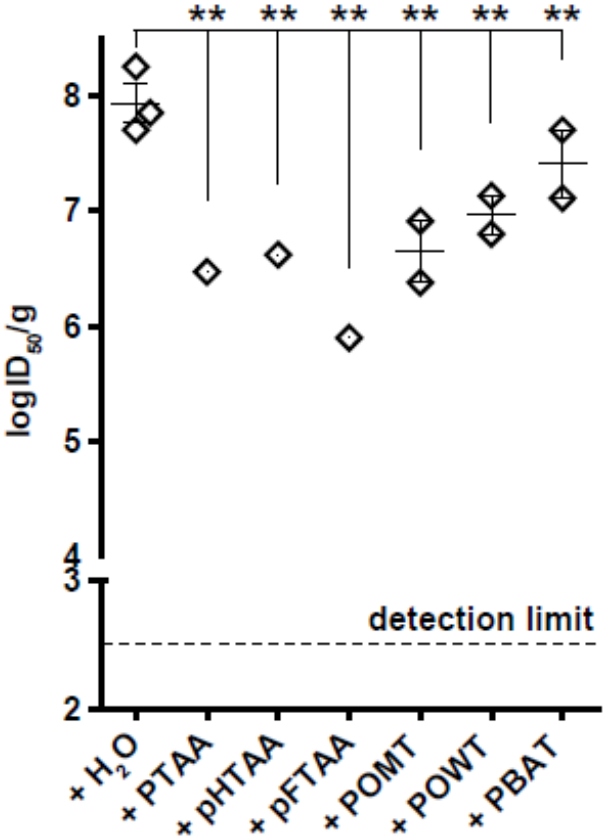

Figure 25: LCPs reduce prion infectivity in the SCEPA

Comparison of the infectivity titres of RML6 after treatment with different LCPs using a concentration of 300 μg/ml. Non-infected (CD1) and RML6-infected BH were incubated with the LCPs and infectivity was determined on 17'000 cells in the SCEPA. Each data point represents one sample determined by serial tenfold dilution steps from 10^{-4} to 10^{-8} on a 96-well plate. Data are shown as mean ± SEM. The ID_{50} represents the number of magnitudes a prion-containing sample has to be diluted in order to decrease its infectious titre by 50%, read as a 50% decrease in positive wells on a 96-well plate. P-values represent statistical difference between LCP-treated and untreated RML BH and were calculated with a Mantel-Haenszel Chi-square test with Bonferroni-Holm correction (Table 7). Detection limit: Theoretical titre based on the observation of false positives at concentrations between 10^{-2} and 10^{-3} of non-infectious inoculum. Part of this analysis was performed by Carlo Suter.

I chose to compare PTAA and its monodisperse derivative pFTAA and studied their effects on the infectivity of RML6 prions in a dose-dependent manner using concentrations ranging between 100-5000 μg/ml for PTAA (Figure 26A) and 75-900 μg/ml for pFTAA (Figure 26B). PTAA reduced the infectious titre of RML6 by 3 logs ID_{50}/g when used at a concentration of 900 μg/ml and completely abolished prion infectivity when RML6 was treated with a concentration of 5000 μg/ml PTAA. The effect of pFTAA on prion infectivity appeared similar to the effect of PTAA given the variability of the SCEPA (+/- 1 logID_{50}/g) (Table 8).

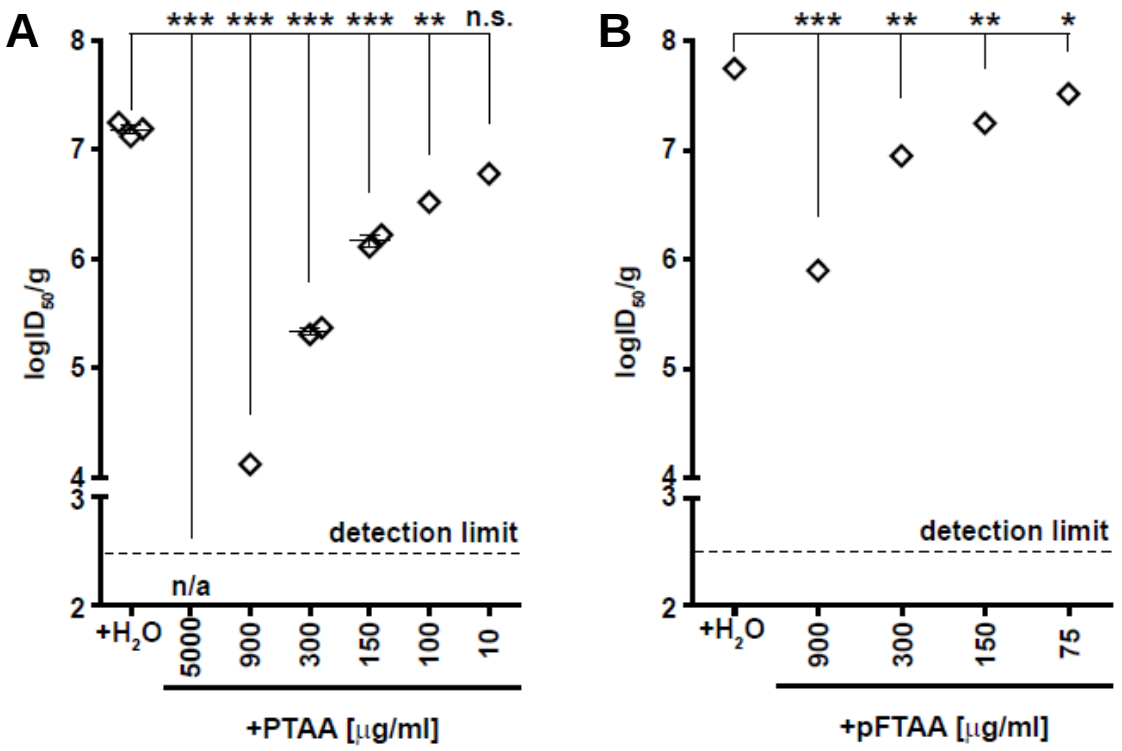

Figure 26: LCPs reduce prion infectivity in the SCEPA

(**A**) Concentration-dependent titration of PTAA.

(**B**) Concentration-dependent titration of pFTAA.

Non-infected (CD1) and RML6-infected BH were incubated with different concentrations of the LCPs as indicated in the Figure and infectivity was determined on 17'000 cells in the SCEPA. Each data point represents one sample determined by serial tenfold dilution steps from 10^{-4} to 10^{-8} on a 96-well plate. Data are shown as mean ± SEM. P-values represent statistical difference between LCP-treated and untreated RML homogenates and were calculated with a Mantel-Haenszel Chi-square test. n/a: no positive wells were observed with this sample between concentrations ranging from 10^{-3} to 10^{-8}. Part of this analysis was performed by Carlo Suter.

Next, I wanted to exclude that the ability of neuroblastoma cells to become infected with prions was affected by the presence of the LCPs themselves. In a first approach (described in Figure 27A) I added a 10-fold excess of RML6 to untreated or PTAA-treated RML6 samples prior to infection of the cells in order to control that the concentration of PTAA present in the infected medium was not affecting the susceptibility of the cells to prions. I observed that the infectivity titres did not significantly differ (Tables 9 and 10), showing that 500 μg/ml PTAA did neither affect the ability of the cells to become infected nor the read-out of the SCEPA. In a second approach (described in Figure 27B) I tested whether the pre-incubation of N2a PK1 cells with PTAA added in the culture medium before infection reduces the susceptibility of the cells to prion infection. For this experiment, I used a PTAA concentration of 10 μg/ml

which corresponds approximately to the amount of PTAA present in the medium used for the infection with the RML6 sample treated with 900 µg/ml shown in Figure 26A. After analysing the data in the SCEPA I obtained $logID_{50}/g$ values that did not significantly differ (Tables 11 and 12), confirming that the susceptibility of PTAA-treated cells to prion infection was not affected.

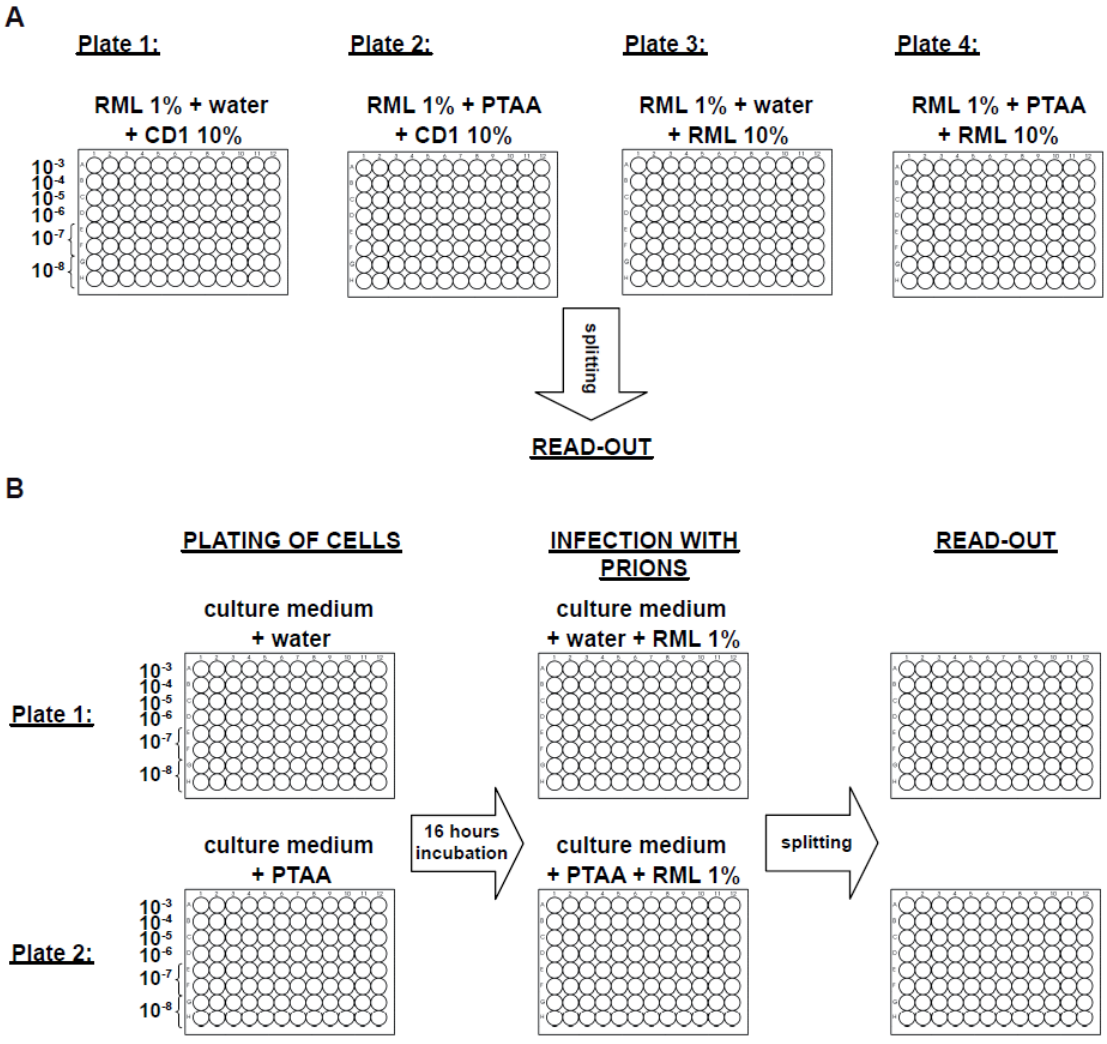

Figure 27: Experimental setup for verification of the susceptibility of PK1-N2a cells to RML6 in the presence of PTAA.

A serial dilution (shown on the left) of each sample indicated in the figure was investigated (results and statistical analysis in Tables 9-12).

(**A**) Each sample was first incubated with water or PTAA before addition of a 10-fold excess of BH, either non-infectious (CD1 BH 10%) or infectious (RML BH 10%). The infectious titre of each sample was then determined according to the normal procedure for SCEPA.

(**B**) Cells were plated either in culture medium (upper) or in culture medium containing PTAA (lower) 16 hours before addition of a prion-infectious inoculum. The infectious titre of all samples was then determined according to the normal procedure for SCEPA. Part of the SCEPA analysis was performed by Carlo Suter.

Finally, I used an MTA assay to exclude the possibility of acute toxicity of PTAA to N2a PK1 cells when spiked in the culture medium (Figure 28). A concentration of 50 μg/ml PTAA in the culture medium (corresponding to the sample treated with 5000 μg/ml PTAA in Figure 26A) did not affect cell viability in this paradigm. Therefore I conclude that LCPs can reliably decrease prion infectivity of RML6 without affecting the sensitivity of the SCEPA.

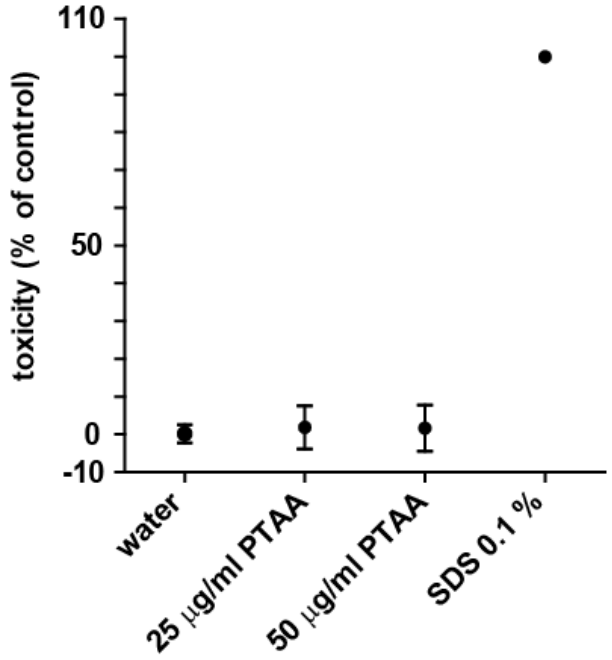

Figure 28: PTAA does not provoke acute toxicity to n2a cells.

MTS assay comparing water-treated and PTAA-treated RML6. Values are indicated as percentage of the negative control (water). The positive control for toxicity is RML6 treated with SDS 0.1 % and is set as 100% toxicity on the graph. The MTA analysis was performed by Carlo Suter.

Bioassay in *tg*a20 mice

Because PTAA-treated RML6 showed a significant reduction in prion infectivity in the SCEPA, I next asked whether PTAA-treated RML6 would also affect the survival time of *tg*a20 mice, a mouse line that overexpresses wild-type PrP about 10-fold (Fischer et al., 1996). Therefore, I intracerebrally inoculated 10-fold serial dilutions of untreated or PTAA-treated RML6 ranging from 10^{-5} to 10^{-8} (dilution of wet brain tissue) into *tg*a20 mice (Figure 29). Mice were observed for clinical signs until they reached the terminal stage of disease. The mean survival time for *tg*a20 mice inoculated with an untreated and a PTAA-treated 10^{-6} dilution of RML6 was 83 ± 0.5 and 88 ± 13.5 days (n= 5), respectively, indicating a slightly prolonged survival time with statistical significance ($p = 0.044$). There was no statistically significant difference between groups of mice inoculated with other concentrations of untreated or PTAA-treated RML.

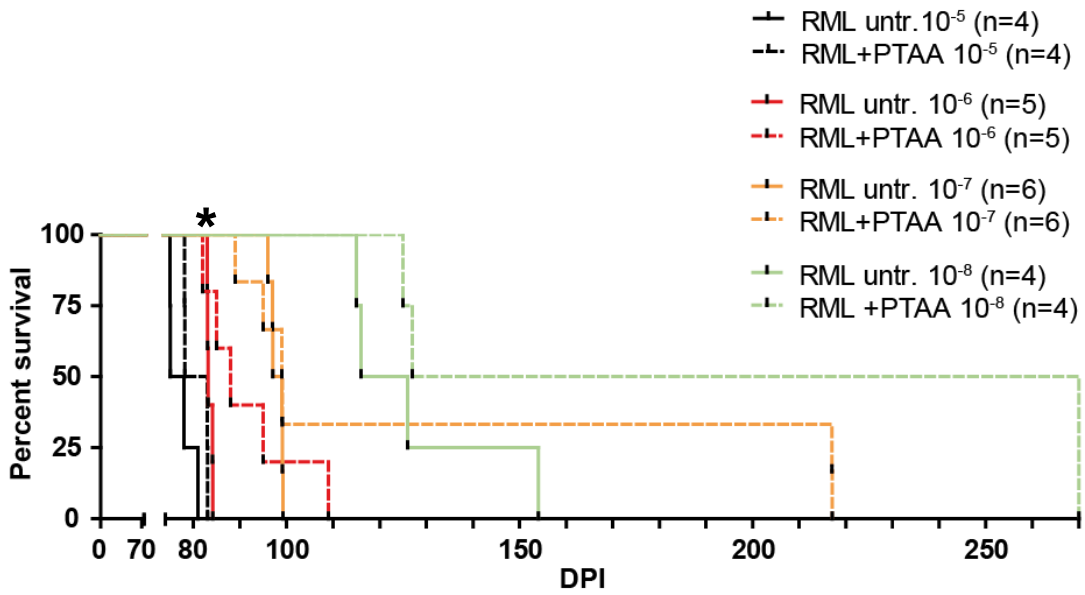

Figure 29: Bioassay in *tg*a20 mice.

A serial 10-fold dilution of untreated or PTAA-treated RML was inoculated into *tg*a20 mice. The curves in red represent the groups inoculated with 10^{-6}-diluted untreated or PTAA-treated RML6. *: p = 0.044. Statistical difference was computed using a Log-rank (Mantel-Cox) test. DPI: days post inoculation.

Reactivity of LCP-treated RML6 prions with prion-specific binding peptoids

Because of my finding that LCPs render PrP^{Sc} more resistant to PK digestion, I decided to use the MPA as a PK-independent tool to further analyse the physical properties of LCP-treated prions. I exposed 1% RML6 BH with different concentrations of the LCPs PTAA, POMT, pHTAA and pFTAA. I chose to focus on PTAA for its availability in large amounts and included POMT because I wanted to investigate a cationic LCP. I also tested the monodisperse versions of PTAA: pHTAA and pFTAA because of their ability to cross the BBB. Figure 30 show that all four compounds affect the number of PrP aggregates in a dose-dependent manner. I observed that the treatment of RML6 with 10 µg/ml of the LCPs PTAA, POMT and pFTAA significantly reduced the signal in the MPA for RML6 prions (p = 0.004, 0.015 and 0.003, respectively, Table 13). PTAA and POMT had the strongest effect at high concentrations of 300 and 100 µg/ml, respectively, whereas pFTAA was found to be more efficient at lower concentrations. Already the treatment with 1 µg/ml pFTAA caused a significant reduction in the MPA signal (p = 0.028). pHTAA appeared to be the less efficient compound (Table 14).

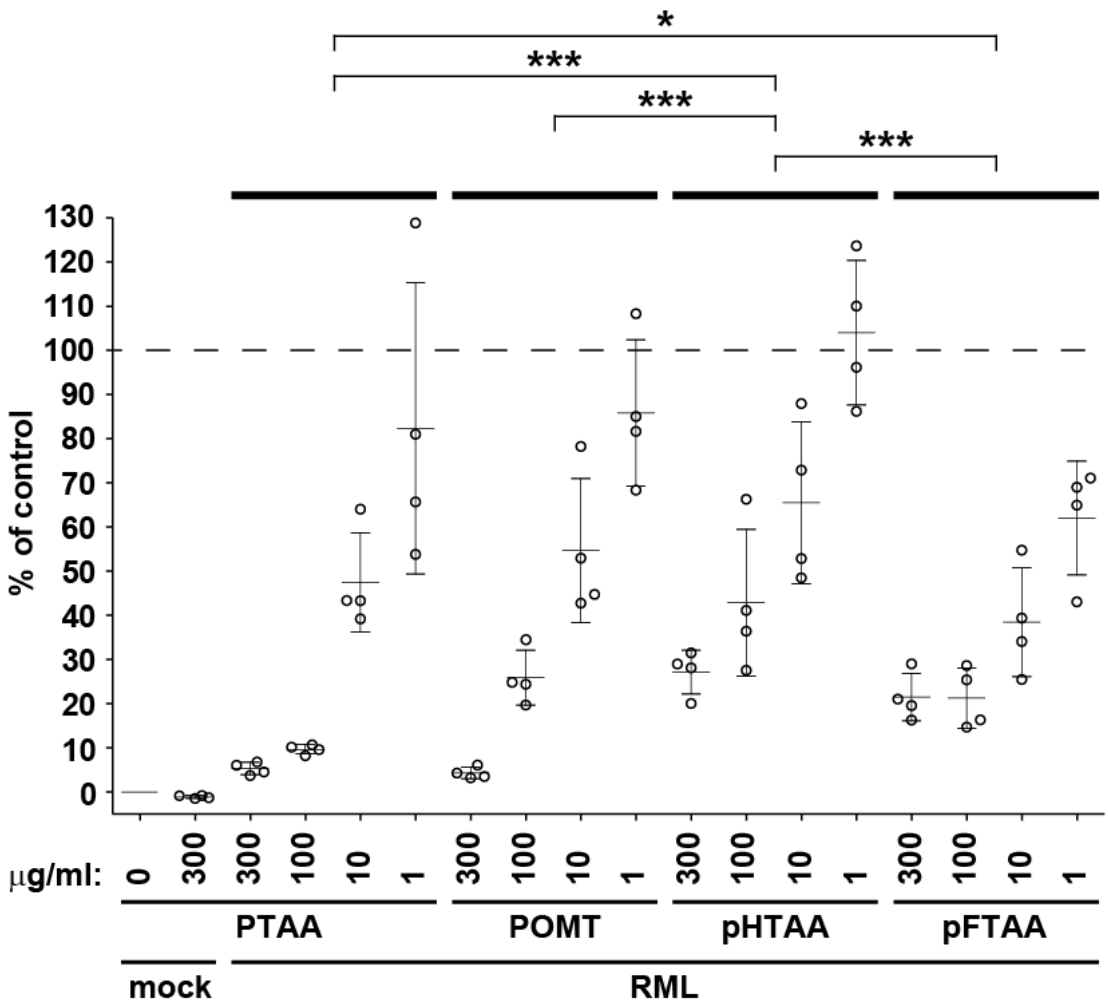

Figure 30: LCPs reduce the signal for prion aggregates in the MPA.

Concentration-dependent titrations of the LCPs PTAA, POMT, pHTAA and pFTAA were performed on RML6 prions and the reactivity with prion-specific binding peptoids was analyzed in the MPA. Each sample was analyzed in technical quadruplicates (circles) and is represented as the mean ± SD. All data were corrected for the negative control (mock: CD1 BH) and represented as relative light units normalized for the control (untreated RML6 BH). Statistical differences were computed to compare LCP-treated RML6 to the control (untreated RML6) (Table 13) or groups of four concentrations of each LCP (Table 14).

In order to verify that the LCPs did not affect the assay by unspecific interaction with the peptoid-coated paramagnetic beads I performed a control experiment in which I incubated the beads with 1 µg/ml PTAA prior to their use. Figure 31 show that pre-treatment of the beads with PTAA had no effect on the capture efficiency of untreated or PTAA-treated RML prions (Table 15). The MPA data show that the LCPs significantly reduce the number of captured aggregates which is in good accordance with the infectivity data obtained in the SCEPA.

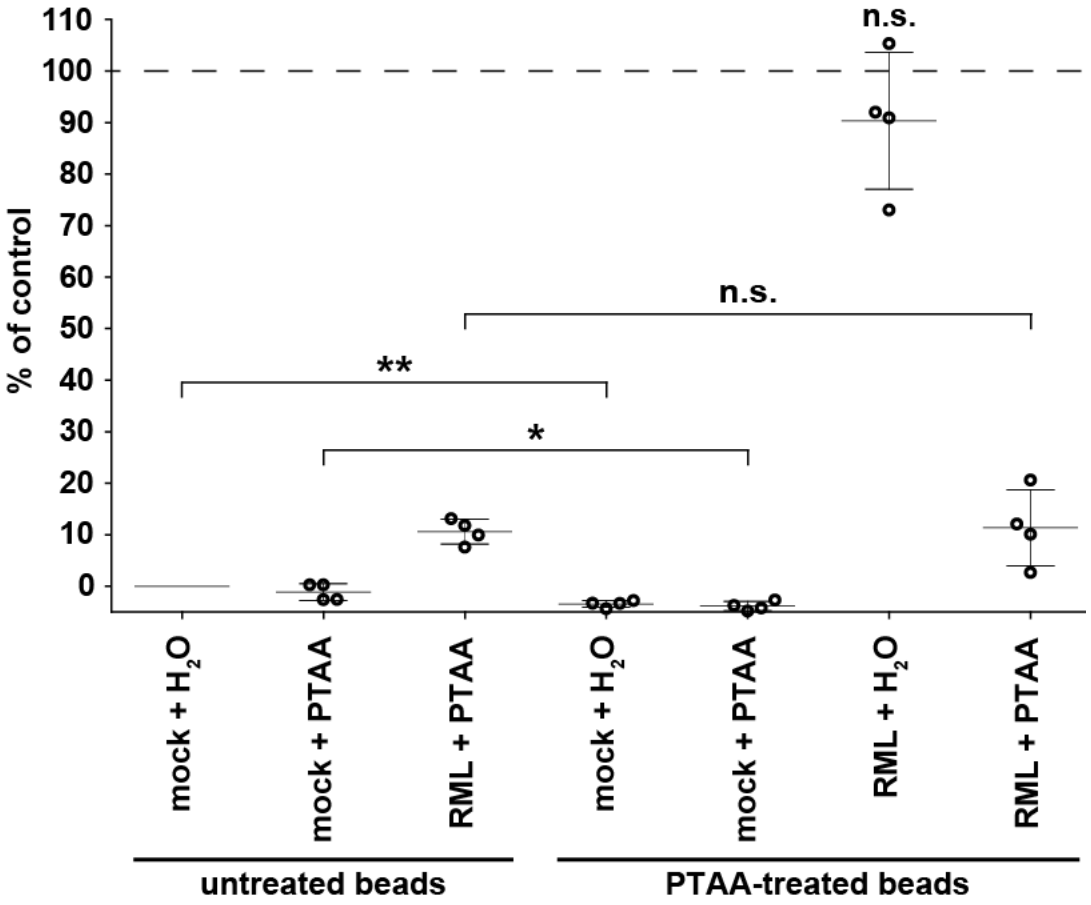

Figure 31: Control experiment for the MPA.

Paramagnetic beads were treated with 100 µg/ml PTAA or left untreated prior to capture of untreated (+H_2O) or PTAA-treated uninfected (mock: CD1 BH) or prion-infected (RML BH) samples. A significant reduction in the signal could be observed for the negative controls (CD1+H2O and CD1+PTAA). This statistical significance can be imputed to the small variability between technical replicas for the samples that yielded low fluorescence, and therefore is to be considered as a statistical artefact.

Conformational stability of PTAA-treated RML prions

I next investigated whether the LCPs change the biochemical properties of RML prions by altering the stability of PTAA-treated RML. I mixed a 1% RML6 BH with two different concentrations of PTAA. Untreated and PTAA-treated RML6 was then incubated with increasing concentrations of GdnHCl for 60 min, digested with PK to remove soluble PrP and analyzed by Western blotting (Thackray et al., 2007). Figure 32 displays that PrP^{Sc} in the untreated samples remained visible even at a concentration of 3 M GdnHCl, whereas in the samples treated with 10 and 100 μg/ml PTAA the signal for PK-resistant material abolished at 2.4 and 2 M GdnHCl, respectively, indicating that PTAA-treated PrP^{Sc} is less stable than untreated PrP^{Sc}. However, the persistence of higher-order aggregates in all samples treated with PTAA suggests that PTAA induces conformational changes of PrP^{Sc} that are not affected by denaturation with GdnHCl.

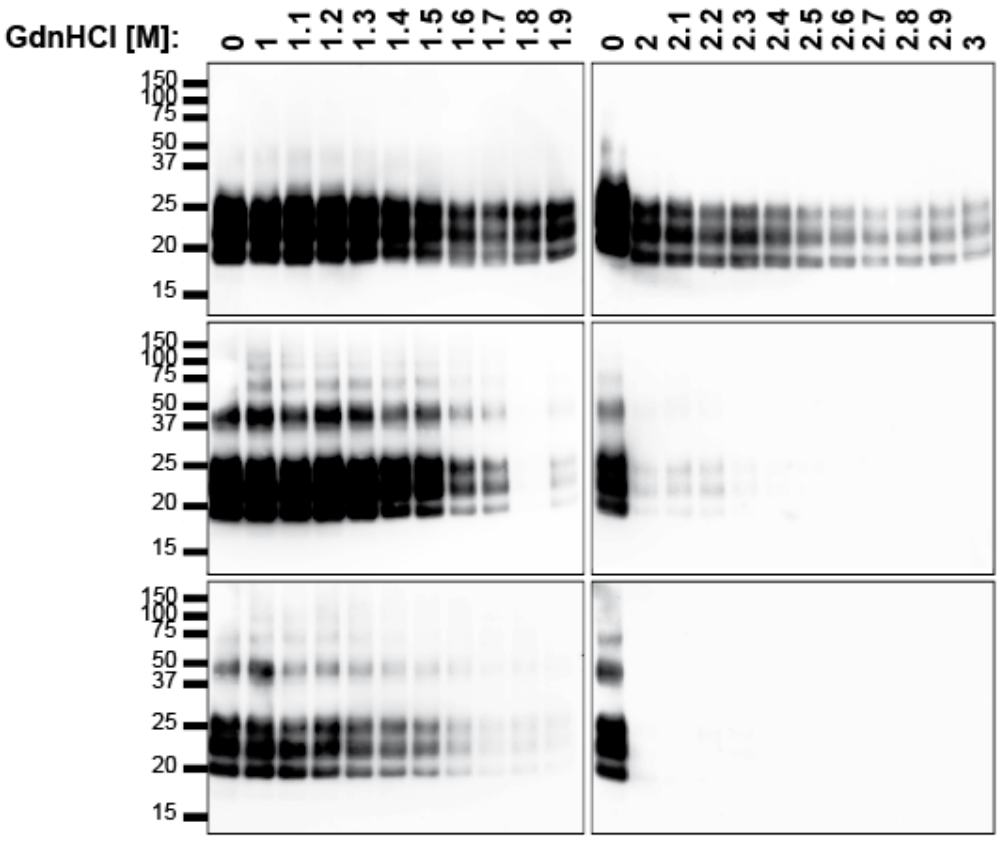

Figure 32: PTAA-treated RML6 prions are more sensitive to denaturation with GndHCl.

Immunoblots of untreated (upper panels) and PTAA-treated RML6 BH at different concentrations of GdnHCl. RML6 BH was treated with either 10 μg/ml (middle panels) or 100 μg/ml PTAA (lower panels). Aliquots of 20 μg protein were denatured with various concentrations of GdnHCl, subsequently digested with PK to remove soluble PrP and loaded to the gel. The anti-PrP antibody POM1 was used for the detection. Molecular sizes are indicated in kDa.

I also compared the stabilities of PrP^{Sc} in untreated and PTAA-treated RML6 BH in a PK independent manner using the MPA. Untreated and PTAA-treated samples were incubated with different concentrations of GdnHCl and the amount of insoluble PrP^{Sc} was detected by the MPA. RML6 prions treated with PTAA exhibited a lower signal in the MPA at all GdnHCl concentrations (Figure 33). The GdnHCl concentrations where 50% of the protein is solubilized and 50% is in the pellet fractions were 1.72 M for the untreated samples and 0.31 M for the PTAA-treated samples. The stability data show that PTAA-treated PrP^{Sc} is less stable than untreated PrP^{Sc}, indicating that PTAA physically alters the conformational stability of PrP^{Sc}.

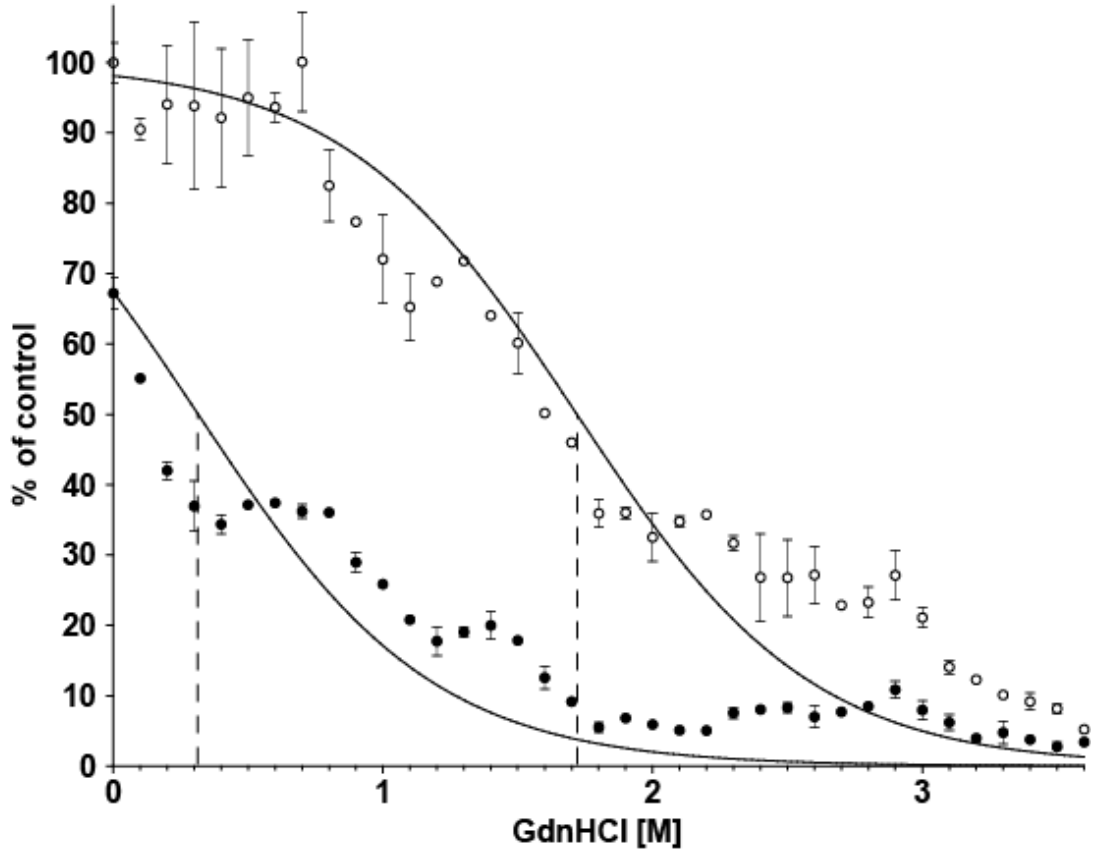

Figure 33: PTAA-treated RML6 prions are more sensitive to denaturation with GndHCl.

MPA of untreated (open circles) and PTAA-treated RML6 BH (filled circles) after denaturation with different concentrations of GdnHCl. PTAA was used at a concentration of 10 µg/ml. Each sample was analyzed in technical duplicates and is represented as the mean ± SD. All data were corrected for the negative control (CD1 BH) and represented as relative light units normalized for RML6 prions. Asymptotic curves were fitted to each dataset with the $[GdnHCl]_{½}$ value at which 50% of the molecules are in a soluble fraction and 50% are in a insoluble fraction indicated by a dotted line at 1.72 M for the untreated and 0.31 M for the PTAA-treated samples.

PTAA-treated recPrP fibers are more resistant to PK digestion

In order to investigate the mechanism of action of the LCPs, I asked, in collaboration with Dr. Simone Hornemann and Cinzia Tiberi, whether PTAA inhibits amyloid fiber formation of the recombinant mouse prion protein mPrP(23-231). Monomeric mPrP(23-231) was grown under slightly denaturating conditions according to a protocol published by Apetri and Surewicz in the presence of different concentrations of PTAA. The time course of fibrillisation was followed by optical density measurements at 350nm for 48h (Apetri et al., 2005). mPrP(23-231) formed amyloid-like fibrils by a nucleation-dependent polymerisation with a lag-phase followed by an exponential growth phase and a plateau phase (Figure 34A). The addition of PTAA significantly reduced the growth rate of the fibers in a dose-dependent manner (Figure 33A). The incubation with the highest dose of 50 μg/ml resulted in a complete inhibition of fiber formation. We further analysed the samples by negatively-stained transmission electron microscopy (TEM) (Figure 34B). Electron micrographs of samples withdrawn after 48h showed that the untreated control samples contained long unbranched fibers. Fibrils grown in the presence of PTAA at concentrations between 1 and 10 μg/ml were coated with small PTAA aggregates in a regular and periodic manner (Figure 34D, E and F), suggesting a specific binding of PTAA to the fibers. With increasing PTAA concentrations we also observed coalescence of the fibers and fiber formation was inhibited (Figure 34B), as evidenced by empty EM grids at PTAA concentrations above 25 μg/ml. Next, we asked whether PTAA directly interacts with preformed mPrP(23-231) fibers. For that purpose, we incubated fibers that were grown for 48h with different concentrations of PTAA and analysed their morphology by TEM. Electron micrographs showed that fibers incubated with PTAA concentrations between 1 and 10 μg/ml were also associated with small aggregates of PTAA as seen for the fibers grown in the presence of PTAA (Figure 34C, D and E). With increasing PTAA concentrations we observed a coalescence of the fibers (Figure 34C), resulting in large associations of the fibers. To determine whether PTAA also renders mPrP(23-231) fibers more resistant to PK digestion, I incubated mPrP(23-231) fibers with 10 μg/ml PTAA and performed a limited proteolysis with different PK concentrations. Figure 34G shows that PTAA-treated fibers are more resistant to PK digestion than untreated fibers as already seen for LCP-treated RML6 prions. Our data show that PTAA inhibits mPrP(23-231) fiber formation and directly interacts with the fibers, causing a coalescence of the fibers into more compact structures upon treatment with PTAA which are also more PK resistant.

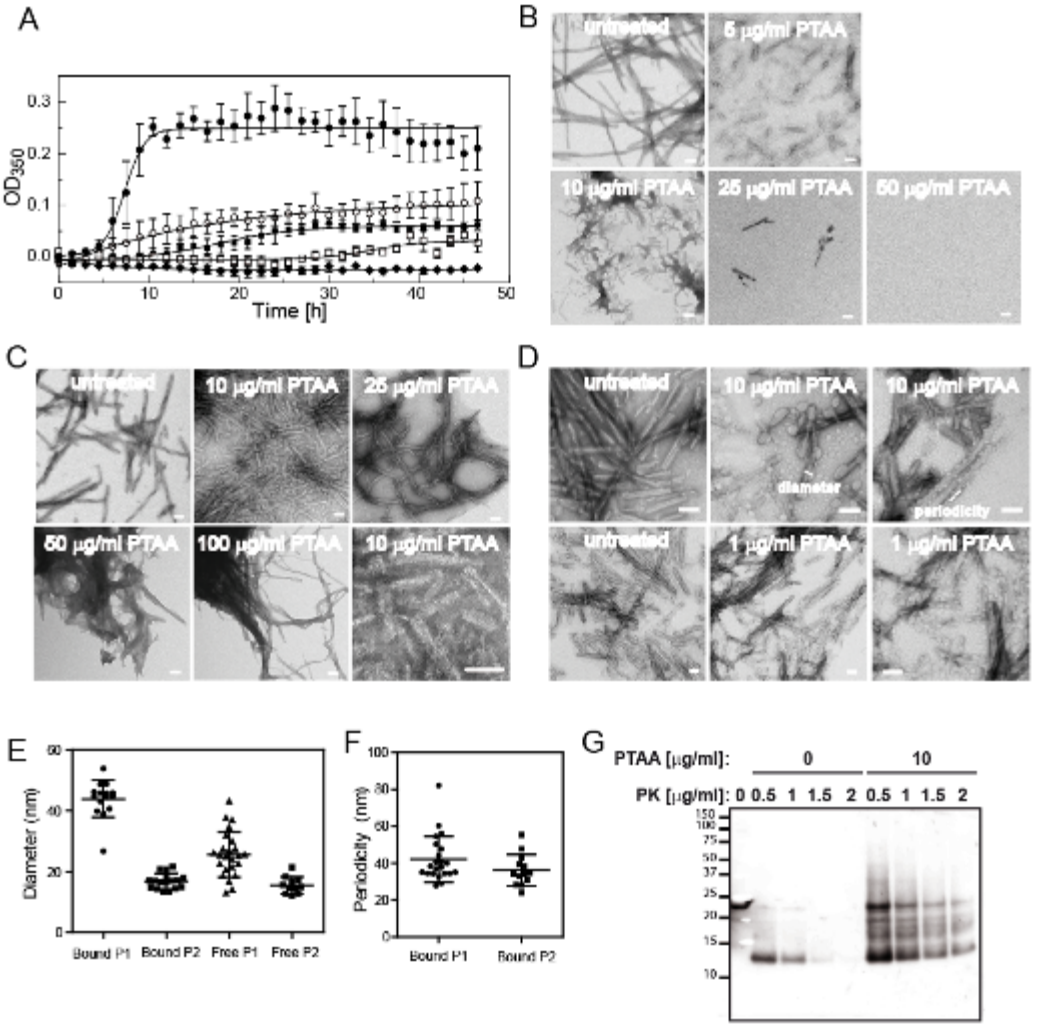

Figure 34: Effect of PTAA on mPrP(23-231) fiber formation and preformed fibers.

(**A**) Time course of mPrP(23-231) fiber formation grown in the absence (filled circles) and presence of PTAA at different concentrations of 5 µg/ml (open circles), 10 µg/ml (filled squares), 25 µg/ml (open squares) and 50 µg/ml (filled diamonds) followed over a period of 48h. Error bars represent the SEM of technical triplicate measurements. (**B**) TEM taken after 48h of control fibers grown in the absence of PTAA and of fibers grown in the presence of different concentrations of PTAA. (**C**) TEM of preformed mPrP(23-231) fibers incubated with different concentrations of PTAA. The electron micrograph in the right lower corner displays the fibrils incubated with 1 µg/ml PTAA at higher magnification. (**D**) TEM of fibers recorded from another independent experiment grown in the presence of 10 µg/ml PTAA (upper panel) and of preformed mPrP(23-231) fibrils mixed with 1 µg/ml PTAA (lower panel). (**E**) PTAA formed two different populations of small aggregates at concentrations between 1 and 10 µg/ml which bound to the fibers with mean diameters of 43.9 ± 2.5 (bound P1) and 16.8 ± 2.8 (bound P2). Free aggregates had mean diameters of 25.6 ± 7.4 for population 1 (Free P1) and 15.4 ± 2.8 (Free P2). Data are represented as the mean ± SD. (**F**) PTAA aggregates were located on the fibers in a periodic manner with distances of 42.2 ±12.5 nm for population 1 and 36.3 ± 8.6 nm for population 2. Data are represented as the mean ± SD. (**G**) PTAA increases the resistance of mPrP(23-231) fibers to PK digestion. Aliquots of mPrP(23-231) fibers were incubated with 10 µg/ml PTAA prior to proteolysis with increasing concentrations of PK. Lane 1 contains non-digested mPrP(23-231) fibers. Scale bar: 100 nm. Molecular sizes are indicated in kDa.

Simone Hornemann performed all work shown in Figure 34A to 34F and prepared the Figure. Cinzia Tiberi performed part of the TEM analysis. Ilan Margalith performed experiments shown in Figure 34G.

DISCUSSION

The high degree of steric specificity of the interaction of LCPs for amyloids had previously been evidenced in the context of the structural differentiation of prion strains (Sigurdson et al., 2007). In addition, LCPs decreased PrP^{Sc} levels in chronically prion-infected neuroblastoma cells (N2a) (Julius C., K. Peter R. Nilsson, not shown), a result similar to the observation made by Caspi et al. with CR. I therefore decided to investigate the potential of LCPs for interfering with stability of PrP^{Sc} and the release of prion infectious particles. Preliminary data from immunoblots of COCSBH from cultures treated with PTAA or PBAT revealed more PK-resistant material and increased presence of higher-order aggregates. These observations suggest a structural modification of prions present at the time of treatment initiation and/or prion replicating during the course of the experiment into a more PK-resistant form. If more compact, such aggregates would also be more stable and therefore less prone to release prion infectivity. As PK-resistant material is only a surrogate marker for prion accumulation I measured the infectivity titre of COCSBH in the SCEPA. Cultures treated with 6 μg/ml PTAA had lower infectivity titres than untreated cultures at 42 DIV. The efficiency of treatment with 6 μg/ml PTAA was comparable to that of 0.3 μg/ml PPS. I have excluded the possibility that PTAA accumulated in cultured tissue could affect the measurement of prion infectivity and therefore conclude that my observations reflect a decrease of prion accumulation in PTAA-treated slice cultures and/or a structural change of pre-existing prions into entities that are less infectious. In addition, treatment with 60 μg/ml PTAA decreased infectivity of COCSBH below the level measured at the time of treatment initiation. This further point towards a structural change, upon PTAA treatment, of pre-existing prions into a form that is less prone to release prion infectious particles.

To further investigate a possible change in prion load in COCSBH I measured prion aggregates in the MPA. This method does not imply digestion with PK and may therefore better reflect prion content. Cultures treated with 0.1 to 60 μg/ml PTAA had lower reactivity with prion-specific binding peptoids than untreated tissue at 42 DIV. This may reflect either a decreased prion load, a structural shift of prions towards larger aggregates that offer less binding surface to prion-specific binding peptoids or a partial disaggregation of prions by PTAA. In addition, the presence of prion aggregates in the MPA correlated remarkably well with the measurements of prion infectivity in the SCEPA and suggests that these two methods are measuring the same entities. To explore the discrepancy between the observation of increased PK-resistant material and higher-order aggregates shown by Western blot and the

decreased prion content evidenced by SCEPA and MPA, I further investigated PK-resistant material in COCSBH by using an ELISA for PK-resistant PrP. PTAA-treated cultures had less PK-resistant material than untreated cultures when measured by ELISA. These results are perfectly in line with the parallel observations of decreased prion infectivity in the SCEPA and decreased prion aggregates in the MPA and further point towards a decreased prion load in PTAA-treated tissue. Of note, a good correlation between the entities measured by MPA, SCEPA and ELISA indicates that the same entity is being affected by PTAA which results in a decrease of measurable PrP^{Sc} aggregates and infectivity. In addition, histoblots from tissue cultured and treated in a similar manner revealed decreased accumulation of PK-resistant PrP^{Sc} in PPS or PTAA-treated tissue. I therefore conclude that PTAA-treated COCS have a decreased prion content compared to untreated tissue. I cannot exclude, however, that PTAA induced a structural shift of prions. The discrepancy between PK-resistant material observed by Western blot and ELISA could be due to an interaction of PTAA with prions that renders them more impervious to PK. As I have shown that guanidine reverses the effect of PTAA, it is possible that PrP^{Sc} investigated by WB was in a more compact state that was unfolded by the guanidine used in the ELISA protocol. Treatment with 60 μg/ml PTAA resulted in a prion load of COCSBH that lies below that of tissue harvested at 21 DIV. In this particular case, PK-resistant material evidenced by Western blot correlated with that shown by ELISA. Furthermore, the signal in the MPA and the prion infectious titre of these cultures were also lower than at 21 DIV. These results may reflect a PTAA-induced partial disaggregation of prions present at the time of treatment initiation or a facilitated removal of such prion levels by scavenging cells. Alternatively it could be due to a structural change of pre-existing prions into a form that is less PK-resistant, less prone to reactivity with prion-specific binding peptoids and releases less infectivity. This would be explained by an enhanced compactness of prion aggregates. In addition, I performed PTAA treatment in a time-resolved manner and investigated prion load by MPA and ELISA. This analysis revealed that PTAA treatment is most effective if initiated before 21 days post-infection. PTAA treatment started at 28 or 35 DIV resulted in an amount of PK-resistant material that was respectively similar or lower than at the time of treatment start and further indicates that PTAA interferes with prion replication within the tissue and possibly transforms pre-existing prions into a form that is less efficiently detected by my methods. In addition, the analysis of this experiment by MPA and ELISA in parallel shows that the measurement of prion aggregates with prion-specific binding peptoids may not be an appropriate method in this particular paradigm, as the MPA could not detect prion aggregates in COCSBH from PTAA-treated cultures. It is possible that the proximal

coating of prion fibrils by PTAA interferes with the interaction of peptoids with binding sites on prion aggregates. Alternatively, it is possible that PTAA interaction with prion aggregates results in a structural change of the latter towards larger structures that offer less interacting surface with peptoid-coated beads. As the interaction of PTAA with RML prions or with recPrP fibril seeds was recently shown to block, respectively, the release of prion infectivity and the fibrilization of murine recPrP (Margalith et al., 2012), it is possible that prion replication within the tissue was impaired by PTAA. It is not clear, however, how this anti-prion seeding effect would be achieved. PTAA could either induce a structural shift towards a more compact, more stable form or on the contrary induce a partial disaggregation of prions. My observations are compatible with both views, to the condition that in the case of a partial disaggregation, PTAA would additionally protect the POM1 epitope from PK, which would explain the observation of increased PK-resistant material by immunoblotting.

My results show that the interaction of PTAA and its derivatives with prion containing BH significantly reduced prion infectivity in the SCEPA. An apparent complete removal of prion infectivity was only achieved at high concentrations of PTAA, however the use of other LCPs show that these molecules generally decrease prion infectivity even at low concentrations. I also performed a titration of infectivity of PTAA-treated RML in *tg*a20 mice to investigate whether PTAA prolongs the survival time. As I only saw a weak difference, I believe that the SCEPA is a stronger tool for measuring variations in prion infectivity: Indeed, prions injected *in vivo*, even if less able to release infectious particles upon PTAA treatment, would remain in the brain for a long time. By contrast, the cells used in the SCEPA are only exposed to prion-containing samples for a short period and therefore may reflect better the release of prion infectivity.

To elucidate the mechanism underlying the above-described phenomena I characterized the influence of LCPs on the resistance to proteolysis of RML prions in a crude brain homogenate. My results show a profound increase in the apparent signal for PK-resistant material on a Western blot of RML prions. Importantly, PK digestion was not affected, as all PK-sensitive PrP was removed and the products of cleavage appeared identical in treated or untreated RML, suggesting that the discrete conformation of PrP^{Sc} was not changed. However, the observation of higher-order aggregates suggests structural changes at the level of the quaternary structure of aggregates in LCP-treated, PK-digested RML prions. Notably, the decoration with PTAA of recPrP fibrils also resulted in improved resistance to PK digestion and electron micrographs revealed coalescence of PTAA-coated recPrP fibrils into more compact structures. Of note, PTAA interacted as small aggregates in a periodic manner

with recPrP fibrils, which underlines the specificity of PTAA for amyloid structures. In addition, all LCPs that decreased prion infectivity also increased the apparent amount of PK-resistant material of RML and PTAA interfered with fibrilization of recPrP, which supports a link between modified infectivity and possible structural changes of associated aggregates.

The antiprion activity of LCPs cannot be attributed to the charges of their side chains, since anionic, cationic and zwitterionic compounds reduced prion infectivity to a similar extent. Also, neither the spacing between the side chains nor the rigidity of the molecules seemed to play a role for their antiprion activity. Based on theoretical considerations, the total avidity of LCPs for amyloids should increase with the number of low-affinity binding sites, and therefore with the length of the polymers. However, very long polymers may have chemical properties limiting their interactions. Hence the activity of LCPs appears to be an intrinsic property of the polythiophene backbone itself. PTAA also caused a left-shift in the conformational stability curve of PrP^{Sc} after exposure to increasing concentrations of the non-surfactant-type chaotrope, GdnHCl. Coalescence of fibrils into more compact structures is not necessarily incompatible with increased denaturation by guanidine: as PK resistance was suggested to depend on conformational state of PrP (Jackson et al., 1999) it is possible that LCP coating of prions results in a perturbation of the structure of aggregates which may create nuclei that are more impervious to PK digestion, yet these nuclei may still be permissive to denaturation by guanidine. In addition, the persistence of higher-order aggregates in PTAA-treated, denatured, PK-digested RML prions suggest that not all of the structural changes induced by PTAA are reversed by denaturation. To further investigate possible structural changes of LCP-treated prions, I used the MPA, an assay which is independent of PK digestion. I observed a good correlation between decreased prion infectivity and decreased signal for prion aggregates in the MPA. This could be due to a coalescence of RML prions into larger structures that are less prone to release prion infectious particles, which would fit to a proposed model in which fibril fragility determines nucleation and further fibril elongation (Knowles et al., 2009). It cannot be excluded, however, that the MPA may be affected by a competition of the LCPs with peptoids for binding sites on prion aggregates. In this study the MPA provided an independent confirmation of structural changes linked with decreased infectivity provoked by an anti-prion compound, in a PK-independent manner. This is interesting because sensitivity of treated prions to PK is not always reliable and therefore might be misleading for testing of therapeutic compounds. I therefore propose to use the MPA as a fast method for the detection of prions and a high throughput assay to screen for novel drugs.

LCPs may act on prion species in different way. PrP^{Sc} was more resistant to PK digestion with low concentrations of the LCPs, which also induced the formation of SDS-stable high-molecular-weight aggregates. Accordingly, PTAA transformed recPrP fibers into more compact structures. Very high concentrations of PTAA and POMT, however, decreased the resistance of PrP^{Sc} to PK. These adverse effects resembles the mechanisms reported for several surfactants which were assumed to affect protein aggregation in a two-concentration dynamic by either interacting as monomers or in equilibrium with small molecule aggregates (Otzen, 2010) and were demonstrated to enhance or reduce the stability and detectability of PK resistant PrP^{Sc} (Caspi et al., 1998; Milhavet et al., 2000; Breyer et al., 2012). A similar mode of action was reported for CR which induces β-sheet formation and self-propagation of monomeric Aβ (Lendel et al., 2010; Abelein et al., 2012). LCPs might promote de novo PrP aggregation by converting PrP into compact aggregates that are more resistant to PK but less infectious. Accordingly, LCPs used at low concentrations (at which the effects cannot be attributed to micelle formation) may prevent prion replication by stabilizing the PrP^{Sc} conformation, which may resultin reduced fiber frangibility, a critical determinant of prion infectivity (Caughey and Lansbury, 2003; Knowles et al., 2009) which controls prion propagation by fragmentation of fibrils and elongation of these infectious particles into new fibrils (Wang et al., 2011). The denseness of LCP-treated PrP^{Sc} aggregates may reduce the release of infectious seeds, resulting in decreased prion infectivity. This possibility is supported by studies showing uncoupling of aggregates size and infectivity (Gabizon et al., 1987; Silveira et al., 2005; Tixador et al., 2010). In conclusion, LCPs can be protective by stabilizing non-compact fibrils. It is also possible that pre-existing prions, and possibly also PrP^{C}, are included into inert structures (Figure 35, Adapted from: (Margalith et al., 2012)).

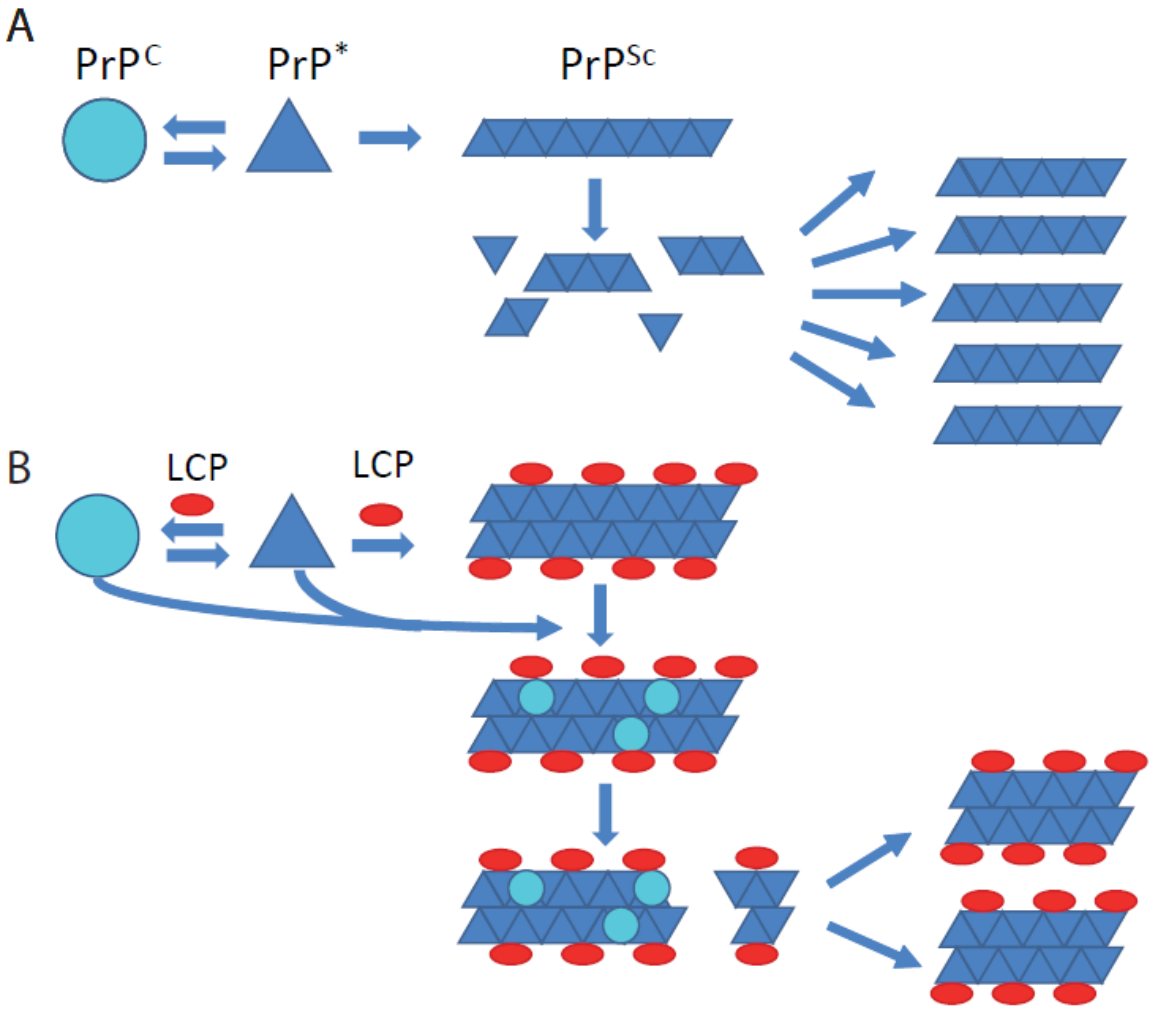

Figure 35: Model for the antiprion activity of the LCPs. Adapted from: (Margalith et al., 2012).

(**A**) In the prion model PrP^{C} is in a reversible thermodynamic equilibrium with PrP*, which further aggregates into amyloid fibrils, PrP^{Sc}. When the fibrils reach a critical length, the fibril becomes more fragile and fragmentation occurs. The newly formed ends of the fibril fragments are new nucleation sites for further fibril growth.

(**B**) The antiprion activity of the LCPs seems to be based on interactions with PrP^{Sc} aggregates, possibly increasing their compactness. LCP coated fibrils further embed preexisting prions and even PrP^{C}. The higher compactness of the PTAA treated aggregates ultimately cause less fragmentation into infectious particles necessary for further prion replication.

Some studies have shown that larger polymers were more PK-resistant than smaller ones (Sklaviadis et al., 1992; Pastrana et al., 2006). Also it has been demonstrated that prion strains with short incubation times had infectivity peaking in the upper part of the sedimentation profile when the respective brain homogenates were subjected to centrifugation in a viscous medium (Tixador et al., 2010), which suggests a link between small forms of PrP^{Sc} and infectivity. My results support this view: LCPs trigger a shift in the size distribution of aggregated recPrP that correlates with increased resistance to PK. PTAA-treated RML prions

also had more PK-resistant material, were less infectious, and had a decreased signal in the MPA that could be interpreted as a decreased binding surface to peptoids of larger prion aggregates. However, this decrease of signal in the MPA could also be interpreted as a partial disaggregation into smaller PrP aggregates. This scenario may fit better with the apparent loss of conformational stability and loss of reactivity in the MPA, however in this paradigm it would be difficult to interpret the increased resistance to PK and higher-order aggregates. Also, disaggregation would rather be expected to increase infectious seeds.

Prions are defined by biochemical and biological parameters such as resistance to proteolysis and prion infectivity and the observation of protease-resistant material tends to correlate with prion infectious titres (Safar et al., 1993). Some experiments, however, have shown that not always a clear correlation between PK resistance and infectivity exists (Sklaviadis et al., 1989; Hsiao et al., 1994; Lasmezas et al., 1997; Shaked et al., 1999; Chiesa et al., 2003; Barron et al., 2007; Piccardo et al., 2007), which points out that PK-resistant material is a surrogate marker for infectivity. The observation of increased PK-resistant material and decreased prion infectivity in this study is a rather unexpected finding since anti-prion compounds rather induce a disruption of PrP^{Sc} which should therefore be more sensitive to PK digestion. Therefore, I conclude that the use of PK digestion only for evaluation of anti-prion compounds may be misleading.

Although the results presented in this thesis underline that LCPs can interact with PrP^{Sc}, their effects on COCS suggest that they may act as well during the transformation of PrP^{C} to PrP^{Sc}. ELISA measurements on COCSBH showed that the PrP^{C} content was reduced approximately two-fold, suggesting that PTAA might remove PrP^{C} from the cell surface or modulate PrP^{C} levels. This may reduce the amount of PrP^{C} available for the formation of PrP^{Sc}. A similar mechanism was reported for other antiprion compounds (Shyng et al., 1995; Pauly and Harris, 1998; Milhavet et al., 2000; Enari et al., 2001; Peretz et al., 2001; Brown and Harris, 2003; Hijazi et al., 2003; Perrier et al., 2004). This interpretation is supported by my finding of a direct interaction of PTAA with PrP^{C} evidenced by an in vitro conversion assay with recPrP in the presence of PTAA in a cell-free environment. PTAA strongly inhibits the formation of recPrP fibers, supporting that it directly interacts with PrP^{C} by either stabilizing the spatial conformation of PrP^{C} or protecting the binding site for the template PrP^{Sc} molecule. Both effects may prevent efficient convertion of PrP^{C} into PrP^{Sc}.

In conclusion, LCPs triggers a structural transformation of PrP^{Sc} in by a mechanism that resembles the one of surfactants. This process depends essentially of the LCP backbone and not on the nature of the side-chains. PrP^{Sc} becomes more resistant to PK digestion upon

incubation with LCPs, while proteolysis of PrP^{C} and other proteins is not affected, and strongly decreases prion infectivity. This body of data also links decreased infectivity to formation of more stable PrP^{Sc} species. Therefore, the LCP scaffold may be used to generate a promising new family of antiprion compounds. The recently developed LCPs, pHTAA and pFTAA, were shown to penetrate the BBB (Aslund et al., 2009) and may represent good candidates for further investigation and for in vivo studies.

OUTLOOK

Further biochemical studies aimed at better defining structure of LCP-treated prions, such as field-flow fractionation, would help elucidate the structural changes that are responsible for the decrease of prion infectivity shown in this study. In addition, the potential of LCPs for curing prion diseases must be investigated in more detail in vivo. To that effect, a project has been started in the laboratory of Prof. A. Aguzzi involving delivery of LCPs to mice through osmotic pumps.

MATERIAL AND METHODS PART I

Preparation of CD1 and RML6 crude brain homogenate

20% wt/vol RML6 or CD1 brain homogenates in 0.32M sucrose in PBS were prepared by three runs in a PreCellys tissue homogenizer with cooling on ice between each run. Protein concentrations of RML6 or CD1 brain homogenates were determined using the bicinchoninic acid assay (Pierce) and normalized to 1 mg/ml total protein with 0.32M sucrose in PBS.

Preparation of LCP stock solutions

The synthesis of the different LCPs has been described elsewhere (Ding et al., 2000). Lyophilized LCPs were resuspended in pure water (B.Braun, Melsungen AG) and stock solutions at a concentration of 1 mg/ml were prepared and stored at 4°C, protected from light. Serial dilutions of the LCPs were prepared in pure water.

Treatment of slice cultures with LCPs

Cerebellar slice cultures were prepared and prion-infected according to Falsig et al. Slice culture medium was changed three times per week and 10 µl of diluted LCP or PPS (30 µg ml^{-1}, Bene pharmachem) was added to 1 ml medium to obtain final concentrations ranging from 0.01 µg/ml to 60 µg/ml PTAA or 0.3 µg ml^{-1} PPS. Treatment was initiated three weeks post-infection or in a time-course manner and maintained until tissue was harvested.

Preparation of slice culture homogenates

Tissue was harvested in PBS and homogenized according to Falsig et al in PBS. Protein concentration was determined using the bicinchoninic acid assay (Pierce) and normalized to 1 mg/ml total protein with PBS.

Quantification of total protein from slice culture homogenates

A BCA Protein Assay Kit was used according to the manufacturer`s protocol (23-225 BCA™ Protein Assay Kit, Pierce) for quantification of total protein from 1% slice culture homogenates.

Proteolysis of COCSBH and Western blot analysis

PrP^{Sc} was detected by limited proteolysis with proteinase K (PK) (Roche) and analysed by Western blotting. 20 µg protein aliquots were digested with 25 µg/ml PK in lysis buffer

containing 0.5% wt/vol sodium deoxycholate, 0.5% vol/vol Nonidet P-40 and 10% vol/vol PBS for 60 min at 37°C and rotating at 700 rpm on a thermoshaker in a total volume of 20 µl. This condition allowed specific detection of PrP^{Sc}. PK digestion was terminated by adding 6.7 µl of 4x LDS loading buffer (NuPAGE, Invitrogen) and boiling the samples at 95 °C for 5 min. 20 µl of the samples were separated on a 12% Bis-Tris SDS polyacrylamide gel (NuPAGE, Invitrogen) and blotted onto a nitrocellulose membrane. Membranes were blocked with 5% wt/vol Topblock (Fluka) in Tris-buffered saline supplemented with Tween (150 mM NaCl, 10 mM Tris HCl, 0.05% Tween 20 (vol/vol)) and incubated with POM1 (Polymenidou et al., 2005) mouse IgG1 antibody to PrP^{C} (anti-PrP^{C}) (200 ng/ml) as primary antibody. Horse radish peroxidase (HRP)-conjugated rabbit anti–mouse IgG1 (1:10,000, Zymed) was used as a secondary antibody. The blots were developed using SuperSignal West Pico chemiluminescent substrate (Pierce) and detected in a LAS3000 system (FUJI).

Scrapie Cell End-Point Assay of COCSBH

COCSBH normalized to 1 mg/ml total protein was diluted 1 to 100 fold in cell culture medium to obtain a final dilution of 10^{-4} from full brain. These samples were then serially diluted in cell culture medium containing a 10^{-4} dilution of CD1 BH and dilutions of COCSBH ranging from 10^{-4} to 10^{-8} were tested in 96-well plates. Experimental runs comprised 4 plates including a COCSBH from six weeks-old prion-infected, untreated tissue as a standard plate. The infection of N2a-PK1 cells and subsequent processing of the SCEPA were performed as previously described (Klohn et al., 2003).

Misfolded protein assay

10 µg total protein (BH or COCSBH prepared as 1% w/v in 0.32 M sucrose in PBS and normalized to 1 mg/ml) was diluted 100 fold in TBSTT [50 mM Tris-HCl (pH 7.5)/137 mM NaCl/1% Tween 20/1% Triton X-100] and incubated 10 min at 37 °C under permanent agitation (850 rpm). 100 µl was then subjected to precipitation using magnetic beads coupled to the peptoid PSR1 (Lau et al., 2007) for 1 h at 37 °C under permanent agitation (750 rpm). Beads were washed and trypsin digestion was performed (12.5 µg/ml trypsin in TBST containing 5 mM $CaCl_2$) for 30 min at 37 °C under permanent agitation (750 rpm) and stopped with 2 mM PMSF for 15 min at RT. Beads were washed and denatured with 0.1 N NaOH. After neutralization (0.3 M Na_2H_2PO4), samples were placed on a magnet, and supernatant was transferred to POM19 (Polymenidou et al., 2005)-coated ELISA plates. After incubation (1 h at 37°C, 300 rpm), plates were washed, and POM2-AP (Polymenidou et al.,

2005) was added. After incubation with substrate (100 µl of Lumiphos Plus substrate (Lumigen, Southfield, MI), plates were read in a luminometry reader (Luminoskan Ascent; Thermo Fisher Scientific).

ELISA

For ELISA, COCSBH were diluted ten-fold in TBSTT [50 mM Tris-HCl (pH 7.5)/137 mM NaCl/1% Tween20/1% Triton X-100] to obtain a final concentration of 0.1 mg/ml total protein. Digestion with proteinase K (PK) was performed in a 96-well plate for 60 min at 37 °C, rotating at 700 rpm on a thermoshaker in a total volume of 50 µl containing 50 µg ml^{-1} PK. Digestion was halted by adding 2 mM phenylmethanesulfonylfluoride (PMSF, Calbiochem) and Complete Mini protease inhibitor cocktail (Roche). Digested samples were denatured with an equal volume of 3 M GdnSCN for 30 min at 37 °C and diluted with four volumes of 0.1 M $NaHCO_3$ pH 8.9. The samples were then detected by sandwich ELISA. Briefly, ELISA plates were coated with POM1-antibodies (400 ng/well) in coating buffer overnight. After washing with PBST, plates were blocked with blocking buffer (5% TopBlock in PBST) for 2 hrs at room temperature. Next, samples were incubated for 2 hours on ELISA plates (Nunc, MaxiSorb). Captured samples were detected with POM19 antibody (1 mg/ml, 1 hour, diluted in sample buffer) and horse radish peroxidase (HRP)-avidin conjugate (1 mg/ml, 1 hour, diluted in sample buffer) (BD Pharmingen). Samples were analysed by ELISA in technical triplicates and washed five times with PBS 0.05% Tween20 between each antibody and conjugate incubations. Finally, TMB substrate (Invitrogen) was added to the wells and incubated for 15 min at room temperature and stopped by adding 0.5 M H_2SO_4. The absorbance was read at 450 nm in a VERSAmax microplate reader and validated with the SOFTmax PRO software.

Histoblots of slice cultures

The histoblot technique was performed according to previously published protocols (Taraboulos et al., 1992) with the following modification for slice cultures: 100% Ethanol-fixed slice cultures of various thicknesses comprised between 50 and 300 µm were pressed on a nitrocellulose membrane wetted in lysis buffer. Membranes were air-dried for at least 24 h. For detection, they were rehydrated in TBST, and limited proteolysis was performed using proteinase K concentrations of 0, 20, 50 and 100 µg/ml in digestion buffer at 37 °C for 4 h. Blots were washed three times in TBST, denatured in 3 M guanidinium thiocyanate for 10 min, washed another three times in TBST and blocked for 1 h in 5% non-fat milk in TBST.

Incubation with primary antibody POM1 was carried out at a dilution of 1:10000 in 1% non-fat milk in TBST at 4°C overnight. Blots were washed three times in TBST and blocked for 5 min in 1% non-fat milk in TBST. Detection was accomplished by adding an alkaline phosphatase-conjugated goat anti-mouse antibody (Dako D0486) at a concentration of 1:2000 for 1 h. Blots were washed three times in TBST and B3 solution (100 mM Tris, 100 mM NaCl, 100 mM $MgCl_2$, pH 9) was applied for 10 min. Visualization was achieved with nitro blue tetrazolium and bromo-chloro-indolyl phosphate solution (Roche) (1 tablet for 10 ml water and 10 µl 1M Levamisole) for 45 min and washing with B4 solution (100 mM Tris, 0.01 mM EDTA, pH 8) for 30 min.

Immunohistochemistry

For immunocytochemistry of *in vitro* material, the organotypic slice cultures were washed twice in PBS and fixed in 4% formalin overnight at 4 °C. Membrane inserts were washed and incubated for 1 h in blocking buffer (0.05% vol/vol Triton X-100 and 3% vol/vol goat serum dissolved in PBS) and incubated with the primary antibody diluted in blocking buffer at 4 °C for 3 days. The primary antibody mouse anti-Neuronal Nuclei (NeuN, 1 µg ml^{-1}, Serotec) was detected using the Alexa-conjugated secondary antibody Alexa Fluor 647 (3 µg ml^{-1}, Molecular Probes) and counterstained with 4,6-diamidino-2-phenylindole (dapi) (1 µg ml^{-1}). Images were recorded at 4x magnification on a fluorescence microscope (BX-61, Olympus) equipped with a cooled black/white CCD camera.

Treatment of RML prions with LCPs

LCPs were diluted into aliquots of normalized crude brain homogenates at final concentrations ranging from 0.1 µg/ml to 5000 µg/ml and to final volumes of 45 µl. All samples were incubated for 30 min at 37°C on a thermo shaker rotating at 700 rpm prior to proteolysis.

Proteolysis of RML6 prions and Western blot analysis

PrP^{Sc} was detected by limited proteolysis with PK (Roche) and analysed by Western blotting. 45 µl samples were digested with 50 µg/ml PK in lysis buffer containing 0.5% wt/vol sodium deoxycholate, 0.5% vol/vol Nonidet P-40 and 10% vol/vol PBS for 60 min at 37°C and rotating at 700 rpm on a thermoshaker. This condition allowed specific detection of PrP^{Sc}. PK digestion was terminated by adding 17 µl of 4x LDS loading buffer (NuPAGE, Invitrogen) and boiling the samples at 95 °C for 5 min. 30 µl of the samples were separated on a 12% Bis-

Tris SDS polyacrylamide gel (NuPAGE, Invitrogen) and blotted onto a nitrocellulose membrane. Membranes were blocked with 5% wt/vol Topblock (Fluka) in Tris-buffered saline supplemented with Tween (150 mM NaCl, 10 mM Tris HCl, 0.05% Tween 20 (vol/vol)) and incubated with POM1 mouse IgG1 antibody to PrP^C (anti-PrP^C) (200 ng/ml) as primary antibody. Horse radish peroxidase (HRP)-conjugated rabbit anti–mouse IgG1 (1:10,000, Zymed) was used as a secondary antibody. The blots were developed using SuperSignal West Pico chemiluminescent substrate (Pierce) and detected in a LAS3000 system (FUJI).

Scrapie Cell End-Point Assay of BH

RML samples consisting of 1% BH containing water or various concentrations of polythiophenes were diluted 1 to 100 fold in cell culture medium to obtain a final dilution of 10^{-4} (dilution of wet brain tissue). These samples were then serially diluted in cell culture medium containing a 10^{-4} dilution of CD1 brain homogenate and dilutions of RML ranging from 10^{-4} to 10^{-8} were tested in 96-well plates. The effect on RML of 3 dilutions of a polythiophene, or 3 different polythiophenes were compared to a standard plate (RML + water) in experimental runs that comprised 4 plates. The infection of N2a-PK1 cells and subsequent processing of the SCEPA were performed as previously described (Klohn et al., 2003).

MTS assay

We used the MTS assay kit from PROMEGA according to the instructions given by the manufacturer.

Bioassay in tga20 mice

A 2% (w/v) RML6 brain homogenate was prepared by dilution of a 20% stock with 0.32M sucrose in PBS and divided into two 25 µl aliquots. These aliquots were supplemented with 25 µl PTAA (20 µg/ml) or with water, yielding 1% brain homogenates containing either 10 µg/ml PTAA or no PTAA and incubated on a thermo shaker for 60min at 37°C, 700 rpm. The samples were then further diluted 100 fold with pure water and 10 fold with PBS, yielding a 10^{-5} dilution (from full brain). Further 10-fold dilutions of these samples in PBS were prepared to inoculate mice with 10^{-6}, 10^{-7} and 10^{-8} dilutions. *tg*a20 mice were maintained under specific pathogen-free (SPF) conditions. Housing and experimental protocols were in accordance with the Swiss Animal Protection Law and mice were held in compliance with the

regulations of the Veterinäramt, Kanton Zürich. Mice were intracerebrally (i.c.) infected with 30 µl of the above-described samples. Numbers of mice inoculated with each dilution is indicated in Figure 29. The mice were then monitored three times per week from the apparition of the first signs of disease. Mice were then sacrificed at terminal stage of prion disease as follows: a sagital section of the brain was fixed in 2% parafomaldehyde for immunohistochemistry. From the second half of the brain, a coronal section was snap-frozen in HANKS medium for histoblot analysis. The remaining brain material was snap-frozen and stored for further biochemical analysis.

Conformational stability assay of RML6 prions

Aliquots of RML brain homogenates normalized to 2 mg/ml protein were prepared and water or PTAA was added to obtain final concentrations of 0, 10 or 100 µg/ml PTAA before incubation for 30 min at 37°C on a thermo shaker rotating at 700 rpm. These samples were divided into 10 µl aliquots containing 20 µg protein and an equal volume of water or 2x concentrated guanidine were added to obtain the final concentrations indicated in the figures. Denaturation was performed by incubating the samples for 10 min at room temperature. For Western blot analysis these samples were digested with PK (15 µg/ml) and 20 µl of the samples were separated on a 12% Bis-Tris SDS polyacrylamide gel (NuPAGE, Invitrogen) and blotted onto a nitrocellulose membrane. For MPA analysis, denaturated aliquots from the preparations containing 0 or 10 µg/ml PTAA were diluted 1:100 fold in TBSTT prior to capture with peptoid-coated beads in the MPA.

Preparation of recombinant mouse mPrP(23-231) and conversion into fibers

Recombinant mouse PrP comprising residues 23-231 was expressed and purified as described elsewhere (Zahn et al., 2000; Lysek and Wüthrich, 2004; Hornemann et al., 2009). mPrP(23-231) fibers were produced by incubating the protein at 37 ºC for 48 hours in 50 µM Tris-HCl, 1 M GdnHCl, 150 mM sodium chloride, pH 7.5, and shaking at 600 (Apetri et al., 2005). To study the inhibition of fiber formation by PTAA, mPrP(23-231) fibers were grown in the absence and presence of different concentrations of PTAA ranging from 1 µg/ml to 50 µg/ml. The time course of fiber formation was followed by measuring the optical density at 350nm with a Tecan Saphire 2 plate reader. After 48h the samples were also analysed by transmission electron microscopy (see below). Preformed fibrils were mixed with PTAA at

concentrations of 10, 25, 50 and 100 μg/ml PTAA for 30 min at 37°C and 600 rpm before they were analysed by transmission electron microscopy as described below.

Transmission electron microscopy

Carbon coated copper grids were placed on 10 μl of the fibril solutions and incubated for 1 min. After removing of excess liquid, grids were washed three times with water prior to staining with 2% aqueous uranyl acetate for 1 min. Samples were analysed on a Philips CM12 electron microscope (transmission electron microscope with an acceleration voltage of 80 keV).

Proteolysis of mPrP(23-231) fibrils in the presence of PTAA

mPrP(23-231) fibrils were incubated in the absence and presence of 10 μg/ml PTAA at 37°C for 60 min on a thermo shaker rotating at 700 rpm. 18 μl of untreated and PTAA-treated recPrP fibrils were digested with PK at concentrations of 0.5, 1, 1.5 and 2 μg ml^{-1} diluted in PBS at 37°C for 60 min on a thermo shaker rotating at 700 rpm. PK digestion was terminated by adding 7 μl of 4x LDS loading buffer (NuPAGE, Invitrogen) and boiling the samples at 95 °C for 5 min prior to loading the samples on a 12% BisTris SDS polyacrylamide gel (NuPAGE, Invitrogen). The tips used for loading as well as the electrophoresis chamber filled with the running buffer were warmed to 80 °C in order to prevent precipitation of the guanidine hydrochloride while loading. After gel electrophoresis, immunoblotting was performed as described above.

Statistical analysis

For Figure 11, P-values were calculated with a one-sample T-test comparing ID_{50} difference to control (COCSBH from untreated cultures harvested after 42 DPI). For Figure 12, Figure 14, Figure 17 and Figure 18 statistical differences were computed to compare each set of biological replica to the control COCSBH using a one-way ANOVA with Tukey's multiple comparison test. For Figure 25, Figure 26 and Figure 27 (SCEPA), proportion of negative wells over dilutions was compared between drugs using a Mantel-Haenszel Chi-square test with a Bonferroni-Holm correction. Confidence interval for common odds ratio is given in the respective tables for non-significant comparisons. For Figure 29 (bioassay in *tg*a20 mice), survival curves were compared using a Log-rank (Mantel-Cox) test. For Figure 30 and Figure 31 (MPA), technical quadruplicates were compared for each individual sample using a T-test.

In Figure 30, the overall effect of individual LCPs was investigated by comparing a group of four concentrations of each individual LCPs using a post-Hoc T-test for analysis of variance.

PART II: PRION STRAIN TYPING USING LCPs

Introduction

The first idea of my thesis project was to adapt prion strain discrimination with LCPs in the POSCA. Since prion aggregates can readily be observed in COCS after three weeks, prion strain discrimination can potentially be performed in a very fast manner while reducing the number of animals to be used for experiments. In addition, the reduced time-scale for generation of successive passages of prion inocula in COCS would also enable the study of strain adaptation using the POSCA. Furthermore, a phenomenon called "prion strain competition" has been reported (Schutt and Bartz, 2008). The POSCA may enable the investigation of prion strain competition by inoculation of COCS with different prion strains and discrimination of strain-specific aggregates with LCPs. To that effect I have dedicated a large effort to the development of a protocol for staining COCS with LCPs and subsequent spectral analysis of prion strains. This has successfully led to the discrimination of mouse-adapted prion strains in COCS on the basis of the spectral signature of prion aggregates. In addition, I have observed that different prion strains replicating in COCS yield aggregates with subtle differences that are generally not obvious in brain sections from prion-inoculated mice, such as deposition pattern and morphology of aggregates. These differences may arise specifically in the cerebellar environment and may provide a new mean of discriminating prion strains.

Spectral profile of mouse-adapted prion strains *in vivo* and *in vitro*

I used a panel of mouse-adapted prion strains that have been largely described in the literature including ME7 (Zlotnik and Rennie, 1963; Bruce, 1993; Bruce et al., 2002; Bruce, 2003), the mouse-adapted goat prion strains 79A (Bruce, 1993) and 139A (Chandler and Fisher, 1963) as well as a natural sheep scrapie isolate that was passaged in mice in our lab, MSS (for mouse-passaged scrapie) and the sheep-derived (Chandler) mouse-adapted prion preparation RML (characterized in (Büeler et al., 1993)) (RML6: passage 6, performed in our lab). In addition, I used the mouse-adapted BSE strain 301C (Bruce et al., 1994). COCS were inoculated and cultured for 35 DIV (Figures 36 and 38A) or 56 DIV (Figures 39 and 40). In parallel, I investigated in a similar manner the prion strains 22L, 79A, 139A, ME7, 135X, MSS and 301C in wild-type (WT) (not shown) and *tg*a20 mice (Figure 37 and 38B) by staining cortical cryosections of terminal mice with PTAA as described by Sigurdson et al. (Sigurdson et al., 2007). The RML strain was omitted from the *in vivo* part of the analysis because PTAA-

stained RML prion aggregates cannot be observed in cryosections of terminal *tg*a20 mice (Sigurdson et al., 2007), although they are abundant in COCS. The isolate 135X (described by Prof. Jean Manson as a variant of the strain ME7) was included as well as the 22L isolate (Bruce, 1993). Staining with PTAA was performed and spectral analysis of prion aggregates from COCS or mice inoculated with the different prion isolates revealed different spectral signatures: the wavelength with the maximal intensity of fluorescence was shifted from 10 to 20 nm in COCS (Figure 36) and about 10 nm in *tg*a20 mice (Figure 37). These spectral differences reveal structural differences between aggregates from different prion strains. In addition, the overall shapes of the curves were different: distribution of fluorescence intensity between 510 and 610 nm was different for aggregates of different prion strains (Figure 36 and 37). This may reveal spectral differences between aggregates or/and contribution of the background (PTAA bound to various entities within tissue, such as DNA and other) to the measured spectra. The latter may result from the fact that the underlying tissue stained with PTAA emits light between 510 and 610 nm. As different prion isolates are expected to provoke prion-induced neurodegeneration to variable extents, it is possible that differences in this region of the spectrum reveal the extent of cell death. For this reason I chose to perform the first part of this analysis by plotting the ratios of light emitted at 517 nm, 685 nm and Emax. It can be appreciated in Figures 36 and 37 that the contribution of the background is the highest between approximately 530-610 nm and that the most obvious differences between spectra, with low background contribution is around 685 nm. These differences are close to the discriminatory sensitivity of the SpectraCube, the machine used for spectral acquisition (10 nm) and some aggregates had a similar maximal emission (Emax) even while displaying overall different spectral curves. For this reason I performed spectral acquisition on a large number of aggregates (n = 5-8) from several individual COCS (n = 5-6) or mice (n = 3-4) (Figure 36-38). It readily appears in Figures 36 and 37 that spectral differences between PTAA-stained aggregates from different prion strains are more evident in COCS than in brain cryosections from terminal mice. This is even more obvious in the ratio plots (Figure 38).

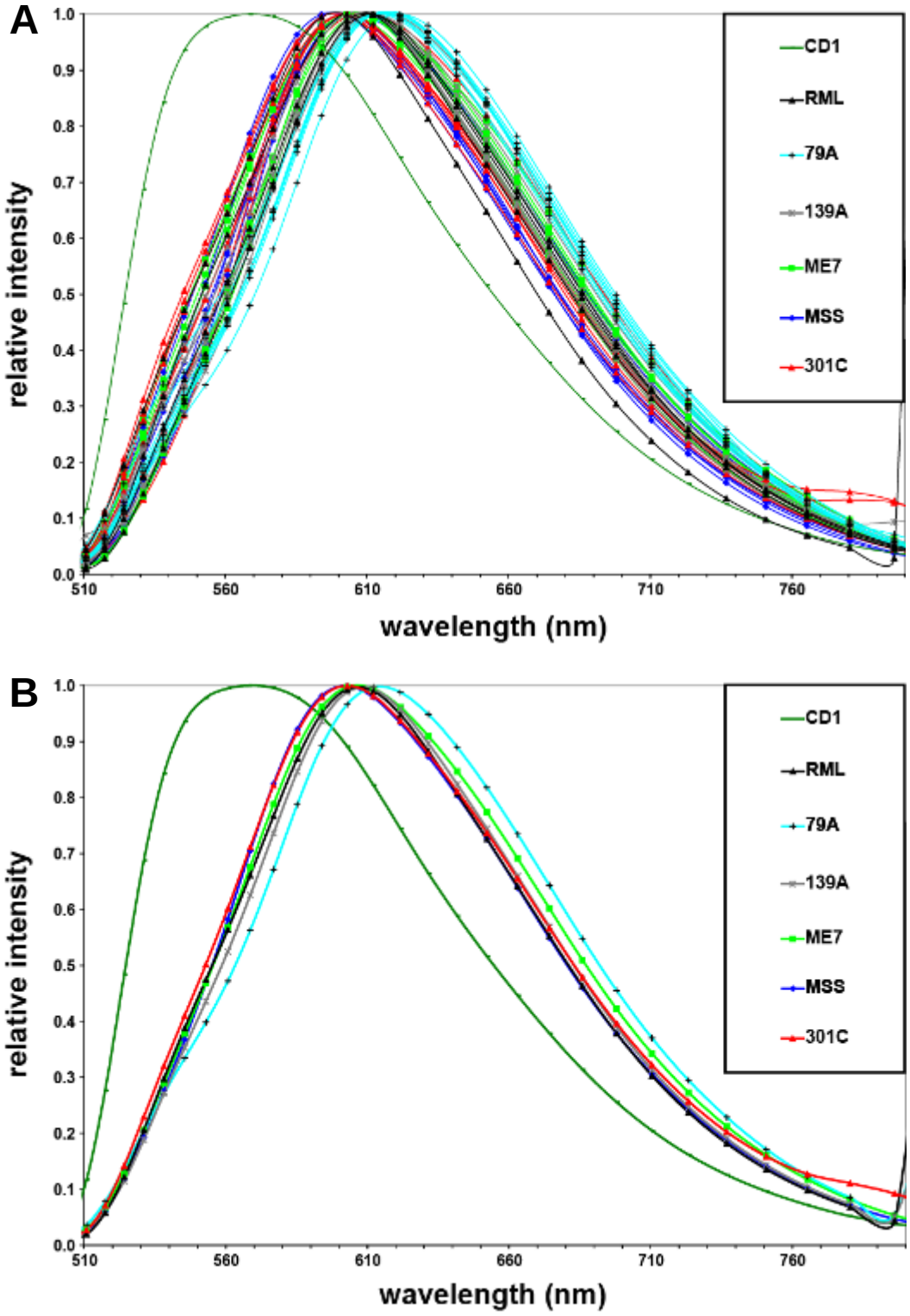

Figure 36: Spectral signature of aggregates from six prion strains *in vitro* after 35 DIV.

(**A**) Fluorescence emission at 510 to 800 nm from 5 to 8 aggregates of the prion strains RML, 79A, 139A, ME7, MSS and 301C *in vitro*. For each aggregate fluorescent emission was acquired from 9 regions of a spectral image and averaged. Spectra from aggregates were acquired in 5 to 6 PTAA-stained COCS (prepared from *tga*20 mice) per strain. Staining of tissue was performed after 35 DIV. CD1: background spectrum from a COCS exposed to non-infectious BH from a CD1 mouse and PTAA-stained after 35 DIV.

(**B**) Average fluorescence emission from aggregates shown in (A).

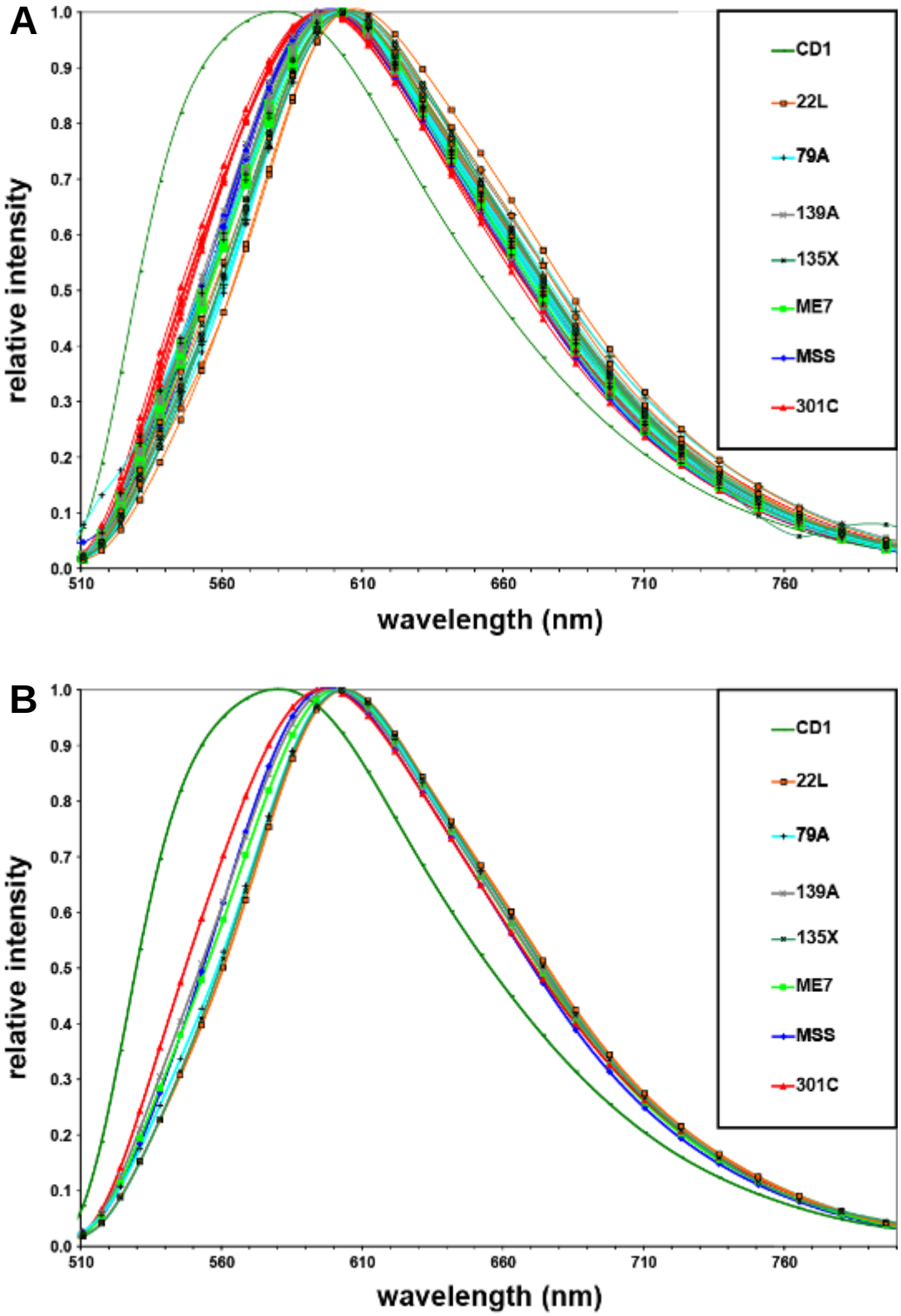

Figure 37: Spectral signature of aggregates from seven prion strains *in vivo*.

(**A**) Fluorescence emission at 510 to 800 nm from 4 to 8 aggregates of the prion strains 22L, 79A, 139A, 135X, ME7, MSS and 301C *in vivo*. For each aggregate fluorescent emission was acquired from 9 regions of the spectral image and averaged. Spectra from aggregates were acquired in PTAA-stained cortical cryosections from 3 to 4 *tg*a20 mice per strain. CD1: PTAA-stained cortical cryosection from a *tg*a20 mouse inoculated with non-infectious BH from a CD1 mouse.

(**B**) Average fluorescence emission from aggregates shown in (A).

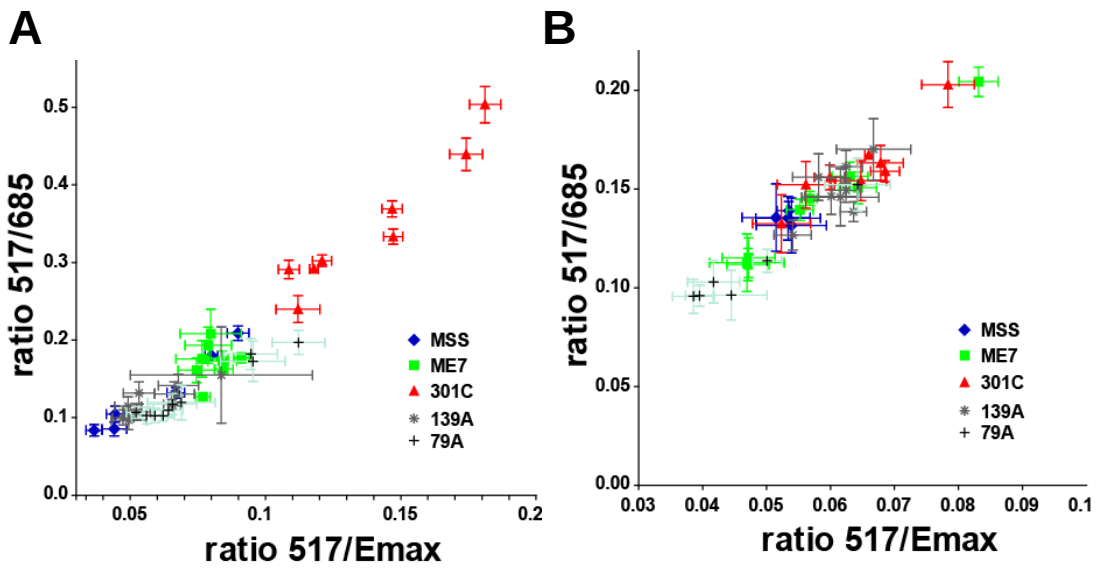

Figure 38: Ratio plots from spectra shown in Figures 36A and 37A.

(**A**) Ratio plot of spectra from Figure 36A (prion strains *in vitro*). For easier comparison between assays only a subset of strains (MSS, ME7, 301C, 139A and 79A) is shown.

(**B**) Ratio plot of spectra from Figure 37A (prion strains *in vivo*).

One technical problem of the analysis of prion aggregates in COCS is the impossibility of obtaining preparations with the same thickness, because COCS are undergoing neurodegeneration to variable extents during culturing and cannot be cut into thinner sections. As a result, the contribution of the background to the spectral signature of aggregates from different prion strains in COCS induces high variability between measurements for one prion strain and possibly differences between strains that are due to variable contribution of the background and not to structural differences of aggregates. As prion aggregates are growing into larger entities with more intense fluorescence during the course of replication I repeated the analysis in COCS with prolongating the culturing period until a total of 56 DIV (Figure 39 and 40). This resulted into larger aggregates with more intense PTAA-fluorescence (about two fold). In addition, more profound neurodegeneration of COCS after 56 DIV contributed to decrease the intensity of the background and possibly to make it more homogenous between COCS infected with different prion strains. For these reasons I chose to include background differences in this analysis by plotting the ratios at 569nm/685nm and 569nm/Emax. Of note, differences around 569 nm are probably not due only to the contribution of the background but also to structural differences between aggregates, as the entire curves are shifted between strains. Figure 40 shows that measurements of fluorescence from PTAA-stained aggregates from five mouse-adapted prion strains segregate into five

homogenous and separated groups. Of note, these five groups also segregate into three groups: the mouse-adapted scrapie prions (RML, 22L), the mouse-adapted goat prions (79A, 139A) and the mouse-adapted bovine prions (301C).

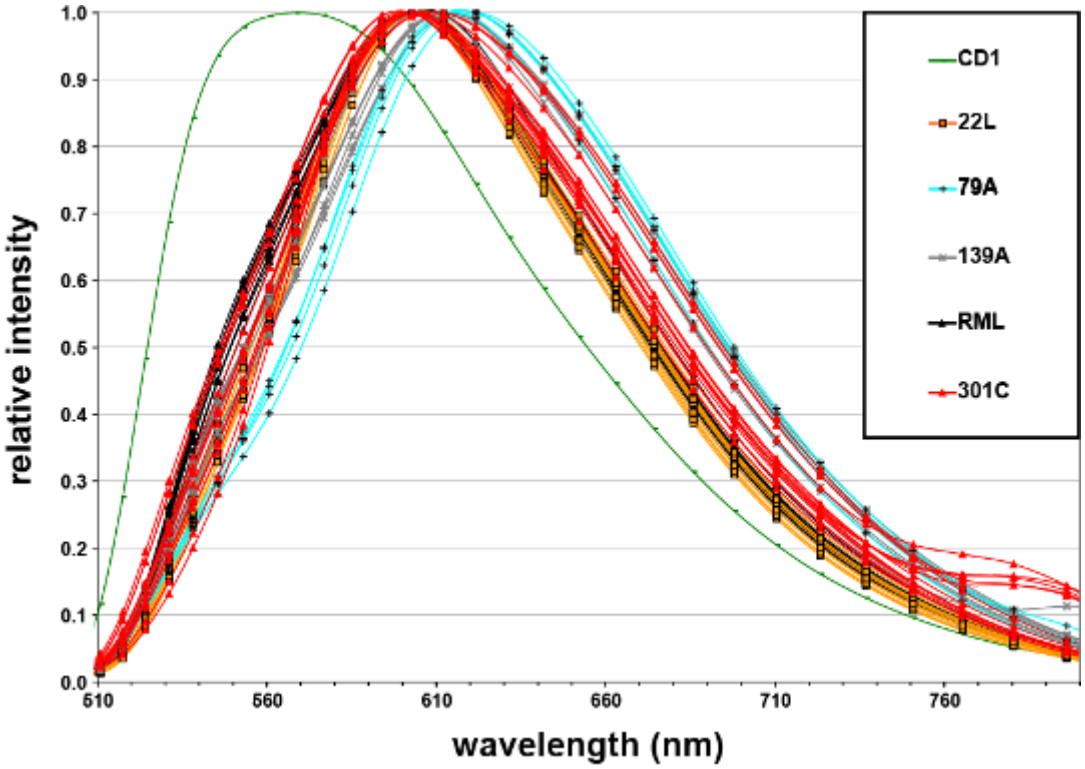

Figure 39: Spectral signature of aggregates from five prion strains *in vitro* after 56 DIV.

Fluorescence emission at 510 to 800 nm from 4 to 13 aggregates of the prion strains 22L, 79A, 139A, RML, and 301C *in vitro*. For each aggregate fluorescent emission was acquired from 9 regions of a spectral image and averaged. Spectra from aggregates were acquired in 5 to 6 PTAA-stained COCS (prepared from *tg*a20 mice) per strain. Staining of tissue was performed after 56 DIV. CD1: background spectrum from a COCS exposed to non-infectious BH from a CD1 mouse and PTAA-stained after 56 DIV.

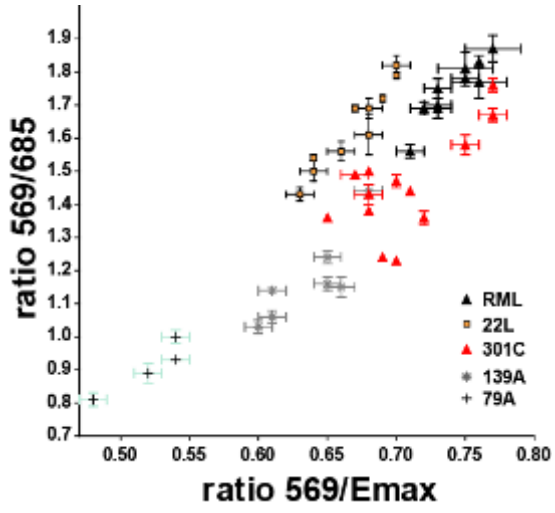

Figure 40: Ratio plots from spectra shown in Figure 39.

Ratios 569/685 and 569/Emax from Figure 38.

To further investigate the spectra of prion aggregates I analyzed the evolution of the spectra from aggregates of the ME7 prion strain *in vivo* and in COCS after 35 or 56 DIV (Figure 41).

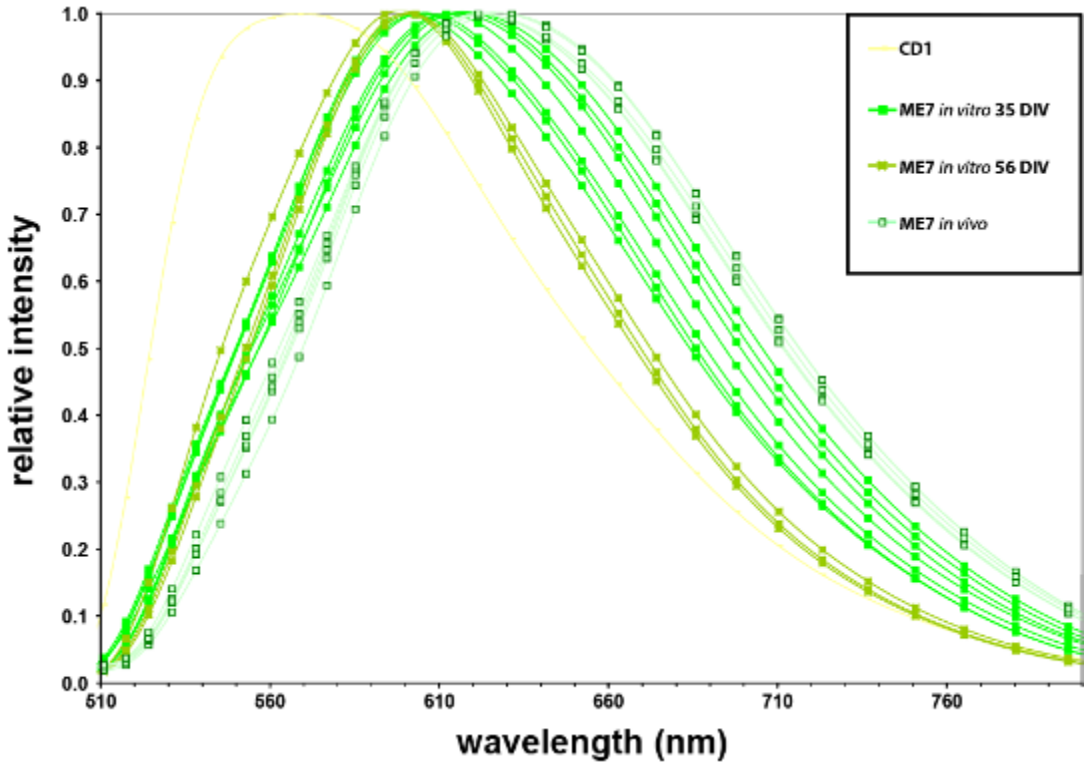

Figure 41: Spectral signature of aggregates from a prion strain *in vivo* or *in vitro*.

Fluorescence emission at 510 to 800 nm from 3 to 7 aggregates of the ME7 prion strain in cortical cryosections from a *tg*a20 mouse or in COCS after 35 or 56 DIV. For each aggregate fluorescent emission was acquired from 9 regions of a spectral image and averaged. CD1: background spectrum from a COCS exposed to non-infectious BH from a CD1 mouse and PTAA-stained after 56 DIV. Note: the background in cortical cryosections from a non-inoculated *tg*a20 mouse is similar to the background in COCS from *tg*a20 mice.

It can be appreciated in Figure 41 that the spectra of ME7 aggregates *in vivo* have a stronger red component than in COCS at 35 or 56 DIV. In addition, spectra of ME7 aggregates in COCS have more green component and further shift towards more green fluorescence during the course of culturing. The maximal emission was also shifted towards green light. It is unlikely that these differences are due to the evolution of the background during culturing as the background may only decrease during the course of the experiment (due to cell death) and would therefore rather decrease the green component of the spectra in COCS. Heterogeneity of fluorescent spectra was stronger in COCS at 35 DIV than after 56 DIV. This was probably due to the facts that (1) aggregates at 56 DIV are larger and therefore emit stronger fluorescence and (2) background of the surrounding tissue is lower than at 35 DIV.

Finally, the structure of prion aggregates from ME7 evolved during the course of culturing of COCS towards entities that emit more green-shifted fluorescence.

Additional features of prion strains in COCS

During the course of this work, several unexpected observations were made. Firstly, prion aggregates from different strains appeared to grow either with a diffuse (RML, 22L, 79A, 139A) or focal morphology (ME7, MSS, 301C). Occasionally RML appeared to yield also some focal aggregates (Figure 42, lower left panel) and ME7 some fibrillar structures. Figure 42 shows as an example aggregates from RML and ME7.

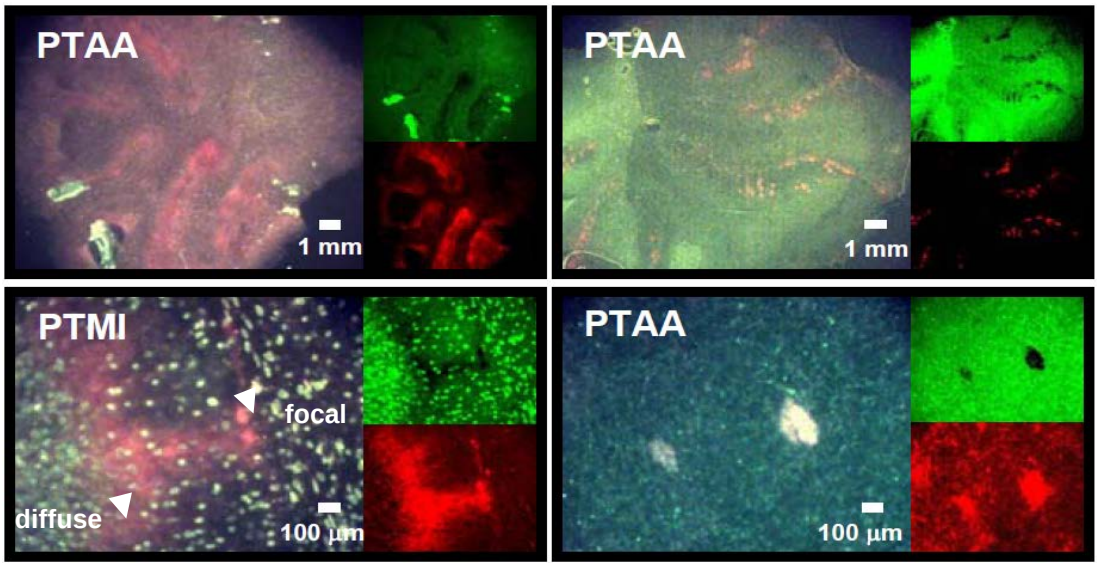

Figure 42: Morphology of aggregates from prion strains in COCS.

Diffuse/focal morphology of RML aggregates (left panels) or focal morphology of ME7 aggregates (right panels). Upper panels: an entire cerebellar slice photographed with a 5x objective. Lower panels: granular layer photographed with a 40x objective. Lower left panel, PTMI: this LCP stains cell nuclei in green, showing the morphology of the different cells composing the different layers of the cerebellum. In all pictures fluorescent light was separated into green channel (LCP bound to various components of the tissue) and red channel (LCP bound to prion aggregates). The objects emitting strong green fluorescence in the upper left panel are artefacts originating occasionally from the culturing process (agarose, dust and other).

Surprisingly, the strains with diffuse aggregates were also the strains that were yielding more PK-resistant material after 35 DIV, presumably growing faster than strains yielding very little PK-resistant material at the same time point (Falsig et al., 2008). The observations made in this study support this view: pictures from LCP-stained COCS show very few focal aggregates in COCS infected with ME7 or MSS, whereas COCS infected with RML, 22L, 79A, 139A had abundant diffuse aggregates covering the entire surface of the slices (most abundant in the area of the Purkinje cell layer). COCS infected with 301C yielded amount of

PK-resistant material intermediate to the two above-described groups and had more abundant aggregates in microscopy images than ME7 and MSS.

Another interesting observation is the preferential, strain-dependent deposition of aggregates in particular areas: Figure 42 shows the deposition of ME7 aggregates mainly near the cerebellar sulci (upper right panel). In addition the occasional focal aggregates of RML were systematically located near the sulci. Deposition of fibrillar aggregates from RML, 22L, 79A and 139A started at in the Purkinje cell and granular layers as shown by staining performed at 21 DPI (Figure 43) and progressively extended towards the molecular layer for ultimately covering the entire slices.

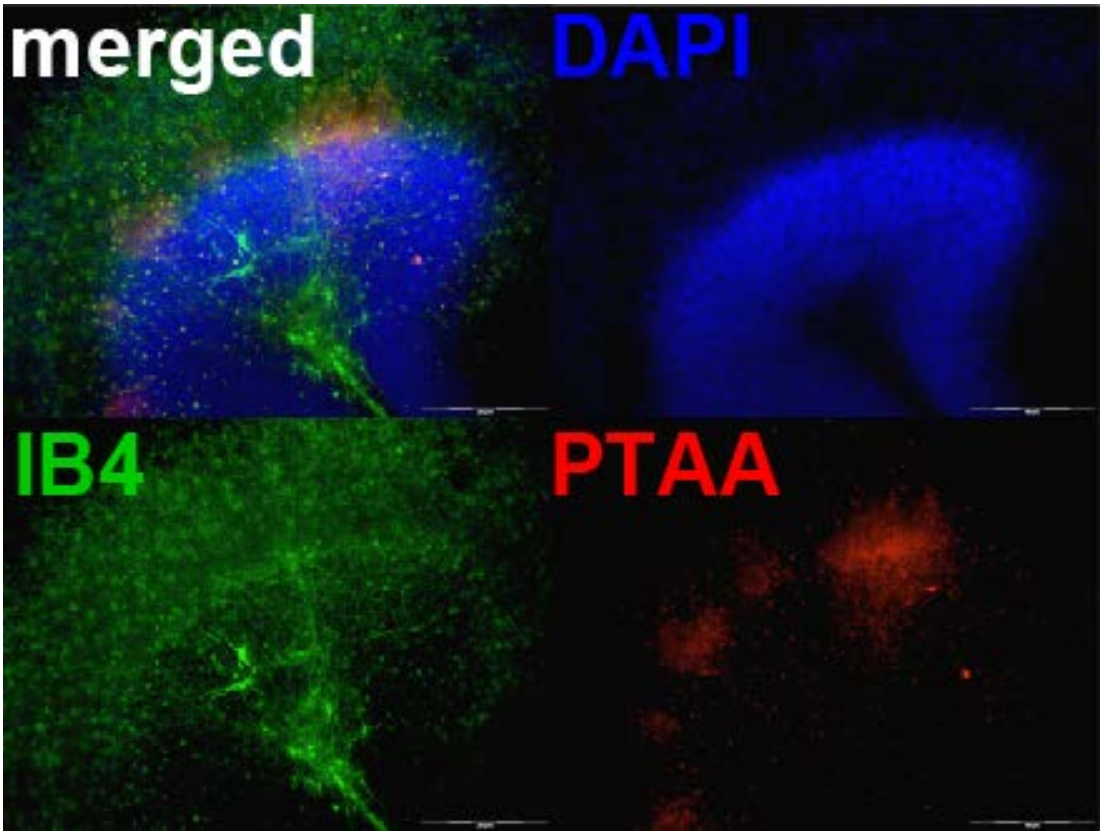

Figure 43: Deposition of prion aggregates in COCS.

Diffuse RML aggregates at 21 DPI. IB4 stands for isolectin B4 and stains microglia and blood vessels. Scale bar: 200 µm.

Aggregates from 301C had a predominantly focal morphology; however, unlike ME7 and MSS, the aggregates were randomly distributed throughout the tissue (not shown). Interestingly, slices from 7 day-old mice yielded more abundant prion accumulation than slices from 14 day-old mice (Figure 44 and Figure 45), suggesting that prion replication is enhanced during phases of intense cell replication and/or migration or by cellular interactions.

However, the deposition pattern was more precise in slices from 14 day-old mice, probably linked with achieved organisation of the cerebellar tissue.

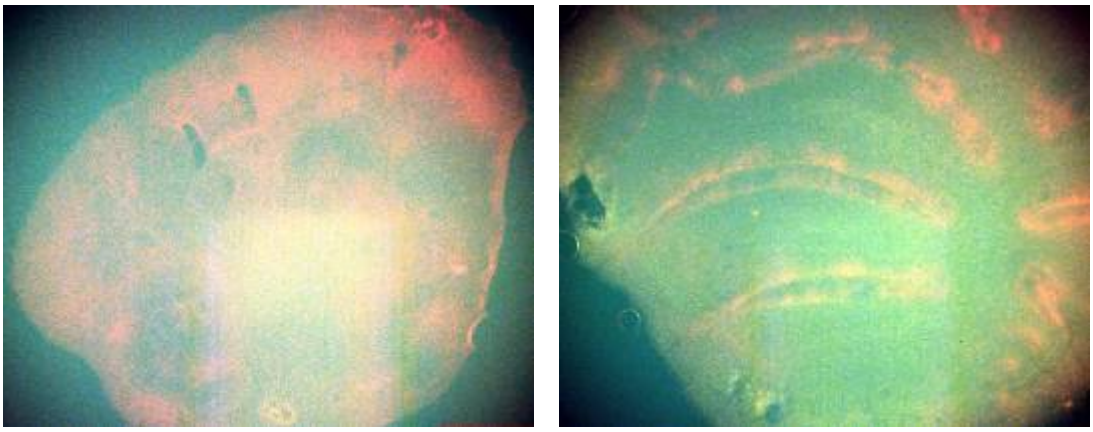

Figure 44: Accumulation of prion aggregates in COCS prepared from 7 or 14 days old pups.

RML aggregates at 35 DPI in PTAA-stained slices from 7 day-old mice (left panel) or 14 day old mice (right panel). Pictures were taken at a 10x magnification. Red fluorescence corresponds to PTAA bound to prion aggregates; green fluorescence corresponds to PTAA bound to various components of the tissue.

Figure 45: Accumulation of RML prions in COCS prepared from 7 or 14 days old pups.

Immunoblots showing PK-resistant material at 35 DPI in COCS from 7 days old mice (third lane: *tg*a20 RML, 7 d.o.) or 14 days old mice (seventh lane: *tg*a20 RML, 14 d.o.). *tg*a20 mock: uninfected COCS. First lane: RML BH undigested, 10 mg. Aliquots of 20 mg protein were digested with PK to remove soluble PrP and loaded to the gel. The anti-PrP antibody POM1 was used for the detection. Molecular sizes are indicated in kDa.

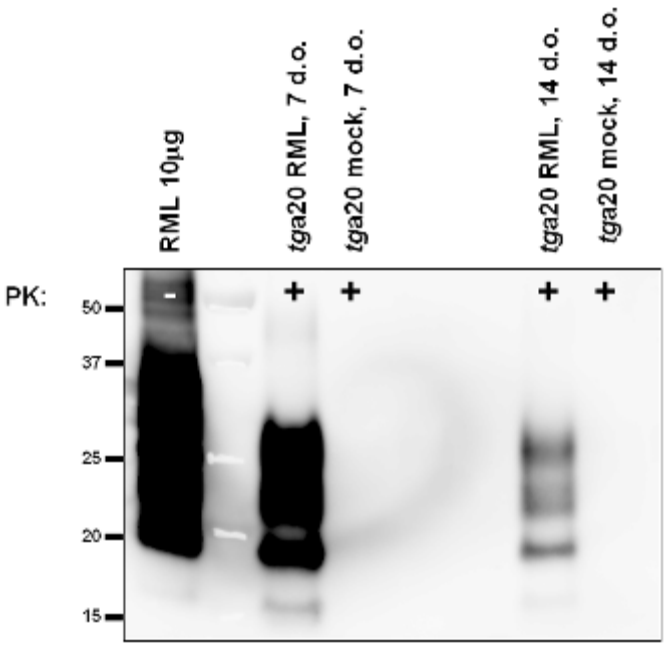

DISCUSSION

Spectral profile of mouse-adapted prion strains *in vivo* and *in vitro*

Although the aim of this work was to point out spectral differences that are linked with structural differences of aggregates, it is difficult to avoid the contribution of the background tissue to the analyzed spectra. However, the extent of contribution of the background reflects the extent of prion-induced neurodegeneration, which is a parameter used in vivo to discriminate prion strains and may therefore strengthen the potential of PTAA-stained COCS for discriminating prion strains. Sigurdson et al. discriminated mouse-adapted prion strains originating from different species (cervid, ovine and bovine prions) (Sigurdson et al., 2007). The present analysis further confirms the efficiency of PTAA for discriminating prion strains originating from different species (caprine, ovine and bovine prions) on the basis of the structure of the aggregates and possibly also on prion-induced neurodegeneration.

Aggregates from the ME7 strain had different spectra in COCS at 35 or 56 DIV or *in vivo*. Of note, these spectra evolved during the course of culturing in COCS from red-shifted (at 35 DIV: closer to spectra of ME7 aggregates *in vivo*) towards green-shifted aggregates. It is possible that ME7 exists *in vivo* as an ensemble of prion aggregates with heterogenous quaternary structures and that the simplified *in vitro*-cultured cerebellar environment provides an advantage to fewer prion forms that prevail after a certain culturing time. It is also possible that the artificial *in vitro*-cultured cerebellar environment enables strain cloning (isolation of a prion "substrain") or even the generation of a new strain. In conclusion, it seems that prion aggregates from the ME7 strain (and possibly from other strains) may have a different structure in *in vitro*-cultured cerebellar tissue than in cortical tissue from terminally-sick mice.

Finally, spectral analysis of prions aggregates from different strains using monodisperse LCP preparation such as H7A, a heptameric and pFTAA, a pentameric version of PTAA, showed the potential of new generations of LCPs to increase the resolution of this method as spectral differences between strains were more marked than with PTAA (data not shown).

Additional features of prion strains in COCS

The prion strains investigated in this work can be discriminated into two groups according to the abundance of PK-resistant material previously observed on WB at 35 DPI: the fast replicating strains RML, 22L, 139A and 79A and the slow replicating ME7, MSS and 301C. The same two groups harbour prion aggregates with distinct morphologies, respectively diffuse or focal PTAA-stained prion deposits. In addition these strains yielded aggregates with

at least three different deposition patterns (location in the molecular layer, sulci or random), which may provide an additional way of classifying prion strains and suggests a link between localization of deposits and cell types present in different locations of the tissue.

OUTLOOK

This work proposes spectral analysis of LCP-stained prions in COCS as a new tool for the characterization of prion strains on the basis of the structure of strain-specific PrP aggregates. Furthermore the replication rate of prion strains and the morphology and deposition pattern of prion aggregates in COCS may be used to generate a new method for prion strain classification. In addition these differences may help pointing out the involvement of different cell types in prion strain replication. Finally, this work may initiate follow-up projects for investigating the phenomena of prion strain adaptation and prion strain competition.

MATERIAL AND METHODS PART II

Preparation of CD1 and RML6 crude brain homogenate

20% wt/vol RML6 or CD1 brain homogenates in 0.32M sucrose in PBS were prepared by three runs in a PreCellys tissue homogenizer with cooling on ice between each run. Protein concentrations of RML6 or CD1 brain homogenates were determined using the bicinchoninic acid assay (Pierce) and normalized to 1 mg/ml total protein with 0.32M sucrose in PBS.

Preparation of LCP stock solutions

The synthesis of the different LCPs has been described elsewhere (Ding et al., 2000). Lyophilized LCPs were resuspended in pure water (B.Braun, Melsungen AG) and stock solutions at a concentration of 1 mg/ml were prepared and stored at 4°C, protected from light. Serial dilutions of the LCPs were prepared in pure water. For PTAA I used a stock with a concentration of approximately 3 mg/ml. This stock was the same as used for the publication from Sigurdson et al. (Sigurdson et al., 2007).

PTAA staining and slides preparation

PTAA staining of COCS was performed directly on the tissue still sitting on the culture membrane and then transferred to a glass slide. First, cultures were washed twice with 5 ml PBS and fixed with pre-cooled (-20°C) 100% ethanol for 10 min at RT. Cultures were rinsed

twice for 15 min in 5ml PBS and staining with LCPs was performed as described in (Sigurdson et al., 2007). The PTAA of PTMI stocks were diluted 1:100 in PBS. After rinsing, tissue transfer to the glass slide was performed as follows: excess PBS was carefully removed with a pipet to avoid the cut membrane to fold and membrane was cut with a scalpel blade and detached with a tweezer. Membrane was placed upside-down on a glass slide moistened with a drop of PBS. Excess PBS was removed with a tissue and glass slide was left to dry under a laminar flow until membrane was almost completely dry (appears then white: tissue attaches to the membrane). PBS was added on top of the membrane for 1 min to allow tissue to detach and then membrane was peeled off with a tweezer. Tissue was mounted with Fluorescent Mounting Medium (Dakocytomation) and slides were sealed with nail polish and decontaminated for 2 h with 2 M NaOH.

Spectral acquisition

I recorded spectra with a Zeiss Axioplan 2 microscope fitted with a Spectraview 4.0 (Applied Spectral Imaging) and a Spectra-Cube (interferometrical optical head SD 300) module with cooled charge-coupled device (CCD) camera, through a 405/30 nm (LP470) or a 470/40 nm (LP515) bandpass filter. The data were processed with SpectraView 3.0 EXPO. I collected spectra from LCP-stained PrP aggregates (8 individual spots for each sample) and other fluorescent entities.

Preparation of slice culture homogenates

Tissue was harvested in PBS and homogenized according to Falsig et al in PBS. Protein concentration was determined using the bicinchoninic acid assay (Pierce) and normalized to 1 mg/ml total protein with PBS.

Proteolysis of COCSBH and Western blot analysis

PrP^{Sc} was detected by limited proteolysis with proteinase K (PK) (Roche) and analysed by Western blotting. 20 μg protein aliquots were digested with 25 μg/ml PK in lysis buffer containing 0.5% wt/vol sodium deoxycholate, 0.5% vol/vol Nonidet P-40 and 10% vol/vol PBS for 60 min at 37°C and rotating at 700 rpm on a thermoshaker in a total volume of 20 μl. This condition allowed specific detection of PrP^{Sc}. PK digestion was terminated by adding 6.7 μl of 4x LDS loading buffer (NuPAGE, Invitrogen) and boiling the samples at 95 °C for 5 min. 20 μl of the samples were separated on a 12% Bis-Tris SDS polyacrylamide gel (NuPAGE, Invitrogen) and blotted onto a nitrocellulose membrane. Membranes were blocked

with 5% wt/vol Topblock (Fluka) in Tris-buffered saline supplemented with Tween (150 mM NaCl, 10 mM Tris HCl, 0.05% Tween 20 (vol/vol)) and incubated with POM1 (Polymenidou et al., 2005) mouse IgG1 antibody to PrP^{C} (anti-PrP^{C}) (200 ng/ml) as primary antibody. Horse radish peroxidase (HRP)-conjugated rabbit anti–mouse IgG1 (1:10,000, Zymed) was used as a secondary antibody. The blots were developed using SuperSignal West Pico chemiluminescent substrate (Pierce) and detected in a LAS3000 system (FUJI).

Immunohistochemistry

For immunocytochemistry of *in vitro* material, the organotypic slice cultures were washed twice in PBS and fixed in 4% formalin overnight at 4 °C. Membrane inserts were washed and incubated for 1 h in blocking buffer (0.05% vol/vol Triton X-100 and 3% vol/vol goat serum dissolved in PBS) and incubated with the primary antibody diluted in blocking buffer at 4 °C for 3 days. The ALEXA488-conjugated mouse antibody IB4 (Isolectin B4, 1 μg ml^{-1}, Molecular Probes) was used for staining microglia and counterstained with 4,6-diamidino-2-phenylindole (dapi) (1 μg ml^{-1}). Additional staining with PTAA was performed and sections sitting on their culture membrane were transferred on glass slides (with tissue facing up, unlike for spectral analysis). Images were recorded on a fluorescence microscope (BX-61, Olympus) equipped with a cooled black/white CCD camera.

PART III: COLLABORATIVE WORK

Humanized mice project

My activities as a Research Assistant included participation to the elaboration of a model of transgenic mice lacking B and T cells ($C\gamma^{-/-}RAG2^{-/-}$) which immune system was reconstituted with human embryonic stem cells. This work was performed in a collaborative framework with PD Dr. Heikenwalder and Dr. Hayback. The main goal of this project is to investigate peripheral prion pathogenesis of human prions. My activities included negotiation of written consents for donation of placental tissue, extraction of blood from placenta, purification of human stem cells, analysis of cells and blood from reconstituted mice with FACS analysis and reconstitution, inoculation with human prions (sCJD) and housing of mice as well as, dissection and tissue analysis by WB of prion-inoculated humanized mice (Figure 46). My work has notably helped obtaining high efficiency of engraftment of human $CD34^+$ cells in $Cg^{-/-}RAG2^{-/-}$ mice (Figure 46). "Humanized" mice showed a high degree of $CD45^+$ cells in peripheral blood as well as human lymphocytes in white pulp follicles of spleens and mesenteric lymph nodes (MLNs) (data not shown). Interestingly, the degree of $CD19^+$ cells in peripheral blood was very high at the age of 8-16 weeks and declined over time (data not shown). Importantly, after inoculation with human prions (sCJD 129MM), spleens and MLNs do not show PK-resistant material at 30 DPI (data not shown). However, PrP^{Sc} can be detected by WB analysis in spleen at 60 and 90 DPI (data not shown) and at 120 DPI (Figure 48A). Optimization by me of the protocol for enrichment for human prions from spleen homogenates of these mice has been necessary for obtaining the results in Figure 48A.

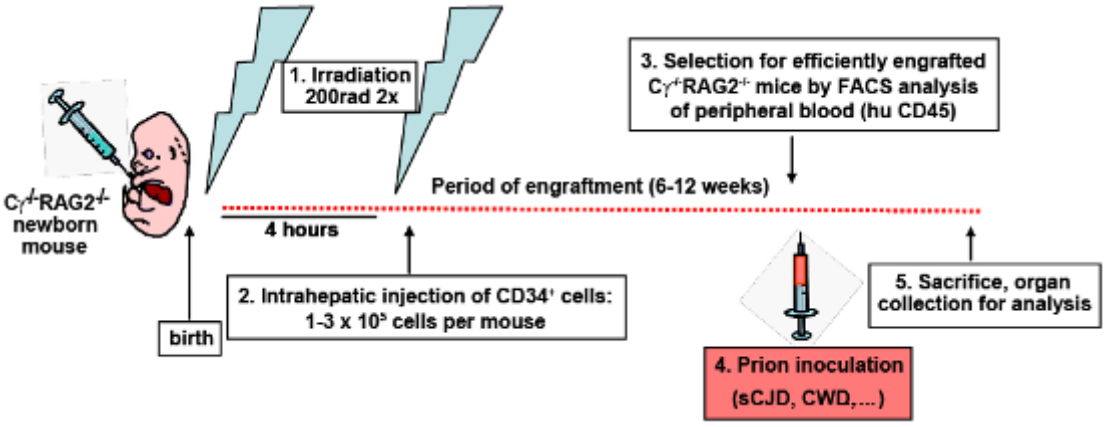

Figure 46: Inoculation scheme.

After birth, $Cg^{-/-}RAG2^{-/-}$ newborn mice are irradiated. After the second irradiation round, $CD34^+$ cells are inoculated intra-hepatically. After assessment of engraftment with hu $CD45^+$ cells by FACS analysis of peripheral blood, human prions (sCJD) are inoculated intra-peritoneally. After various time points organs are collected for further analysis.

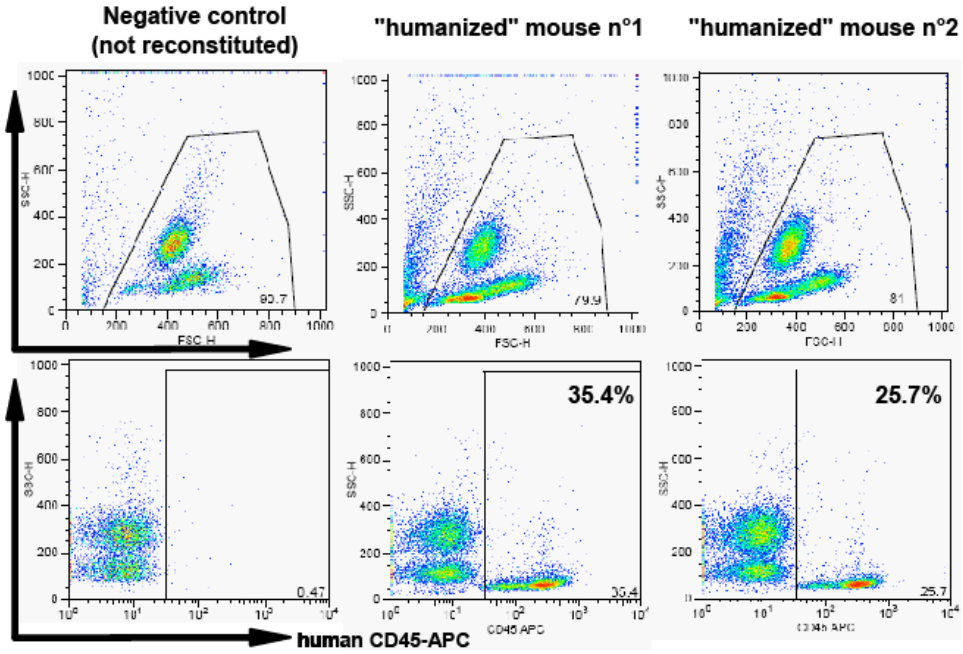

Figure 47: Control of efficiency of engraftment with CD34^{+} cells.

FACS analysis for human CD45-APC^{+} cells in peripheral blood from reconstituted mice at 6-12 weeks post reconstitution. Upper panels: Gate for living cells isolated from blood. Lower panels: Living cells gated for human CD45. Efficiency of engraftment (percentage of hu-CD45^{+} cells) shows a variation (e.g. 34.4%, 25.7%). Approximately 70% of all mice have an engraftment larger than 5%. Cg$^{-/-}$RAG2$^{-/-}$ non reconstituted mice analyzed as negative controls show a negligible background (e.g. 0.47%). SSC = sideward scatter. FSC = forward scatter. Human CD45 is used as a panleucocytic marker (leukocyte common antigen).

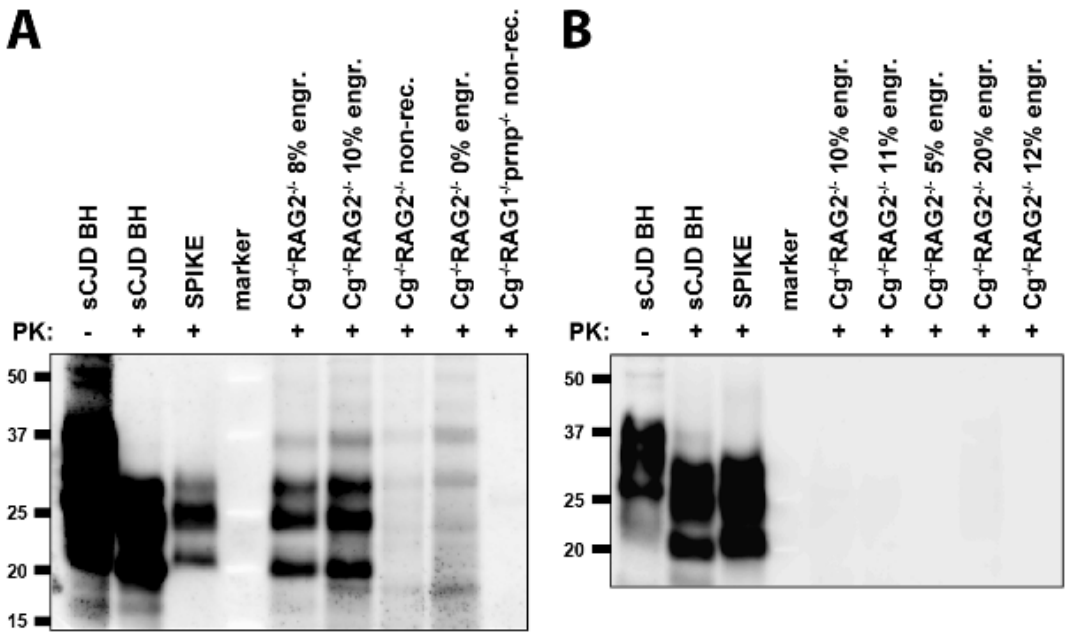

Figure 48: PK-resistant material in sCJD prion-infected humanized mice

Immunoblots of spleens from (**A**) sCJD-inoculated humanized mice and (**B**) CWD-inoculated humanized mice at 120 DPI. Spleens are homogenized in PBS. Sodium phosphotungstic acid precipitation is used to concentrate PrP^{Sc} from 500 µl spleen homogenate (lanes 3-9). The resulting pellet undergoes PK digestion and is loaded on a SDS-Gel (12%). The nitrocellulose membrane is probed with 3F4 (anti-human PrP antibody). SPIKE: 120 µg sCJD BH (from a terminally sick patient) in 500 µl Cγ$^{-/-}$RAG2$^{-/-}$ spleen homogenate (10%). sCJD BH: 40 µg (-PK) or 80 µg (+PK) sCJD BH (from a terminally sick patient). Molecular sizes are indicated in kDa.

OUTLOOK

Further analysis by histoblot and transmission of spleen homogenates will validate our results. Of note, mice inoculated with BH pooled from several cervids that succumbed to CWD (homogenate kindly provided by Dr. C.J. Sigurdson) do not show PK-resistant material at 90 DPI in spleens (Figure 48B) neither in MLNs (data nor shown). Mice challenged with BSE prions also failed to replicate prions (data not shown).

MATERIAL AND METHODS PART III

Extraction of embryonic stem cells from cord blood

A mixture of cord blood and anticoagulant was distributed in 50 ml Ficoll tubes (50 ml Falcon with filter and 15 ml Ficoll briefly centrifuged at 300g) using PBS to adjust volumes. About 20 ml undiluted blood was poured in each Ficoll tube. Tubes were centrifuged for 20 min at 600g, RT, without brakes to avoid disturbance of the white blood cell interface formed during centrifugation. SN was aspirated and then cells of interest were isolated including liquid up to the filter. This mixture was then dispatched to new 50 ml Falcon tubes, pouring 15 ml per tube and adding washing buffer (PBS supplemented with 2mM EDTA). Centrifugation (150g, 10 min, RT) to get rid of thrombocytes, SN was aspirated and cells were pooled and diluted to 50 ml with washing buffer. At that point a 30 µl aliquot was set aside for cell counting. After another round of centrifugation (300g, 7 min, RT) SN was aspirated and cells were resuspended in MACS buffer (PBS supplemented with 2mM EDTA and 0.5% v/v BSA) and supplemented with FCR-blocker (Miltenyi Biotech GmbH) and antibody-coupled beads (Miltenyi Biotech GmbH) (300 µl MACS buffer, 100 µl FCR-blocker and 100 µl beads per 100 mio cells) and incubated for 30 min at 4°C in a fridge. After this point, only cold MACS buffer was used (4°C). Cells were washed in 20 ml cold MACS buffer and centrifuged (300g, 7 min, RT), SN was discarded. Cells were resuspended in 5 ml cold MACS buffer and kept on ice. Two LS columns (Miltenyi Biotech GmbH) were pre-rinsed with 3 ml MACS buffer prior to placement in a magnetic field (QuadroMACS magnet, Miltenyi Biotech GmbH). Cells were applied to the first column and non-target fraction (NTF) was collected in a 50 ml Falcon tube. Column was washed 3 times with 3 ml MACS buffer while non-target fraction was collected in the 50 ml Falcon tube. Column was then placed in a 15 ml Falcon tube, away from the magnetic field, and target fraction (TF) was flushed out using 2 times 2.5 ml MACS buffer. TF in the 15 ml Falcon tube was then applied to the second column in the magnetic

field and handled in the same manner with collecting NTF in the 50 ml Falcon tube. Finally, TF was flushed out from the second column into a 15 ml Falcon tube using 3 ml MACS buffer. Aliquots were taken from both fractions (50 µl from TF, 200 µl from NTF) for cell counting and FACS analysis. TF and NTF were centrifuged (300 g, 7 min, RT), resuspended in freshly prepared freezing medium (90% v/v Foetal Calf Serum, 10% v/v DMSO) and aliquoted (TF: 1.2 mio cells in 1 ml, NTF: 30-40 mio cells in 1 ml). Tubes were placed in a freezing box filled with isopropanol and stored in a fridge for 60 min and then in a -80°C freezer overnight. Tubes were then transferred to a liquid nitrogen tank for longer storage.

Cell staining for FACS analysis

TF was stained as follows: 20 µl TF, 30 µl FACS buffer (PBS supplemented with 2 mM EDTA and 0.1% w/v sodium azide), 1 µl CD34-APC, 1 µl CD3-PE. NTF was stained as follows: 50 µl NTF, 50 µl FACS buffer, 2 µl CD34-APC, 2 µl CD3-PE or left unstained: 50 µl NTF, 50 µl FACS buffer. All aliquots were incubated for 30 min at 4 °C and washed once with 2 ml FACS buffer. Cell viability was briefly checked with trypan blue staining (10 µl TF, 10 µl trypan blue stain 0.4%, Invitrogen). If stained cells were not analyzed by FACS immediately (not ideal), cells were fixed as follows: cells were resuspended in 1 ml FACS buffer supplemented with 0.5% v/v paraformaldehyde (PF), centrifuged (300 g, 3 min, RT), resuspended in 150 µl FACS buffer and stored overnight at 4°C in the dark. Cells obtained from tail blood from humanized mice were stained as follows: 4-5 drops of tail blood were collected in 2 ml FACS buffer and centrifuged (300 g, 7 min, RT). SN was aspirated and cells were stained with a mastermix (50 µl mastermix per pellet) prepared with human CD45-APC (human lymphocytes), CD4-FITC (helper T cells) and CD19-PE (B cells) (each Ab diluted 1:20 in FACS buffer). Samples were vortexed and incubated for 30 min at 4°C in the dark. 1 ml BD FACS lysis solution was added, samples were vortexed and incubated for 10 min at RT in the dark. Samples were washed twice with 2 ml FACS buffer and centrifuged (300 g, 7 min, RT). SN was removed until about 100 µl was left in the tube and cells were resuspended with FACS buffer. FACS analysis was performed until about 20,000 events were recorded.

Isolation of DNA from NTF or whole blood

Isolation of DNA from either NTF or whole blood obtained from humanized mice was performed using a DNA isolation kit from QIAGEN according to the manufacturer's instructions. DNA purity was checked in a spectrophotometer and samples were handed over

to Prof. Zimmermann (University Hospital, Zürich) for sequencing of the region of the *prnp* gene containing the 129 codon. Mice engrafted with stem cells originating from a patient harbouring the 129MM phenotype are ideal candidates for exposure to human prions.

Reconstitution of newborn mice with human stem cells

Frozen aliquots of human stem cells were thawn at 37°C in a water bath and centrifuged (300 g, 5 min, RT). SN was removed, leaving about 100 µl and cells were resuspended in 1 ml PBS. Cells were centrifuged (300 g, 5 min, RT) and SN was removed, leaving about 50 µl. Cells were resuspended in PBS to obtain about 100-200 mio cells per 30 µl. 30 µl was inoculated in the liver of irradiated newborns from $C\gamma^{-/-}RAG2^{-/-}$ mice. Mice were housed for 6-12 weeks post reconstitution prior to challenge with BSE, human or CWD prions.

Sodium phosphotungstic acid precipitation and Western blot analysis

Enrichment for prions was performed on organ homogenates from sacrificed mice using a previously published protocol (Ligios et al., 2007) with the following modifications:
1. A 5- 10% organ homogenate was used when organs were too small. 2. The final pellet was resuspended in 500 µl PBS and ultracentrifuged (150,000 g for 1 h at 4°C). SN was removed and pellet was resuspended in 50-100 µl PBS. 3. After digestion with PK (50 µg/ml) samples were applied to a 1.5 mm thick 12% Bis-Tris SDS polyacrylamide gel (NuPAGE, Invitrogen) to allow loading of up to 80 µl sample (note: blotting such a gel needs increasing transfer time by 1 h). Western blot analysis was performed as described above with the following modifications: 1. Blocking of the membrane was performed in 2% w/v BSA in TBST. 2. The Ab 3F4 (1:2000 in 2% w/v BSA in TBST) was used as a primary Ab with IGg2a (1:5000 in 2% w/v BSA in TBST) as a secondary Ab. Picture acquisition was performed for 15 min in a LAS3000 system (FUJI).

REFERENCES

Abelein A, Bolognesi B, Dobson CM, Graslund A, Lendel C (2012) Hydrophobicity and conformational change as mechanistic determinants for nonspecific modulators of amyloid beta self-assembly. Biochemistry 51:126-137.

Aguzzi A (1996) Pathogenesis of spongiform encephalopathies: an update. Int Arch Allergy Immunol 110:99-106.

Aguzzi A (2006) Prion diseases of humans and farm animals: epidemiology, genetics, and pathogenesis. J Neurochem 97:1726-1739.

Aguzzi A, Weissmann C (1996) Spongiform encephalopathies: a suspicious signature. Nature 383:666-667.

Aguzzi A, Weissmann C (1997) Prion research: the next frontiers. Nature 389:795-798.

Aguzzi A, Haass C (2003) Games played by rogue proteins in prion disorders and Alzheimer's disease. Science 302:814-818.

Aguzzi A, Polymenidou M (2004a) Mammalian prion biology: one century of evolving concepts. Cell 116:313-327.

Aguzzi A, Polymenidou M (2004b) Mammalian prion biology. One century of evolving concepts. Cell 116:313-327.

Aguzzi A, Calella AM (2009) Prions: protein aggregation and infectious diseases. Physiol Rev 89:1105-1152.

Aguzzi A, Heikenwalder M, Polymenidou M (2007) Insights into prion strains and neurotoxicity. Nat Rev Mol Cell Biol 8:552-561.

Aguzzi A, Baumann F, Bremer J (2008) The prion's elusive reason for being. Annu Rev Neurosci 31:439-477.

Alper T, Haig DA, Clarke MC (1966) The exceptionally small size of the scrapie agent. Biochem Biophys Res Commun 22:278-284.

Alper T, Cramp WA, Haig DA, Clarke MC (1967) Does the agent of scrapie replicate without nucleic acid? Nature 214:764-766.

Apetri AC, Vanik DL, Surewicz WK (2005) Polymorphism at residue 129 modulates the conformational conversion of the D178N variant of human prion protein 90-231. Biochemistry 44:15880-15888.

Appleby BS, Lyketsos CG (2011) Rapidly progressive dementias and the treatment of human prion diseases. Expert Opin Pharmacother 12:1-12.

Aslund A, Herland A, Hammarstrom P, Nilsson KP, Jonsson BH, Inganas O, Konradsson P (2007) Studies of luminescent conjugated polythiophene

derivatives: enhanced spectral discrimination of protein conformational states. Bioconjug Chem 18:1860-1868.

Aslund A, Sigurdson CJ, Klingstedt T, Grathwohl S, Bolmont T, Dickstein DL, Glimsdal E, Prokop S, Lindgren M, Konradsson P, Holtzman DM, Hof PR, Heppner FL, Gandy S, Jucker M, Aguzzi A, Hammarstrom P, Nilsson KP (2009) Novel pentameric thiophene derivatives for in vitro and in vivo optical imaging of a plethora of protein aggregates in cerebral amyloidoses. ACS Chem Biol 4:673-684.

Baker HE, Poulter M, Crow TJ, Frith CD, Lofthouse R, Ridley RM (1991) Aminoacid polymorphism in human prion protein and age at death in inherited prion disease. Lancet 337:1286.

Barron RM, Campbell SL, King D, Bellon A, Chapman KE, Williamson RA, Manson JC (2007) High titers of transmissible spongiform encephalopathy infectivity associated with extremely low levels of PrPSc in vivo. J Biol Chem 282:35878-35886.

Basler K, Oesch B, Scott M, Westaway D, Walchli M, Groth DF, McKinley MP, Prusiner SB, Weissmann C (1986) Scrapie and cellular PrP isoforms are encoded by the same chromosomal gene. Cell 46:417-428.

Bendheim PE, Barry RA, DeArmond SJ, Stites DP, Prusiner SB (1984) Antibodies to a scrapie prion protein. Nature 310:418-421.

Benito-Leon J (2004) Combined quinacrine and chlorpromazine therapy in fatal familial insomnia. Clin Neuropharmacol 27:201-203.

Beringue V, Vilotte JL, Laude H (2008) Prion agent diversity and species barrier. Vet Res 39:47.

Bolton DC, McKinley MP, Prusiner SB (1982) Identification of a protein that purifies with the scrapie prion. Science 218:1309-1311.

Bolton DC, Meyer RK, Prusiner SB (1985) Scrapie PrP 27-30 is a sialoglycoprotein. J Virol 53:596-606.

Borchelt DR, Scott M, Taraboulos A, Stahl N, Prusiner SB (1990) Scrapie and cellular prion proteins differ in their kinetics of synthesis and topology in cultured cells. J Cell Biol 110:743-752.

Brandner S, Raeber A, Sailer A, Blattler T, Fischer M, Weissmann C, Aguzzi A (1996) Normal host prion protein (PrPC) is required for scrapie spread within the central nervous system. Proc Natl Acad Sci U S A 93:13148-13151.

Bremer J, Baumann F, Tiberi C, Wessig C, Fischer H, Schwarz P, Steele AD, Toyka KV, Nave KA, Weis J, Aguzzi A (2010) Axonal prion protein is required for peripheral myelin maintenance. Nat Neurosci 13:310-318.

Breyer J, Wemheuer WM, Wrede A, Graham C, Benestad SL, Brenig B, Richt JA, Schulz-Schaeffer WJ (2012) Detergents modify proteinase K resistance of

PrP(Sc) in different transmissible spongiform encephalopathies (TSEs). Vet Microbiol 157:23-31.

Brockes JP (1999) Topics in prion cell biology. Curr Opin Neurobiol 9:571-577.

Brown LR, Harris DA (2003) Copper and zinc cause delivery of the prion protein from the plasma membrane to a subset of early endosomes and the Golgi. J Neurochem 87:353-363.

Bruce M, Chree A, McConnell I, Foster J, Pearson G, Fraser H (1994) Transmission of bovine spongiform encephalopathy and scrapie to mice: strain variation and the species barrier. Philos Trans R Soc Lond B Biol Sci 343:405-411.

Bruce ME (1993) Scrapie strain variation and mutation. Br Med Bull 49:822-838.

Bruce ME (2003) TSE strain variation. Br Med Bull 66:99-108.

Bruce ME, Boyle A, Cousens S, McConnell I, Foster J, Goldmann W, Fraser H (2002) Strain characterization of natural sheep scrapie and comparison with BSE. J Gen Virol 83:695-704.

Büeler HR, Aguzzi A, Sailer A, Greiner RA, Autenried P, Aguet M, Weissmann C (1993) Mice devoid of PrP are resistant to scrapie. Cell 73:1339-1347.

Büeler HR, Fischer M, Lang Y, Bluethmann H, Lipp HP, DeArmond SJ, Prusiner SB, Aguet M, Weissmann C (1992) Normal development and behaviour of mice lacking the neuronal cell-surface PrP protein. Nature 356:577-582.

Cancellotti E, Wiseman F, Tuzi NL, Baybutt H, Monaghan P, Aitchison L, Simpson J, Manson JC (2005) Altered glycosylated PrP proteins can have different neuronal trafficking in brain but do not acquire scrapie-like properties. J Biol Chem 280:42909-42918.

Capobianco R et al. (2007) Conversion of the BASE prion strain into the BSE strain: the origin of BSE? PLoS Pathog 3:e31.

Casalone C, Zanusso G, Acutis P, Ferrari S, Capucci L, Tagliavini F, Monaco S, Caramelli M (2004) Identification of a second bovine amyloidotic spongiform encephalopathy: molecular similarities with sporadic Creutzfeldt-Jakob disease. Proc Natl Acad Sci U S A 101:3065-3070.

Caspi S, Halimi M, Yanai A, Sasson SB, Taraboulos A, Gabizon R (1998) The anti-prion activity of Congo red. Putative mechanism. J Biol Chem 273:3484-3489.

Caughey B, Lansbury PT (2003) Protofibrils, pores, fibrils, and neurodegeneration: separating the responsible protein aggregates from the innocent bystanders. Annu Rev Neurosci 26:267-298.

Caughey B, Race RE, Ernst D, Buchmeier MJ, Chesebro B (1989) Prion protein biosynthesis in scrapie-infected and uninfected neuroblastoma cells. J Virol 63:175-181.

Chandler RL, Fisher J (1963) Experimental Transmission of Scrapie to Rats. Lancet 2:1165.

Chesebro B, Race R, Wehrly K, Nishio J, Bloom M, Lechner D, Bergstrom S, Robbins K, Mayer L, Keith JM, et al. (1985) Identification of scrapie prion protein-specific mRNA in scrapie-infected and uninfected brain. Nature 315:331-333.

Chesebro B, Trifilo M, Race R, Meade-White K, Teng C, LaCasse R, Raymond L, Favara C, Baron G, Priola S, Caughey B, Masliah E, Oldstone M (2005) Anchorless prion protein results in infectious amyloid disease without clinical scrapie. Science 308:1435-1439.

Chiesa R, Piccardo P, Quaglio E, Drisaldi B, Si-Hoe SL, Takao M, Ghetti B, Harris DA (2003) Molecular distinction between pathogenic and infectious properties of the prion protein. J Virol 77:7611-7622.

Christen B, Hornemann S, Damberger FF, Wuthrich K (2009) Prion protein NMR structure from tammar wallaby (Macropus eugenii) shows that the beta2-alpha2 loop is modulated by long-range sequence effects. J Mol Biol 389:833-845.

Collinge J (2005) Molecular neurology of prion disease. J Neurol Neurosurg Psychiatry 76:906-919.

Collinge J, Palmer MS, Dryden AJ (1991) Genetic predisposition to iatrogenic Creutzfeldt-Jakob disease. Lancet 337:1441-1442.

Collinge J, Sidle KC, Meads J, Ironside J, Hill AF (1996) Molecular analysis of prion strain variation and the aetiology of 'new variant' CJD. Nature 383:685-690.

Collinge J, Whittington MA, Sidle KC, Smith CJ, Palmer MS, Clarke AR, Jefferys JG (1994) Prion protein is necessary for normal synaptic function. Nature 370:295-297.

Collinge J, Whitfield J, McKintosh E, Beck J, Mead S, Thomas DJ, Alpers MP (2006) Kuru in the 21st century--an acquired human prion disease with very long incubation periods. Lancet 367:2068-2074.

Collinge J, Gorham M, Hudson F, Kennedy A, Keogh G, Pal S, Rossor M, Rudge P, Siddique D, Spyer M, Thomas D, Walker S, Webb T, Wroe S, Darbyshire J (2009) Safety and efficacy of quinacrine in human prion disease (PRION-1 study): a patient-preference trial. Lancet Neurol 8:334-344.

Cuille J, Chelle PL (1939) Experimental transmission of trembling to the goat. C R Seances Acad Sci 208:1058-1160.

DeArmond SJ (1993) Alzheimer's disease and Creutzfeldt-Jakob disease: overlap of pathogenic mechanisms. Curr Opin Neurol 6:872-881.

DeArmond SJ, McKinley MP, Barry RA, Braunfeld MB, McColloch JR, Prusiner SB (1985) Identification of prion amyloid filaments in scrapie-infected brain. Cell 41:221-235.

Ding L, Jonforsen M, Roman LS, Andersson M, Inganäs O (2000) Photovoltaic cells with a conjugated poly electrolyte. Synth Met 110:133 140

Dodelet VC, Cashman NR (1998) Prion protein expression in human leukocyte differentiation. BLOOD 91:1556-1561.

Donne DG, Viles JH, Groth D, Mehlhorn I, James TL, Cohen FE, Prusiner SB, Wright PE, Dyson HJ (1997) Structure of the recombinant full-length hamster prion protein PrP(29-231): the N terminus is highly flexible. Proc Natl Acad Sci U S A 94:13452-13457.

Edgeworth JA, Gros N, Alden J, Joiner S, Wadsworth JD, Linehan J, Brandner S, Jackson GS, Weissmann C, Collinge J (2010) Spontaneous generation of mammalian prions. Proc Natl Acad Sci U S A 107:14402-14406.

Eiden M, Hoffmann C, Balkema-Buschmann A, Muller M, Baumgartner K, Groschup MH (2010) Biochemical and immunohistochemical characterization of feline spongiform encephalopathy in a German captive cheetah. J Gen Virol 91:2874-2883.

Enari M, Flechsig E, Weissmann C (2001) Scrapie prion protein accumulation by scrapie-infected neuroblastoma cells abrogated by exposure to a prion protein antibody. Proc Natl Acad Sci U S A 98:9295-9299.

Falsig J, Aguzzi A (2008) The prion organotypic slice culture assay--POSCA. Nat Protoc 3:555-562.

Falsig J, Julius C, Margalith I, Schwarz P, Heppner FL, Aguzzi A (2008) A versatile prion replication assay in organotypic brain slices. Nat Neurosci 11:109-117.

Fischer M, Rülicke T, Raeber A, Sailer A, Moser M, Oesch B, Brandner S, Aguzzi A, Weissmann C (1996) Prion protein (PrP) with amino-proximal deletions restoring susceptibility of PrP knockout mice to scrapie. EMBO J 15:1255-1264.

Ford MJ, Burton LJ, Morris RJ, Hall SM (2002) Selective expression of prion protein in peripheral tissues of the adult mouse. Neuroscience 113:177-192.

Gabizon R, McKinley MP, Prusiner SB (1987) Purified prion proteins and scrapie infectivity copartition into liposomes. Proc Natl Acad Sci U S A 84:4017-4021.

Gajdusek DC (1977) Unconventional viruses and the origin and disappearance of kuru. Science 197:943-960.

Gajdusek DC, Gibbs CJ, Alpers M (1966) Experimental transmission of a Kuru-like syndrome to chimpanzees. Nature 209:794-796.

Gibbs CJ, Jr., Gajdusek DC, Asher DM, Alpers MP, Beck E, Daniel PM, Matthews WB (1968) Creutzfeldt-Jakob disease (spongiform encephalopathy): transmission to the chimpanzee. Science 161:388-389.

Griffith JS (1967) Self-replication and scrapie. Nature 215:1043-1044.

Harris DA, Lele P, Snider WD (1993) Localization of the mRNA for a chicken prion protein by in situ hybridization. Proc Natl Acad Sci U S A 90:4309-4313.

Haybaeck J, Heikenwalder M, Klevenz B, Schwarz P, Margalith I, Bridel C, Mertz K, Zirdum E, Petsch B, Fuchs TJ, Stitz L, Aguzzi A (2011) Aerosols transmit prions to immunocompetent and immunodeficient mice. PLoS Pathog 7:e1001257.

Heikenwalder M, Zeller N, Seeger H, Prinz M, Klohn PC, Schwarz P, Ruddle NH, Weissmann C, Aguzzi A (2005) Chronic lymphocytic inflammation specifies the organ tropism of prions. Science 307:1107-1110.

Herland A, Nilsson KP, Olsson JD, Hammarstrom P, Konradsson P, Inganas O (2005) Synthesis of a regioregular zwitterionic conjugated oligoelectrolyte, usable as an optical probe for detection of amyloid fibril formation at acidic pH. J Am Chem Soc 127:2317-2323.

Herms JW, Kretzchmar HA, Titz S, Keller BU (1995) Patch-clamp analysis of synaptic transmission to cerebellar purkinje cells of prion protein knockout mice. Eur J Neurosci 7:2508-2512.

Hijazi N, Shaked Y, Rosenmann H, Ben-Hur T, Gabizon R (2003) Copper binding to PrPC may inhibit prion disease propagation. Brain Res 993:192-200.

Ho HA, Boissinot M, Bergeron MG, Corbeil G, Dore K, Boudreau D, Leclerc M (2002) Colorimetric and fluorometric detection of nucleic acids using cationic polythiophene derivatives. Angew Chem Int Ed Engl 41:1548-1551.

Hornemann S, Christen B, von Schroetter C, Perez DR, Wuthrich K (2009) Prion protein library of recombinant constructs for structural biology. Febs J 276:2359-2367.

Hornemann S, Korth C, Oesch B, Riek R, Wider G, Wuthrich K, Glockshuber R (1997) Recombinant full-length murine prion protein, mPrP(23-231): purification and spectroscopic characterization. FEBS Lett 413:277-281.

Hosszu LL, Baxter NJ, Jackson GS, Power A, Clarke AR, Waltho JP, Craven CJ, Collinge J (1999) Structural mobility of the human prion protein probed by backbone hydrogen exchange. Nat Struct Biol 6:740-743.

Hsiao KK, Groth D, Scott M, Yang SL, Serban H, Rapp D, Foster D, Torchia M, Dearmond SJ, Prusiner SB (1994) Serial transmission in rodents of neurodegeneration from transgenic mice expressing mutant prion protein. Proc Natl Acad Sci U S A 91:9126-9130.

Ingrosso L, Ladogana A, Pocchiari M (1995) Congo red prolongs the incubation period in scrapie-infected hamsters. J Virol 69:506-508.

Jackson GS, Hill AF, Joseph C, Hosszu L, Power A, Waltho JP, Clarke AR, Collinge J (1999) Multiple folding pathways for heterologously expressed human prion protein. Biochim Biophys Acta 1431:1-13.

Jarrett JT, Lansbury PT, Jr. (1993) Seeding "one-dimensional crystallization" of amyloid: a pathogenic mechanism in Alzheimer's disease and scrapie? Cell 73:1055-1058.

Khoor A, Gray ME, Hull WM, Whitsett JA, Stahlman MT (1993) Developmental expression of SP-A and SP-A mRNA in the proximal and distal respiratory epithelium in the human fetus and newborn. J Histochem Cytochem 41:1311-1319.

Klohn PC, Stoltze L, Flechsig E, Enari M, Weissmann C (2003) A quantitative, highly sensitive cell-based infectivity assay for mouse scrapie prions. Proc Natl Acad Sci U S A 100:11666-11671.

Knowles TP, Waudby CA, Devlin GL, Cohen SI, Aguzzi A, Vendruscolo M, Terentjev EM, Welland ME, Dobson CM (2009) An analytical solution to the kinetics of breakable filament assembly. Science 326:1533-1537.

Korth C, May BC, Cohen FE, Prusiner SB (2001) Acridine and phenothiazine derivatives as pharmacotherapeutics for prion disease. Proc Natl Acad Sci U S A 98:9836-9841.

Kranich J, Krautler NJ, Falsig J, Ballmer B, Li S, Hutter G, Schwarz P, Moos R, Julius C, Miele G, Aguzzi A (2010) Engulfment of cerebral apoptotic bodies controls the course of prion disease in a mouse strain-dependent manner. J Exp Med 207:2271-2281.

Lasmezas CI, Deslys JP, Robain O, Jaegly A, Beringue V, Peyrin JM, Fournier JG, Hauw JJ, Rossier J, Dormont D (1997) Transmission of the BSE agent to mice in the absence of detectable abnormal prion protein. Science 275:402-405.

Lau AL, Yam AY, Michelitsch MM, Wang X, Gao C, Goodson RJ, Shimizu R, Timoteo G, Hall J, Medina-Selby A, Coit D, McCoin C, Phelps B, Wu P, Hu C, Chien D, Peretz D (2007) Characterization of prion protein (PrP)-derived peptides that discriminate full-length PrPSc from PrPC. Proc Natl Acad Sci U S A 104:11551-11556.

Lendel C, Bolognesi B, Wahlstrom A, Dobson CM, Graslund A (2010) Detergent-like interaction of Congo red with the amyloid beta peptide. Biochemistry 49:1358-1360.

Li J, Browning S, Mahal SP, Oelschlegel AM, Weissmann C (2010) Darwinian evolution of prions in cell culture. Science 327:869-872.

Ligios C, Cancedda GM, Margalith I, Santucciu C, Madau L, Maestrale C, Basagni M, Saba M, Heikenwalder M (2007) Intraepithelial and interstitial deposition of pathological prion protein in kidneys of scrapie-affected sheep. PLoS ONE 2:e859.

Ligios C, Sigurdson CJ, Santucciu C, Carcassola G, Manco G, Basagni M, Maestrale C, Cancedda MG, Madau L, Aguzzi A (2005) PrPSc in mammary glands of sheep affected by scrapie and mastitis. Nat Med 11:1137-1138.

Lledo PM, Tremblay P, Dearmond SJ, Prusiner SB, Nicoll RA (1996) Mice Deficient For Prion Protein Exhibit Normal Neuronal Excitability and Synaptic Transmission in the Hippocampus. Proceedings of the National Academy of Sciences of the United States of America 93:2403-2407.

Llewelyn CA, Hewitt PE, Knight RS, Amar K, Cousens S, Mackenzie J, Will RG (2004) Possible transmission of variant Creutzfeldt-Jakob disease by blood transfusion. Lancet 363:417-421.

Lu X, Wintrode PL, Surewicz WK (2007) Beta-sheet core of human prion protein amyloid fibrils as determined by hydrogen/deuterium exchange. Proc Natl Acad Sci U S A 104:1510-1515.

Lysek DA, Wüthrich K (2004) Prion protein interaction with the C-terminal SH3 domain of Grb2 studied using NMR and optical spectroscopy. Biochemistry 43:10393–10399.

MacGregor IR, Prowse CV (2004) Impacts and concerns for vCJD in blood transfusion: current status. Curr Mol Med 4:361-373.

MacGregor IR, Dawes J, Pepper DS, Prowse CV, Stocks J (1985) Metabolism of sodium pentosan polysulphate in man measured by a new competitive binding assay for sulphated polysaccharides--comparison with effects upon anticoagulant activity, lipolysis and platelet alpha-granule proteins. Thromb Haemost 53:411-414.

Mallucci G, Dickinson A, Linehan J, Klohn PC, Brandner S, Collinge J (2003) Depleting neuronal PrP in prion infection prevents disease and reverses spongiosis. Science 302:871-874.

Mallucci GR, Ratte S, Asante EA, Linehan J, Gowland I, Jefferys JG, Collinge J (2002) Post-natal knockout of prion protein alters hippocampal CA1 properties, but does not result in neurodegeneration. Embo J 21:202-210.

Mallucci GR WM, Farmer M, Dickinson A, Khatun H, Powell AD, Brandner S, Jefferys JG, Collinge J. (2007) Targeting cellular prion protein reverses early cognitive deficits and neurophysiological dysfunction in prion-infected mice. Neuron 53:325-335.

Manuelidis L, Fritch W, Xi YG (1997) Evolution of a strain of CJD that induces BSE-like plaques. Science 277:94-98.

Margalith I, Suter C, Ballmer B, Schwarz P, Tiberi C, Sonati T, Falsig J, Nystrom S, Hammarstrom P, Aslund A, Nilsson KP, Yam A, Whitters E, Hornemann S, Aguzzi A (2012) Polythiophenes inhibit prion propagation by stabilizing PrP aggregates. J Biol Chem.

Marsh RF, Hadlow WJ (1992) Transmissible mink encephalopathy. Rev Sci Tech 11:539-550.

Martinez-Lage JF, Rabano A, Bermejo J, Martinez Perez M, Guerrero MC, Contreras MA, Lunar A (2005) Creutzfeldt-Jakob disease acquired via a dural graft: failure

of therapy with quinacrine and chlorpromazine. Surg Neurol 64:542-545, discussion 545.

Mastrianni JA (2010) The genetics of prion diseases. Genet Med 12:187-195.

Mathiason CK, Powers JG, Dahmes SJ, Osborn DA, Miller KV, Warren RJ, Mason GL, Hays SA, Hayes-Klug J, Seelig DM, Wild MA, Wolfe LL, Spraker TR, Miller MW, Sigurdson CJ, Telling GC, Hoover EA (2006) Infectious prions in the saliva and blood of deer with chronic wasting disease. Science 314:133-136.

Mead S, Stumpf MP, Whitfield J, Beck JA, Poulter M, Campbell T, Uphill JB, Goldstein D, Alpers M, Fisher EM, Collinge J (2003) Balancing selection at the prion protein gene consistent with prehistoric kurulike epidemics. Science 300:640-643.

Medori R, Tritschler HJ, LeBlanc A, Villare F, Manetto V, Chen HY, Xue R, Leal S, Montagna P, Cortelli P, et al. (1992) Fatal familial insomnia, a prion disease with a mutation at codon 178 of the prion protein gene. N Engl J Med 326:444-449.

Meyer RK, McKinley MP, Bowman KA, Braunfeld MB, Barry RA, Prusiner SB (1986) Separation and properties of cellular and scrapie prion proteins. Proc Natl Acad Sci U S A 83:2310-2314.

Milhavet O, Mange A, Casanova D, Lehmann S (2000) Effect of Congo red on wild-type and mutated prion proteins in cultured cells. J Neurochem 74:222-230.

Moser M, Colello RJ, Pott U, Oesch B (1995) Developmental expression of the prion protein gene in glial cells. Neuron 14:509-517.

Nilsson KP, Inganas O (2003) Chip and solution detection of DNA hybridization using a luminescent zwitterionic polythiophene derivative. Nat Mater 2:419-424.

Nilsson KP, Rydberg J, Baltzer L, Inganas O (2003) Self-assembly of synthetic peptides control conformation and optical properties of a zwitterionic polythiophene derivative. Proc Natl Acad Sci U S A 100:10170-10174.

Nilsson KP, Herland A, Hammarstrom P, Inganas O (2005) Conjugated polyelectrolytes: conformation-sensitive optical probes for detection of amyloid fibril formation. Biochemistry 44:3718-3724.

Nilsson KP, Hammarstrom P, Ahlgren F, Herland A, Schnell EA, Lindgren M, Westermark GT, Inganas O (2006) Conjugated polyelectrolytes--conformation-sensitive optical probes for staining and characterization of amyloid deposits. Chembiochem 7:1096-1104.

Nilsson KP, Ikenberg K, Aslund A, Fransson S, Konradsson P, Rocken C, Moch H, Aguzzi A (2010) Structural typing of systemic amyloidoses by luminescent-conjugated polymer spectroscopy. Am J Pathol 176:563-574.

Nilsson KP, Aslund A, Berg I, Nystrom S, Konradsson P, Herland A, Inganas O, Stabo-Eeg F, Lindgren M, Westermark GT, Lannfelt L, Nilsson LN, Hammarstrom P (2007) Imaging distinct conformational states of amyloid-beta fibrils in Alzheimer's disease using novel luminescent probes. ACS Chem Biol 2:553-560.

Nonno R, Bari MA, Cardone F, Vaccari G, Fazzi P, Dell'omo G, Cartoni C, Ingrosso L, Boyle A, Galeno R, Sbriccoli M, Lipp HP, Bruce M, Pocchiari M, Agrimi U (2006) Efficient transmission and characterization of creutzfeldt-jakob disease strains in bank voles. PLoS Pathog 2:e12.

Oesch B, Westaway D, Walchli M, McKinley MP, Kent SB, Aebersold R, Barry RA, Tempst P, Teplow DB, Hood LE, Weissmann C (1985a) A cellular gene encodes scrapie PrP 27-30 protein. Cell 40:735-746.

Oesch B, Westaway D, Walchli M, McKinley MP, Kent SB, Aebersold R, Barry RA, Tempst P, Teplow DB, Hood LE, et al. (1985b) A cellular gene encodes scrapie PrP 27-30 protein. Cell 40:735–746.

Otzen DE (2010) Amyloid formation in surfactants and alcohols: membrane mimetics or structural switchers? Curr Protein Pept Sci 11:355-371.

Ouidja MO, Petit E, Kerros ME, Ikeda Y, Morin C, Carpentier G, Barritault D, Brugere-Picoux J, Deslys JP, Adjou K, Papy-Garcia D (2007) Structure-activity studies of heparan mimetic polyanions for anti-prion therapies. Biochem Biophys Res Commun 363:95-100.

Palmer MS, Dryden AJ, Hughes JT, Collinge J (1991) Homozygous prion protein genotype predisposes to sporadic Creutzfeldt-Jakob disease. Nature 352:340-342.

Pastrana MA, Sajnani G, Onisko B, Castilla J, Morales R, Soto C, Requena JR (2006) Isolation and characterization of a proteinase K-sensitive PrPSc fraction. Biochemistry 45:15710-15717.

Pauly PC, Harris DA (1998) Copper stimulates endocytosis of the prion protein. J Biol Chem 273:33107-33110.

Pearson GR, Gruffydd-Jones TJ, Wyatt JM, Hope J, Chong A, Scott AC, Dawson M, Wells GA (1991) Feline spongiform encephalopathy. Vet Rec 128:532.

Peretz D, Williamson RA, Kaneko K, Vergara J, Leclerc E, Schmitt-Ulms G, Mehlhorn IR, Legname G, Wormald MR, Rudd PM, Dwek RA, Burton DR, Prusiner SB (2001) Antibodies inhibit prion propagation and clear cell cultures of prion infectivity. Nature 412:739-743.

Perrier V, Solassol J, Crozet C, Frobert Y, Mourton-Gilles C, Grassi J, Lehmann S (2004) Anti-PrP antibodies block PrPSc replication in prion-infected cell cultures by accelerating PrPC degradation. J Neurochem 89:454-463.

Piccardo P, Manson JC, King D, Ghetti B, Barron RM (2007) Accumulation of prion protein in the brain that is not associated with transmissible disease. Proc Natl Acad Sci U S A 104:4712-4717.

Piro JR, Harris BT, Nishina K, Soto C, Morales R, Rees JR, Supattapone S (2009) Prion protein glycosylation is not required for strain-specific neurotropism. J Virol 83:5321-5328.

Pocchiari M, Schmittinger S, Masullo C (1987) Amphotericin B delays the incubation period of scrapie in intracerebrally inoculated hamsters. J Gen Virol 68 (Pt 1):219-223.

Polymenidou M, Stoeck K, Glatzel M, Vey M, Bellon A, Aguzzi A (2005) Coexistence of multiple PrPSc types in individuals with Creutzfeldt-Jakob disease. Lancet Neurol 4:805-814.

Polymenidou M, Prokop S, Jung HH, Hewer E, Peretz D, Moos R, Tolnay M, Aguzzi A (2011) Atypical prion protein conformation in familial prion disease with PRNP P105T mutation. Brain Pathol 21:209-214.

Priola SA, Chesebro B, Caughey B (2003) Biomedicine. A view from the top--prion diseases from 10,000 feet. Science 300:917-919.

Prusiner SB (1982) Novel proteinaceous infectious particles cause scrapie. Science 216:136-144.

Prusiner SB (1991) Molecular biology of prion diseases. Science 252:1515-1522.

Prusiner SB (1998) Prions. Proc Natl Acad Sci U S A 95:13363–13383.

Ravichandran R, Sundarrajan S, Venugopal JR, Mukherjee S, Ramakrishna S (2010) Applications of conducting polymers and their issues in biomedical engineering. J R Soc Interface 7 Suppl 5:S559-579.

Riek R, Hornemann S, Wider G, Glockshuber R, Wuthrich K (1997) NMR characterization of the full-length recombinant murine prion protein, mPrP(23-231). FEBS Lett 413:282-288.

Riek R, Hornemann S, Wider G, Billeter M, Glockshuber R, Wuthrich K (1996a) NMR structure of the mouse prion protein domain PrP(121-321). Nature 382:180-182.

Riek R, Hornemann S, Wider G, Billeter M, Glockshuber R, Wuthrich K (1996b) NMR structure of the mouse prion protein domain PrP(121-231). Nature 382:180-182.

Rivera-Milla E, Stuermer CA, Malaga-Trillo E (2003) An evolutionary basis for scrapie disease: identification of a fish prion mRNA. Trends Genet 19:72-75.

Safar J, Roller PP, Gajdusek DC, Gibbs CJ, Jr. (1993) Thermal stability and conformational transitions of scrapie amyloid (prion) protein correlate with infectivity. Protein Sci 2:2206-2216.

Safar J, Wille H, Itri V, Groth D, Serban H, Torchia M, Cohen F, Prusiner S (1998) Eight prion strains have PrP^{Sc} molecules with different conformations. Nat Med 4:1157-1165.

Schutt CR, Bartz JC (2008) Prion interference with multiple prion isolates. Prion 2:61-63.

Seeger H, Heikenwalder M, Zeller N, Kranich J, Schwarz P, Gaspert A, Seifert B, Miele G, Aguzzi A (2005) Coincident scrapie infection and nephritis lead to urinary prion excretion. Science 310:324-326.

Shaked GM, Fridlander G, Meiner Z, Taraboulos A, Gabizon R (1999) Protease-resistant and detergent-insoluble prion protein is not necessarily associated with prion infectivity. J Biol Chem 274:17981-17986.

Shyng SL, Lehmann S, Moulder KL, Harris DA (1995) Sulfated glycans stimulate endocytosis of the cellular isoform of the prion protein, PrPC, in cultured cells. J Biol Chem 270:30221-30229.

Sigurdson CJ, Aguzzi A (2007) Chronic wasting disease. Biochim Biophys Acta 1772:610-618.

Sigurdson CJ, Nilsson KP, Hornemann S, Manco G, Polymenidou M, Schwarz P, Leclerc M, Hammarstrom P, Wuthrich K, Aguzzi A (2007) Prion strain discrimination using luminescent conjugated polymers. Nat Methods 4:1023-1030.

Silveira JR, Raymond GJ, Hughson AG, Race RE, Sim VL, Hayes SF, Caughey B (2005) The most infectious prion protein particles. Nature 437:257-261.

Simonic T, Duga S, Strumbo B, Asselta R, Ceciliani F, Ronchi S (2000) cDNA cloning of turtle prion protein. FEBS Lett 469:33-38.

Sklaviadis T, Dreyer R, Manuelidis L (1992) Analysis of Creutzfeldt-Jakob disease infectious fractions by gel permeation chromatography and sedimentation field flow fractionation. Virus Res 26:241-254.

Sklaviadis TK, Manuelidis L, Manuelidis EE (1989) Physical properties of the Creutzfeldt-Jakob disease agent. J Virol 63:1212-1222.

Solassol J, Crozet C, Lehmann S (2003) Prion propagation in cultured cells. Br Med Bull 66:87-97.

Stahl N, Borchelt DR, Hsiao K, Prusiner SB (1987) Scrapie prion protein contains a phosphatidylinositol glycolipid. Cell 51:229-240.

Stahl N, Baldwin MA, Teplow DB, Hood L, Gibson BW, Burlingame AL, Prusiner SB (1993) Structural studies of the scrapie prion protein using mass spectrometry and amino acid sequencing. Biochemistry 32:1991-2002.

Steele AD, Emsley JG, Ozdinler PH, Lindquist S, Macklis JD (2006) Prion protein (PrPc) positively regulates neural precursor proliferation during developmental and adult mammalian neurogenesis. Proc Natl Acad Sci U S A 103:3416-3421.

Strumbo B, Ronchi S, Bolis LC, Simonic T (2001) Molecular cloning of the cDNA coding for Xenopus laevis prion protein. FEBS Letters 508:170-174.

Supattapone S, Piro JR, Rees JR (2009) Complex polyamines: unique prion disaggregating compounds. CNS Neurol Disord Drug Targets 8:323-328.

Tagliavini F et al. (1997) Effectiveness of anthracycline against experimental prion disease in Syrian hamsters. Science 276:1119-1122.

Taraboulos A, Jendroska K, Serban D, Yang SL, DeArmond SJ, Prusiner SB (1992) Regional mapping of prion proteins in brain. Proc Natl Acad Sci U S A 89:7620-7624.

Telling GC, Scott M, Mastrianni J, Gabizon R, Torchia M, Cohen FE, DeArmond SJ, Prusiner SB (1995) Prion propagation in mice expressing human and chimeric PrP transgenes implicates the interaction of cellular PrP with another protein. Cell 83:79-90.

Terada T, Tsuboi Y, Obi T, Doh-ura K, Murayama S, Kitamoto T, Yamada T, Mizoguchi K (2010) Less protease-resistant PrP in a patient with sporadic CJD treated with intraventricular pentosan polysulphate. Acta Neurol Scand 121:127-130.

Thackray AM, Hopkins L, Klein MA, Bujdoso R (2007) Mouse-adapted ovine scrapie prion strains are characterized by different conformers of PrPSc. J Virol 81:12119-12127.

Tixador P, Herzog L, Reine F, Jaumain E, Chapuis J, Le Dur A, Laude H, Beringue V (2010) The physical relationship between infectivity and prion protein aggregates is strain-dependent. PLoS Pathog 6:e1000859.

Tobler I, Gaus SE, Deboer T, Achermann P, Fischer M, Rülicke T, Moser M, Oesch B, McBride PA, Manson JC (1996) Altered circadian activity rhythms and sleep in mice devoid of prion protein. Nature 380:639-642.

Tsuboi Y, Doh-Ura K, Yamada T (2009) Continuous intraventricular infusion of pentosan polysulfate: clinical trial against prion diseases. Neuropathology 29:632-636.

Viles JH, Donne D, Kroon G, Prusiner SB, Cohen FE, Dyson HJ, Wright PE (2001) Local structural plasticity of the prion protein. Analysis of NMR relaxation dynamics. Biochemistry 40:2743-2753.

Wadsworth JD, Asante EA, Desbruslais M, Linehan JM, Joiner S, Gowland I, Welch J, Stone L, Lloyd SE, Hill AF, Brandner S, Collinge J (2004) Human prion protein with valine 129 prevents expression of variant CJD phenotype. Science 306:1793-1796.

Wang YQ, Buell AK, Wang XY, Welland ME, Dobson CM, Knowles TP, Perrett S (2011) Relationship between prion propensity and the rates of individual molecular steps of fibril assembly. J Biol Chem 286:12101-12107.

Weissmann C (1991) A 'unified theory' of prion propagation. Nature 352:679-683.

Weissmann C (2004) The state of the prion. Nat Rev Microbiol 2:861-871.

Weissmann C, Enari M, Klohn PC, Rossi D, Flechsig E (2002) Transmission of prions. J Infect Dis 186 Suppl 2:S157-165.

Wells GA, Scott AC, Johnson CT, Gunning RF, Hancock RD, Jeffrey M, Dawson M, Bradley R (1987) A novel progressive spongiform encephalopathy in cattle. Vet Rec 121:419-420.

Wilesmith JW (1988) Bovine spongiform encephalopathy. Vet Rec 122:614.

Williams ES, Young S (1980) Chronic wasting disease of captive mule deer: a spongiform encephalopathy. J Wildl Dis 16:89-98.

Windl O, Dempster M, Estibeiro JP, Lathe R, de Silva R, Esmonde T, Will R, Springbett A, Campbell TA, Sidle KC, Palmer MS, Collinge J (1996) Genetic basis of Creutzfeldt-Jakob disease in the United Kingdom: a systematic analysis of predisposing mutations and allelic variation in the PRNP gene. Hum Genet 98:259-264.

Wroe SJ, Pal S, Siddique D, Hyare H, Macfarlane R, Joiner S, Linehan JM, Brandner S, Wadsworth JD, Hewitt P, Collinge J (2006) Clinical presentation and pre-mortem diagnosis of variant Creutzfeldt-Jakob disease associated with blood transfusion: a case report. Lancet 368:2061-2067.

Yull HM, Ritchie DL, Langeveld JP, van Zijderveld FG, Bruce ME, Ironside JW, Head MW (2006) Detection of type 1 prion protein in variant Creutzfeldt-Jakob disease. Am J Pathol 168:151-157.

Zahn R, Liu A, Luhrs T, Riek R, von Schroetter C, Lopez Garcia F, Billeter M, Calzolai L, Wider G, Wuthrich K (2000) NMR solution structure of the human prion protein. Proc Natl Acad Sci U S A 97:145-150.

Zanusso G, Farinazzo A, Prelli F, Fiorini M, Gelati M, Ferrari S, Righetti PG, Rizzuto N, Frangione B, Monaco S (2004) Identification of distinct N-terminal truncated forms of prion protein in different Creutzfeldt-Jakob disease subtypes. J Biol Chem 279:38936-38942.

Zhang CC, Steele AD, Lindquist S, Lodish HF (2006) Prion protein is expressed on long-term repopulating hematopoietic stem cells and is important for their self-renewal. Proc Natl Acad Sci U S A 103:2184-2189.

Zlotnik I, Rennie JC (1963) Further observations on the experimental transmission of scrapie from sheep and goats to laboratory mice. J Comp Pathol 73:150-162.

ACKNOWLEDGMENTS

I would like to express my deepest gratitude to Professor Adriano Aguzzi for his support, brilliant ideas and guidance throughout my Ph.D. thesis.

Furthermore, I would like to express my gratitude to a number of people who have helped me throughout:

Especially warm thanks to Dr. Simone Hornemann who supervised the last two years of my thesis. She spent a large amount of time writing with me the manuscript “Polythiophenes inhibit prion propagation by stabilizing PrP aggregates”. In addition, her help was critical in the writing of my thesis. She always supported me and gave me guidance and critical input.

PD. Dr. Mathias Heikenwalder deserves many thanks for having supervised the first years of my thesis. He introduced me into the laboratory and taught me various techniques of molecular biology and animal work.

Dr. Jeppe Falsig got me started with the organotypic slice cultures.

Dr. Christina Sigurdson’s friendly way was very motivating throughout my time in the lab.

Dr. Johannes Habaeck always behaved as a very helpful and motivated team worker.

Dr. Peter Nilsson got me started with the use of polythiophenes and spectral analysis. Furthermore he always gave me support and precious technical input. He also participated actively on the development of my main PhD project.

Warm thanks to Giuseppe Manco, Petra Schwartz and Rita Moos and the BZL-team for taking care of my mice and helping with the genotyping thereof.

I would also like to thank all my former colleagues at the Institute for Neuropathology, especially Carlo Suter for his help with SCEPA analysis and MTS assay and Ahmet Varol for helping me with the occasional medium change and tissue harvesting.

I would also like to extend my gratitude to Zentrum für Neurowissenschaften Zurich (ZNZ).

I would like to express my outmost gratitude and affection to my parents, brothers and friends, as well as to my daughter Gila.

Finally, I would like to express my infinite love and extreme gratitude to Angela Batschelet, the most important person in my life.

CURRICULUM

Ilan Margalith
Maienzugstrasse 6b, 5000 Aarau
079 371 69 92
ilan.margalith@hotmail.com

Single
22.02.1978
Nationality: Swiss
Native place: Lausanne

EDUCATION

08.06 – 09.11 **PhD student.** Graduation in April 2013
Institute of Neuropathology (Prof A. Aguzzi), University Hospital of Zurich

10.03 – 06.05 **Master of Science in Biology** (includes one year for equivalence of studies)
University of Geneva (final note: 5.5)

10.00 – 10.03 **Bachelor in Biology**
University of Neuchatel

10.98 – 04.99 **Law School**
University of Neuchatel

07.97 **Graduation Science Diploma**
High school (Lycée Denis-de-Rougemont), Neuchatel

ONGOING FORMATION

04.04 – 09.04 **Certificate for Ongoing Training in Biosecurity**
University Institute for the Study of Development ("IUED"), Geneva

PROFESSIONNAL EXPERIENCE IN THE FRAME OF STUDIES

09.11 – pres. **Scientific collaborator**
School of Agricultural, Forest and Food Sciences HAFL, Zollikofen

08.06 – 07.11 **Researcher in molecular biology, neurodegenerative disorders**
(PhD thesis)
Institute of Neuropathology (Prof A. Aguzzi), University Hospital of Zurich

10.03 – 06.05 **Researcher in transgenic plant biotechnology** (Master thesis)
Federal Agronomic Research Station Agroscope, Changins

PROFESSIONNAL EXPERIENCE IN PARALLEL TO STUDIES

08.05 – 08.06 **Medical Research Assistant**
Institute of Neuropathology (Prof A. Aguzzi), University Hospital of Zurich

10.03 – 10.04 **Graduate Assistant**
Science Faculty, University of Geneva

08.02 – 09.02 **Stock Administrator**
Mary Kay Inc., Le Crêt-du-Locle

07.00 – 07.03 **Private teaching** (biology, mathematics, chemistry, physics, French, English)
High-school level, Neuchatel

05.99 – 08.99 **Quality Controller**
Philip Morris SA, Neuchatel

08.97 – 01.98 **Shipping Department Operator and Process Group Employee**
Silicon Graphics Inc., Boudry

PUBLICATION LIST

1. **Ilan Margalith**, Carlo Suter, Boris Ballmer, Petra Schwarz, Cinzia Tiberi, Tiziana Sonati, Jeppe Falsig, Sofie Nyström, Per Hammarström, Andreas Åslund, K. Peter R. Nilsson, Alice Yam, Eric Whitters, Simone Hornemann and Adriano Aguzzi
   "Polythiophenes inhibit prion propagation by stabilizing PrP aggregates"
   Journal of Biological Chemistry 2012 Apr
2. Christina J. Sigurdson, Shivanjali Joshi-Barr, Cyrus Bett, Olivia Winson, Giuseppe Manco, Petra Schwarz, Thomas Rülicke, Peter Nilsson, **Ilan Margalith**, Alex Raeber, David Peretz, Simone Hornemann, Kurt Wüthrich and Adriano Aguzzi
   "Spongiform Encephalopathy in Transgenic Mice Expressing a Point Mutation in the β2–α2 Loop of the Prion Protein"
   Journal of Neuroscience 2011 Sep
3. Johannes Haybaeck, Mathias Heikenwalder, Britta Klevenz, Petra Schwarz, **Ilan Margalith**, Bridel Claire, Mertz Kirsten, Zirdum Elizabeta, Benjamin Petsch, Thomas J. Fuchs, Lothar Stitz, Adriano Aguzzi
   "Aerosols Transmit Prions to Immunocompetent and Immunodeficient Mice"
   PLoS Pathogen 2011 Jan
4. Jeppe Falsig, Christian Julius, **Ilan Margalith**, Petra Schwarz, Frank L. Heppner, Adriano Aguzzi
   "A Versatile Prion Replication Assay in Organotypic Brain Slices"
   Nature Neuroscience 2008 Jan
5. Mathias Heikenwalder, Michael O. Kurrer, **Ilan Margalith**, Jan Kranich, Nicolas Zeller, Johannes Haybaeck, Magdalini Polymenidou, Mathias Matter, Juliane Bremer, Walker S. Jackson, Susan Lindquist, Christina J. Sigurdson, Adriano Aguzzi
   "Lymphotoxin-Dependent Prion Replication in Inflammatory Stromal Cells of Granulomas"
   Immunity 2008 Dec
6. Ciriaco Ligios, Giovanna Maria Cancedda, **Ilan Margalith**, Cinzia Santucciu, Laura Madau, Caterina Maestrale, Massimo Basagni, Mariangela Saba and Mathias Heikenwalder
   "Intraepithelial and Interstitial Deposition of Pathological Prion Protein in Kidneys of Scrapie-Affected Sheep"
   PLoS ONE 2007 Sep

APPENDIX

Tables

Table 1

Statistical analysis of prion infectivity titres shown in Figure 11 using a Mantel-Haenszel Chi-square test with Bonferroni correction comparing ID_{50} difference to control (COCSBH from untreated cultures harvested after 42 DPI).

Figure 11	p-value	conf. interval for c. o. r.
untreated (21 DIV)	p = 0.007	-1.71(-2.35 to -1.07)
PPS 0.3 μg/ml	p = 0.012	1.99(-2.96 to -1.03)
PTAA 60 μg/ml	p < 0.001	-3.32(-3.62 to -3.01)
PTAA 6 μg/ml	p = 0.001	-2(-2.19 to -1.81)
PTAA 1 μg/ml	p = 0.106	-0.66(-1.66 to 0.34)
PTAA 0.1 μg/ml	p = 0.695	-0.13(-1.36 to 1.10)
PTAA 0.01 μg/ml	n/a	n/a

Table 2

Statistical analysis of data shown in Figure 12 using a one-way ANOVA with Tukey's multiple comparison test.

Figure 12	p-value	95% c.i. of difference
untreated (21 DIV)	p < 0.0001	-228.7(-309.8 to -147.6)
PPS 0.3 μg/ml	p < 0.0001	216.9(135.8 to 298.0)
PTAA 60 μg/ml	p < 0.0001	236.1(155.0 to 317.1)
PTAA 6 μg/ml	p < 0.0001	233.9(152.8 to 315.0)
PTAA 1 μg/ml	p < 0.0001	229.0(147.9 to 310.1)
PTAA 0.1 μg/ml	p < 0.0001	199.4(118.4 to 280.5)
PTAA 0.01 μg/ml	n/s	-46.9(-128.0 to 34.18)

Table 3

Statistical analysis of data shown in Figure 14A using a one-way ANOVA with Tukey's multiple comparison test.

Figure 14A	**p-value**	**95% c.i. of difference**
untreated (21 DIV)	p < 0.001	-41.79(-66.96 to -16.62)
PPS 0.3 μg/ml	p < 0.001	37.56(12.39 to 62.73)
PTAA 60 μg/ml	p < 0.001	42.94(17.77 to 68.11)
PTAA 6 μg/ml	p < 0.001	40.57(15.40 to 65.74)
PTAA 1 μg/ml	p < 0.001	35.09(9.917 to 60.26)
PTAA 0.1 μg/ml	p < 0.001	26.51(1.36 to 51.70)
PTAA 0.01 μg/ml	p = 0.450	12.11(-13.06 to 37.28)

Table 4

Statistical analysis of data shown in Figure 14B using a one-way ANOVA with Tukey's multiple comparison test.

Figure 14B	**p-value**	**95% c.i. of difference**
PTAA 60 μg/ml	p < 0.05	47.70(0.65 to 94.75)

Table 5

Statistical analysis shown in Figure 17 using a one-way ANOVA with Tukey's multiple comparison test.

Fig. 17A	p-values	95% c.i. of difference
7 DIV	Ns	-9(-108.8 to 90.80)
19 DIV	Ns	-13.86(-113.7 to 85.94)
21 DIV	Ns	-23.77(-123.6 to 76.03)
28 DIV	Ns	-60.36(-160.2 to 39.44)
35 DIV	p < 0.001	-205.5(-305.3 to -105.7)
42 DIV	p < 0.001	-252.8(-352.6 to 153.0)
From 7 DIV	Ns	-2.11(-101.9 to 97.68)
From 19 DIV	Ns	-1.26(-101.1 to 98.54)
From 21 DIV	Ns	0(-99.80 to 99.80)
From 28 DIV	Ns	-0.49(-100.3 to 99.30)
From 35 DIV	Ns	-0.04(-99.84 to 99.75)

Fig. 17B	p-values	95% c.i. of difference
7 DIV	n/s	0(-38 to 38)
19 DIV	n/s	-0.09(-38 to 38)
21 DIV	n/s	-0.95(-39 to 37)
28 DIV	n/s	-6.2(-44 to 32)
35 DIV	n/s	-16(-54 to 21)
42 DIV	$p < 0.001$	-54(-92 to -17)
45 DIV	$p < 0.001$	-113(-151 to -76)
49 DIV	$p < 0.001$	-114(-152 to -76)
56 DIV	$p < 0.001$	-114(-152 to -77)
From 7 DIV	n/s	-0.43(-38 to 37)
From 19 DIV	n/s	0(-38 to 38)
From 21 DIV	n/s	0(-38 to 38)
From 28 DIV	n/s	-4.6(-42 to 33)
From 35 DIV	n/s	-21(-59 to 17)
42 DIV vs. from 7 DIV	$p < 0.001$	54(16 to 92)
42 DIV vs. from 19 DIV	$p < 0.001$	54(17 to 92)
42 DIV vs. from 21 DIV	$p < 0.001$	54(17 to 92)
42 DIV vs. from 28 DIV	$p < 0.01$	50(12 to 87)
42 DIV vs. from 35 DIV	n/s	33(-4.5 to 71)

Fig. 17C	p-values	95% c.i. of difference
7 DIV	Ns	44(-174 to 261)
19 DIV	Ns	71(-146 to 289)
21 DIV	Ns	67(-151 to 284)
28 DIV	Ns	52(-165 to 270)
35 DIV	Ns	162(-55 to 380)
42 DIV	Ns	53(-165 to 270)
45 DIV	Ns	107(-110 to 325)
49 DIV	Ns	14(-203 to 232)
56 DIV	Ns	88(-130 to 305)
From 7 DIV	Ns	211(-6.6 to 428)

From 19 DIV	Ns	196(-22 to 413)
From 21 DIV	$p < 0.05$	223(5.7 to 441)
From 28 DIV	Ns	189(-28 to 407)
From 35 DIV	$p < 0.05$	236(18 to 453)
42 DIV vs. from 7 DIV	Ns	158(59 to 376)
42 DIV vs. from 19 DIV	Ns	143(-74 to 361)
42 DIV vs. from 21 DIV	Ns	170(-47 to 388)
42 DIV vs. from 28 DIV	Ns	136(-81 to 354)
42 DIV vs. from 35 DIV	Ns	183(-34 to 400)

Statistical analysis using a one-way ANOVA with Tukey's multiple comparison test. Unless stated otherwise, time points are compared to the non-infected COCS. For 42 DIV vs. From 7 DIV, for instance, the value obtained for COCS harvested at 42 DIV is compared to the value obtained for COCS harvested at 42 DIV with treatment from 7 DIV.

Table 6

Statistical analysis of data shown in Figure 18 using a one-way ANOVA with Tukey's multiple comparison test.

Figure 18	**p-value**	**95% c.i. of difference**
CD1 untr. VS CD1 +PPS 0.3 μg/ml	n/s	-41.79(-66.96 to -16.62)
CD1 untr. VS CD1 +PTAA 60 μg/ml	n/s	37.56(12.39 to 62.73)
CD1 untr. VS CD1 +PTAA 6 μg/ml	$p < 0.01$	42.94(17.77 to 68.11)
CD1 untr. VS RML untreated	$p < 0.001$	40.57(15.40 to 65.74)
CD1 untr. VS RML +PPS 0.3 μg/ml	n/s	35.09(9.917 to 60.26)
CD1 untr. VS RML +PTAA 60 μg/ml	n/s	26.51(1.36 to 51.70)
CD1 untr. VS RML +PTAA 6 μg/ml	n/s	12.11(-13.06 to 37.28)
RML untr. VS RML +PPS 0.3 μg/ml	$p < 0.001$	35.09(9.917 to 60.26)
RML untr. VS RML +PTAA 60 μg/ml	$p < 0.001$	26.51(1.36 to 51.70)
RML untr. VS RML +PTAA 6 μg/ml	$p < 0.001$	12.11(-13.06 to 37.28)

Table 7

Statistical analysis of the difference between prion infectivity titre of untreated RML6 (control) compared to LCP-treated RML6 and for pHTAA-, pFTAA- and PTAA-treated RML6 compared to each other (Figure 25). Differences were computed by using a Mantel-Haenszel Chi-square test for comparing number of negative wells at each dilution (10^{-4} to 10^{-8}) of a sample in the SCEPA.

Figure 25	**μg/ml**	**p-values**	**conf. interval for c. o. r.**
Control to PTAA	300	p < 0.001	
Control to pHTAA	300	p < 0.001	
Control to pFTAA	300	p < 0.001	
Control to PBAT	300	p < 0.001	
Control to POMT	300	p < 0.001	
Control to POWT	300	p < 0.001	
pHTAA VS PTAA	300	p = 0.450	1.69(0.61-4.67)
pFTAA VS PTAA	300	p = 0.005	0.13(0.03-0.50)
pFTAA VS pHTAA	300	p = 0.001	10(2.66-37.64)

Table 8

Statistical analysis of the difference between prion infectivity titre of untreated RML6 (control) compared to LCP-treated RML6 (Figure 26). Differences were computed by using a Mantel-Haenszel Chi-square test for comparing number of negative wells at each dilution (10^{-4} to 10^{-8}) of a sample in the SCEPA.

Figure 26A	**μg/ml**	**p-values**	**conf. interval for c. o. r.**
Control to pFTAA	900	p < 0.0001	
	300	p = 0.002	0.07(0.01-0.36)
	150	p = 0.004	0.15(0.04-0.52)
	75	p = 0.047	0.32(0.12-0.87)

Figure 26B	**μg/ml**	**p-values**	**conf. interval for c. o. r.**
Control to PTAA	5000	p < 0.0001	
	900	p < 0.0001	
	300	p < 0.0001	
	150	p < 0.0001	

	100	$p < 0.0003$	0.16(0.06-0.43)
	10	$p = 0.081$	0.34(0.12-0.99)

Table 9

Infectivity titres of samples described in Figure 27A.

Plate n°:	1	2	3	4
Infectivity titre ($logID_{50} \times g^{-1}$):	7.91	6.83	8.05	7.80

Table 10

Comparisons between infectivity titres reported in Table 9. Differences were computed by using a Mantel-Haenszel Chi-square test for comparing number of negative wells at each dilution (10^{-4} to 10^{-8}) of a sample in the SCEPA.

Plate n°:	1	2	3	4
1		$p < 0.001$	$p = 0.398$ 1.89(0.62-5.79)	$p = 0.826$ 0.78(0.29-2.15)
2			$p < 0.001$	$p < 0.001$
3				$p = 0.178$ 0.39(0.13-1.24)

Table 11

Infectivity titres of samples described in Figure 27B.

Plate n°:	1	2
PTAA (μg/ml):	0	10
Infectivity titre ($logID_{50} \times g^{-1}$):	8.05	7.78

Table 12

Comparisons between Infectivity titres reported in Table 11. Differences were computed by using a Mantel-Haenszel Chi-square test for comparing number of negative wells at each dilution (10^{-4} to 10^{-8}) of a sample in the SCEPA.

Plate n°:	1	2
1		$p = 0.551$ (n.s.) 0.58(0.17-1.92)

Table 13

Statistical analysis of the difference between MPA signals for untreated CD1 brain homogenate (mock), LCP-treated CD1 brain homogenate, untreated RML6 (control) and LCP-treated RML6 (Figure 30). Differences were computed by using a T- test comparing the $\log_{10}$ RLU signals in the MPA.

	µg/ml	**p-values**	**conf. interval for mean ratio**
mock + H_2O to mock + PTAA	0 to 300	p = 0.001	1.21(1.12-1.30)
Control to PTAA	300	p < 0.001	8.95(6.57-12.20)
	100	p < 0.001	6.50(4.89-8.65)
	10	p = 0.004	1.97(1.37-2.82)
	1	p = 0.348	1.23(0.74-2.04)
Control to POMT	300	p < 0.001	9.80(7.21-13.33)
	100	p < 0.001	3.27(2.30-4.67)
	10	p = 0.015	1.75(1.17-2.63)
	1	p = 0.374	1.15(0.81-1.62)
Control to pHTAA	300	p < 0.001	3.14(2.25-4.38)
	100	p = 0.007	2.21(1.37-3.55)
	10	p = 0.057	1.49(0.86-2.25)
	1	p = 0.737	0.95(0.69-1.32)
Control to pFTAA	300	p < 0.001	3.79(2.66-5.41)
	100	p < 0.001	3.86(2.57-5.80)
	10	p = 0.003	2.39(1.56-3.68)
	1	p = 0.028	1.55(1.07-2.25)

Table 14

Statistical analysis of the difference between MPA signals for RML6 treated with different LCPs (Figure 30). The overall effect of individual LCPs was investigated by comparing a group of four concentrations of each individual LCPs using a post-Hoc T-test for analysis of variance.

	μg/ml	p-values	conf. interval for mean ratio
PTAA to POMT	All conc.	p = 0.078	1.20(0.66-1.01)
PTAA to pHTAA	All conc.	p < 0.001	0.51(0.42-0.63)
PTAA to pFTAA	All conc.	p = 0.017	0.79(0.64-0.97)
POMT to pHTAA	All conc.	p < 0.001	0.62(0.51-0.77)
POMT to pFTAA	All conc.	p = 1.000	1.04(0.78-0.85)
pHTAA to pFTAA	All conc.	p < 0.001	1.53(1.24-1.89)

Table 15

Statistical analysis of samples described in Figure 31.

	bead treatment	p-values	conf. interval for mean ratio
CD1+H_2O to CD1+PTAA	No	p = 0.339	1.08(0.90-1.31)
CD1+H_2O to CD1+H_2O	Yes	p = 0.004	1.29(1.12-1.49)
CD1+PTAA to CD1+PTAA	Yes	p = 0.024	1.24(1.04-1.48)
RML+PTAA to RML+PTAA	Yes	p = 0.992	1.00(0.69-1.45)
Control to RML+H_2O	Yes	P = 0.274	1.10(0.91-1.32)